MOLECULAR AND CELLULAR DYNAMICS OF THE HEALING RESPONSE ASSOCIATED WITH IMPLANTED EXPANDED POLYTETRAFLUOROETHYLENE

by

Mark Aaron Schwartz

A Dissertation Submitted to the Faculty of the

GRADUATE INTERDISCIPLINARY PROGRAM IN BIOMEDICAL ENGINEERING

In Partial Fulfillment of the Requirements
For the Degree of

DOCTOR OF PHILOSOPHY

In the Graduate College

THE UNIVERSITY OF ARIZONA

2005

THE UNIVERSITY OF ARIZONA
GRADUATE COLLEGE

As members of the Dissertation Committee, we certify that we have read the dissertation prepared by Mark A. Schwartz entitled Molecular and Cellular Dynamics of the Healing Response Associated with Implanted Expanded Polytetrafluoroethylene and recommend that it be accepted as fulfilling the dissertation requirement for the Degree of Doctor of Philosophy

_____ Date: 12/05/05
James B. Hoying

_____ Date: 12/05/05
Stuart K. Williams

_____ Date: 12/05/05
Scott A. Boitano

_____ Date: 12/05/05
Scott E. Klewer

_____ Date: 12/05/05
Mark R. Riley

Final approval and acceptance of this dissertation is contingent upon the candidate's submission of the final copies of the dissertation to the Graduate College.

I hereby certify that I have read this dissertation prepared under my direction and recommend that it be accepted as fulfilling the dissertation requirement.

_____ Date: 12/05/05
Dissertation Director: James B. Hoying

_____ Date: 12/05/05
Dissertation Director: Stuart K. Williams

STATEMENT BY AUTHOR

This dissertation has been submitted in partial fulfillment of requirements for an advanced degree at the University of Arizona and is deposited in the University Library to be made available to borrowers under rules of the Library.

Brief quotations from this dissertation are allowable without special permission, provided that accurate acknowledgment of source is made. Requests for permission for extended quotation from or reproduction of this manuscript in whole or in part may be granted by the head of the major department or the Dean of the Graduate College when in his or her judgment the proposed use of the material is in the interests of scholarship. In all other instances, however, permission must be obtained from the author.

Mark A. Schwartz

ACKNOWLEDGEMENTS

First, I would like to thank my mentors, Jay Hoying and Stuart Williams for their continued guidance and support. I have learned much about life and science from you during my graduate career. You are both the kind of scientist I hope to be.

I would also like to thank the other members of my committee, Scott Boitano, Scott Klewer, and Mark Riley, whose insights and counsel were much appreciated. I could not have chosen a better committee.

Thank you to the members of the Hoying lab, Kevin Greer, Gabi Gruionu, Chris Sullivan, Trevor Cardinal, Carlos Chang, Greg Dion, Shaleen Beck, and Helen Chen for your friendship and ideas. You have all made this an extraordinary experience.

Thank you also to the members of the Williams lab, especially Alice Stone whose expertise was greatly appreciated. Thank you to Sam Powis, Cindy Smith, Edward Parkin, Alton Hiscox, Faith Rice, Leigh Kleinert, and Vangie Patula for all of your help.

I would never have gotten through the Biomedical Engineering Program without the watchful eyes of Charlotte Todd, Lori Taylor, and Debbi Howard. Thanks for making sure that I was always where I needed to be.

I would like to thank my father, Leonard, and mother, Mary, for always believing in me. Your encouragement, as well as the examples you have set throughout my life have inspired me to achieve all that I possibly can. I love you guys.

Lastly, I would like to thank my wife, Lili, the best thing that has ever happened to me. Without whose love, patience, encouragement, and smile none of this would ever have been possible.

DEDICATION

To Samuel

TABLE OF CONTENTS

TABLE OF CONTENTS – *Continued*

LIST OF FIGURES

LIST OF TABLES

ABSTRACT

Implantation of biomaterials leads to the formation of an avascular, fibrotic capsule that isolates the implant from the surrounding tissue. Previous studies have demonstrated that ECM-modification of ePTFE promotes increased vascularity and decreased fibrosity in peri-implant tissue, two desired characteristics of engineered medical devices. However, little is known as to what is happening at the molecular level in tissue surrounding both ECM-modified and non-modified ePTFE during the healing process, or for that matter, what cellular pathway is responsible for the increased vascularity and improved healing response. Large-scale gene expression analysis using DNA microarrays was used to assemble gene expression patterns of peri-implant tissue. This data revealed that tissue surrounding ECM-modified ePTFE is more transcriptionally dynamic than tissue surrounding non-modified ePTFE. The microarray data also exposed a set of macrophage-relevant genes that directed investigation into how the ECM modification of ePTFE affected macrophage activation. It was demonstrated that ECM proteins secreted by the keratincocyte cell line HaCaT promoted fusion of macrophages to form multinucleated foreign body giant cells (FBGC's), as more FBGC's were seen at the material-tissue interface of the ECM modified ePTFE. The results of this work suggest a molecular mechanism through which ECM proteins induce FBGC formation. Taken together, this research advances the knowledge of material-associated healing which will lead to the improved biocompatibility of implanted medical devices.

1. POLYMER-ASSOCIATED HEALING

Introduction

The use of implanted medical devices has become so prevalent that it is difficult to track exact numbers. Current estimates place the number of devices that are implanted each year in the millions (Ratner 2002). The rationale behind the use of implanted medical devices is to either restore or enhance the desired function of biological systems. This has often focused on the use of materials that can be used to replace tissues in such areas as orthopedics (e.g. hip replacement), dentistry (root implants), and vascular surgery (vascular grafts). Materials have been used for millennia to replace lost function, as illustrated by the use of ivory by the ancient Egyptians as false teeth (Lemons et al. 1986). Until recently, materials were used solely based on availability. It was again in the field of dentistry that a significant advance in the use of materials to regain lost function occurred. In 1952, Swedish professor Per-Ingvar Brånemark discovered that it was impossible to remove his bone-anchored titanium microscopes (Branemark 1983). Not only had the bone fused to the titanium, Brånemark observed very little inflammation at the material-tissue interface, an atypical result seen when a foreign material was placed in the body.

Implantation of foreign objects, often in the form of medical devices constructed from synthetic materials, disrupts the normal healing response. Normal wound healing follows a temporal, overlapping set of events that are initiated at the site of injury. The stages of this progression are: inflammation, tissue formation, and tissue remodeling

(Clark 1996). While many of the stages of healing may be similar when a device is implanted, the amplitude and duration of each stage are altered. The last 50 years have seen a surge in research to make materials more biocompatible, that is to say, lessen the adverse reactions between the body and the implant.

Biocompatibility has been defined as "the ability of a material to perform with an appropriate host response in a specific application" (Williams 1987). As a majority of the millions of devices that are implanted each year are labeled biocompatible by the FDA, it is easy to see how the general public has come to see medical devices as biologically inert. To the contrary, biocompatibility is a continuing dynamic process (Wataha 2001). An initial favorable response to an implanted material may change to an unfavorable response due to material fatigue or wear. All materials, regardless of composition, elicit a similar response upon implantation. This effect, termed the foreign body response, results in continued low level inflammation and the eventual formation of an avascular, fibrous capsule as the body attempts to isolate itself from the implant (Ratner 2002). The formation of this capsule can pose serious consequences for implanted medical devices, especially for devices such as indwelling glucose sensors, where metabolite transport between device and tissue is critical (Wisniewski et al. 2000).

Often when a new device is being designed a considerable amount of focus, aside from what function the device will perform, is devoted to decreasing the presence of the fibrous capsule while increasing the number of blood vessels. Several approaches have been explored to improve material-associated healing including, but not limited to, modifying materials with biomolecules and manipulating the material's physical

properties (surface morphology, porosity, etc.) (Golden et al. 1990; Tassiopoulos et al. 2000; van Bilsen et al. 2004).

Material-associated healing is often assessed at the cellular level, as in the case of measuring fibrous capsule thickness, or by counting the number of macrophages in the peri-implant tissue to determine the level of inflammation (Salzmann et al. 1999). However, these cellular responses are frequently driven by changes at the molecular level, whether it be at the gene transcription level, or by secreted proteins like cytokines (Kirkpatrick et al. 2002). As the pursuit for more biocompatible devices continues, it is clear that materials must be engineered to create an appropriate tissue environment, keeping in mind the impact of both molecular and cellular function.

Biomaterials/Medical Devices

The number of biomaterials that are implanted into humans each year numbers in the millions. Biomaterials are commonly used to construct medical devices with the intent of recovering lost biological function. Implantation of these devices saves millions of lives each year, while the quality of life for millions of more recipients is significantly improved. Examples of some of the causes for biomaterial-based medical device implantation are: faulty heart valves, vascular occlusion, cataracts, and joint dysfunction (Lysaght et al. 2000). The history of the use of materials to improve quality of life dates back thousands of years. As the understanding of material properties improved over time, materials were chosen to more accurately replace the function of the damaged or diseased tissue. The biological diversity of the human body has lead to the use of various biomaterials, each possessing characteristics favorable to address a specific process.

History

Materials, natural or man-made, have been used for millennia to replace or restore function to a body tissue. The first appearance of the use of materials to replace lost tissue function was in the area of dentistry, as archaeological findings show that ancient Egyptian and South American cultures were crafting false teeth using ivory and wood (Vandgama 2003). Injury tended to be a driving force behind the use of materials, with their utilization serving both medical and aesthetic purposes. A 16th century painting of the astronomer Tycho Brahe, who lost part of his nose in a duel, depicts a metal nose

prosthesis (Bier 2000). In 1670, a xenograft of canine bone was used to repair the injured skull of a Russian peasant (Rah 2000).

Until the 20th century, materials were used in medicine based on availability, without much concern for their interactions with the body. Early surgeons were unaware of concepts like sterile technique and the biological reaction (discussed in the next section), thus the medical implants they implemented were destined to fail. The beginning of the modern era of medical implants has been attributed to an observation made by the British ophthalmologist Harold Ridley (Ratner et al. 2004). During World War II, Ridley was examining fighter pilots who had shards of canopy plastic embedded into their eyes as a result of enemy fire. Ridley noticed that the tissue surrounding the plastic, poly(methyl methacrylate), was healing normally with no sign of adverse reaction. With this knowledge, Ridley replaced a cataractous lens by implanting a lens constructed from poly(methyl methacrylate) in 1949 (Ratner et al. 2004). This was an exciting time in the world of medical devices, as other scientists were designing devices that would revolutionize the medical field. Charnley was developing an artificial hip, Vorhees the vascular graft, and Hufnagel a ball and cage heart valve (Long et al. 1998; Butany et al. 2002; Ratner et al. 2004).

Events of this era led to a discussion between scientists and engineers of multiple disciplines of what design properties medical devices should have, both in terms of materials and their biological implications. The term biomaterial is now used to classify those materials used for medical device construction. A biomaterial is defined as “a

nonviable material used in a medical device, intended to interact with biological systems" (Williams 1987).

The past 50 years has seen tremendous growth in the number of applications where medical devices are being used to treat, repair, or cure damaged or diseased tissue. Fields of study where implanted medical devices are now being used include: orthopedics, cardiovascular applications, dental applications, and wound healing (Davis et al. 2003). The medical device industry has evolved into a multi-billion dollar enterprise as the number of devices implanted into patients continues to increase (Table 1.1) (Lysaght et al. 2000). Since each tissue has unique physical properties, the types of biomaterials used to construct medical devices are often chosen to mimic the native characteristics.

Types of Biomaterials

Medical devices are now constructed using a variety of biomaterials (Table 1.2). Examples of these biomaterials are: metals, ceramics, glasses, composite materials, and polymers. Current knowledge of the mechanical properties (i.e. elasticity, hardness, fatigue, etc.) of these biomaterials has given materials scientists and biomedical engineers the ability to customize medical devices based on biological need. These materials have been used to build devices that have improved the quality of life for numerous people. Although significant advances in these devices have taken place over the past 50 years, they are far from being perfect substitutes for native tissue. This is apparent as the life-span of these devices is often limited due to inadequate interaction between the material

and host. Following is a discussion of various diseases and conditions, and examples of some biomaterials that are presently used to treat these diseses.

Osteoarthritis (OA), also known as degenerative arthritis, is the most common form of arthritis with roughly 5% of the U.S. population having OA of the hip or knee (Wendelboe et al. 2003). This condition leads to the breakdown of cartilage causing tremendous pain, especially in the hips where bone then rubs on bone. As the hip bears a great deal of load, materials with high stiffness must be used. Titanium alloys have become a prominent metal used in the field of orthopedics because of their load bearing ability and their capacity for long-term implantation (Langlais 1985). Patients receiving hip replacements can expect their new hips to last for about 15 years. This is a consequence of poor bone-to-metal bonding. The metallic hip replacement implant is about five to six times stiffer than bone. Stress shielding leads to bone atrophy as bone needs to be subjected to load to regenerate (Katti 2004). Twenty percent of hip replacement operations are done to replace the previous hip implant.

Ceramics have also been used in orthopedics, particularly total joint replacement, because of their low coefficient of friction and their bone bonding potential (Hannouche et al. 2005). Initial studies displayed an excellent tolerance of the material, and the new joint relieved the pain experienced by the patient. However, the ceramic implants were prone to fracture, again leading to replacement of the replacement (Hannouche et al. 2005).

Titanium alloys and ceramics are examples of biomaterials that are generally limited to field of orthopedics based on their physical and mechanical properties. Other

classes of biomaterials exist with properties that have the potential to be used in multiple fields and applications. Polymers are biomaterials that have been used in various applications, and whose mechanical and physical properties can be altered by manipulating their chemical structures.

Polymeric Biomaterials

The possibilities for using polymer-based medical devices are nearly endless. A polymer is a substance that has a large molar mass and is made up of repeating units called “mers”. Polymers are abundant in the natural world. For example starch and cellulose are natural polymers. Today, the synthetic polymer industry has become one of the largest manufacturing industries, with polymers having innumerable applications. As biomaterials, polymers have been used as intraocular lenses, vascular grafts, and drug delivery systems (Lloyd et al. 1999; Kannan et al. 2005; Saito et al. 2005).

Polymeric biomaterials can be classified into two groups: degradable and non-degradable. Polymers that fall into these classifications each have their strengths and weaknesses. However, the goal of utilizing both non-degradable and degradable polymers when designing a medical device is to provide a structure with suitable mechanical properties that will support new tissue.

Izhar et al. performed an experiment evaluating the effectiveness of using a degradable polymer as a vascular graft (Izhar et al. 2001). Poly(ether urethane) was filament-wound into tubular structures and implanted in to dog carotid arteries, and grafts remained patent 3 months post-implantation. The attractiveness of using this particular

type of material is that it is extremely compliant, thus displaying a pulsatile behavior similar to native vessels. Additionally, at the end of the trial, little of the original graft remained as it was replaced with cells. Limitations do exist, however, when using degradable polymers. For instance Ratcliffe explains that the mechanical properties of degradable polymers are such that they are prone to burst or rupture (Ratcliffe 2000).

Non-degradable polymers have been used to construct vascular grafts that resist bursting and rupturing while still providing necessary support and patency. One non-degradable polymer that has been used extensively for vascular grafts is expanded polytetrafluoroethylene (ePTFE) (Zdrahala 1996). Studies using tubular ePTFE as vascular grafts have shown that the 3 elements of constructing an artificial vessel as described by Kakisis are met: a structural scaffold, cells, and a nurturing environment (Kakisis et al. 2005). Kleinert et al. demonstrated that by sodding ePTFE with endothelial cells prior to implantation, extracellular matrix proteins are deposited and a neointima with cell density similar to normal arterial media is observed (Kleinert et al. 1996). As with many non-degradable polymers, ePTFE is rigid and as a result does not exhibit the pulsatile characteristics of a normal vessel. And like all polymers, degradable or non-degradable, implanted ePTFE elicits a foreign body response.

Because ePTFE is used widely for the construction of implanted biomaterials, some background of this material is presented. In 1938, Dr. Roy Plunkett, a DuPont chemist, discovered polytetrafluoroethylene (PTFE) while working with Freon® and tetrafluoroethylene (DuPont). The polymer PTFE is formed by addition polymerization of tetrafluoroethylene (CF_2=CF_2) giving rise to the chemical structure:

PTFE is hydrophobic, chemically inert, has a low coefficient of friction, and maintains physical properties over a large temperature range (-270ºC to 385ºC).

In 1969, Bill Gore discovered the ability to expand PTFE, giving rise to expanded polytetrafluoroethylene (ePTFE). The result was a material that possessed the same chemical properties of PTFE but was highly porous, making it favorable for cellular penetration. The first sale of ePTFE as a vascular graft was made in 1975 (Gore 2005). Today, ePTFE is used in applications such as vascular grafts, hernia patches, surgical sutures, and lip augmentation (Bauer et al. 1999; Hanke 2002).

Table 1.1: Medical devices and number implanted (Adapted from (Ratner 2001).

Device	Number of Implants/Year (U.S.)
Intraocular Lenses	>2,700,000
Cardiovascular Stents	1,700,000
Dental Implants	>300,000
Hip and Knee Prostheses	>300,000
Vascular Grafts	>100,000
Heart Valves	>80,000

Table 1.2: Materials used to construct various medical devices (Adapted from (Ratner 2001).

Device	Material
Intraocular Lenses	Polymers
Cardiovascular Stents	Metals
Dental Implants	Metals, Ceramics
Hip and Knee Prostheses	Metals, Ceramics
Vascular Grafts	Polymers
Heart Valves	Polymers, Metals

Host Response

The injury that results from placing a medical device within the body initiates a wound healing response. Wound healing is the body's attempt to reestablish the integrity of damaged tissue, which it does through a progression of interdependent activities. These activities involve processes that take place at the cellular, and molecular level, which sum to the overall tissue response. The interaction of these factors determines the ultimate success of the wound repair. To improve our understanding of wound healing in response to polymer-based medical implants, each of these factors; tissue response, cellular response, and molecular response must be addressed.

Tissue Response

Normal wound healing consists of temporal, overlapping functions that include: inflammation, new tissue formation, and tissue remodeling (Clark 1996) (Figure 1.1). Tissue injury initiates the repair process as platelets release a variety of cytokines and growth factors, such as platlet-derived growth factor (PDGF) and transforming growth factor-beta (TGF-β) (Martin 1997; Diegelmann et al. 2004). These proteins signal inflammatory cells to the area of injury. Within minutes of injury, neutrophils convene at the site of damaged tissue. Monocytes and lymphocytes are the next to arrive and produce proteinases to defend against microorganisms. A couple of days after the injury has taken place, monocyte-derived macrophages emerge and are involved in phagocytosis of cellular debris and release growth factors and cytokines of their own to initiate the new tissue formation stage of wound healing (Werner et al. 2003). During

this stage, keratinocytes deposit extracellular matrix and myofibroblasts form to contract the wound. Concurrently, substantial angiogenesis is taking place, giving rise to the formation of the connective tissue known as granulation tissue (Li et al. 2003). The termination of the normal wound healing process is recognized by a transition between granulation tissue and mature scar tissue marked by the synthesis of collagen by the fibroblasts.

The basic cell types and signaling molecules that are present in normal wound healing also appear during polymer-associated healing, however the levels and duration of each stages are altered (Figure 1.2). Material-associated healing is also categorized into three unique stages: acute inflammation, chronic inflammation, and the foreign body response (Anderson 1988). Upon implantation, vessel injury results in alterations in serum proteins, such as fibrinogen that can be adsorbed to the polymeric material through the Vroman effect (Vroman et al. 1980) (Figure 1.3A). Accumulation of the proteins has been termed biofouling (Wisniewski et al. 2000). The existence of this protein layer appears within a few hours and cannot be removed even with powerful detergents (Tang et al. 1995).

As is the case during the acute inflammatory stage of the normal healing pathway, neutrophils and monocytes are the first inflammatory cells to arrive at the site of injury. Because of the protein layer surrounding the biomaterial, these inflammatory cells cannot directly contact the implant. Macrophages that stem from monocytes normally direct the wound healing response by secreting cytokines that attract other cell types needed for healing (keratinocyte, fibroblast, etc.) (Ratner 2002). In the course of polymer-

associated healing, the macrophage is unable to recognize the adsorbed protein layer and spreads over the surface, adopting it's phagocytic role (Figure 1.3B).

The next step in the altered healing pathway is chronic inflammation, which is distinguished by the proliferation of macrophages and fibroblasts (Fournier et al. 2003). As implanted devices are usually too large for individual macrophages to successfully ingest, macrophages that are in close proximity will fuse forming multinuclear cells called foreign body giant cells (FBGCs). The formation of FBGCs is believed to reflect frustrated phagocytosis and is a simple attempt to protect the host (Shen et al. 2004) (Figure 1.3C). During chronic inflammation cell signaling is modulated, and cytokines that support fibroblast recruitment are up-regulated.

The final stage of polymer-associated healing is the foreign body response. Fibroblasts begin synthesizing collagen and an avascular, fibrous capsule is established to isolate the device from the host (Mikos et al. 1998) (Figure 1.3D). Microdialysis studies have been used to investigate the impact the tissue response has on the function of implanted polymer-based devices (Wisniewski et al. 2001). Wisniewski et al. implemented microdialysis probes to separate the contributions that both biofouling and the fibrous capsule have on analyte transport through the porous polymer. Their findings show that the tissue capsule is the predominate barrier to analyte transport. Fibrous tissue encapsulation is also to blame for the failure of glaucoma shunt devices to effectively drain fluid and relieve intraocular pressure (Boswell et al. 1999). These studies suggest that the formation of the collagenous, fibrous, avascular tissue is the primary source of device failure.

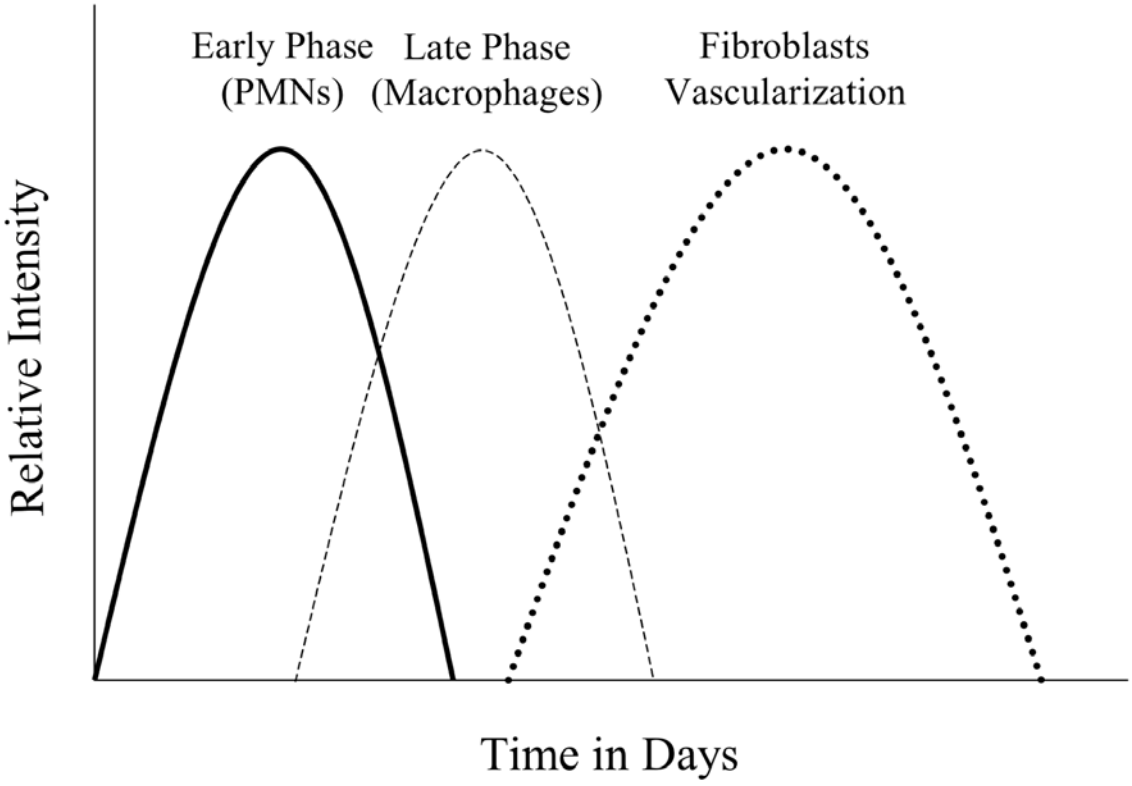

Figure 1.1 Normal wound healing begins with an early phase of inflammation, characterized by the initial presence of polymorphonuclear leukocytes (PMNs). This step is followed by late phase inflammation and the infiltration of macrophages. Inflammation is resolved by an increase in fibroblasts and vascularization (Adapted from Clark, 1996).

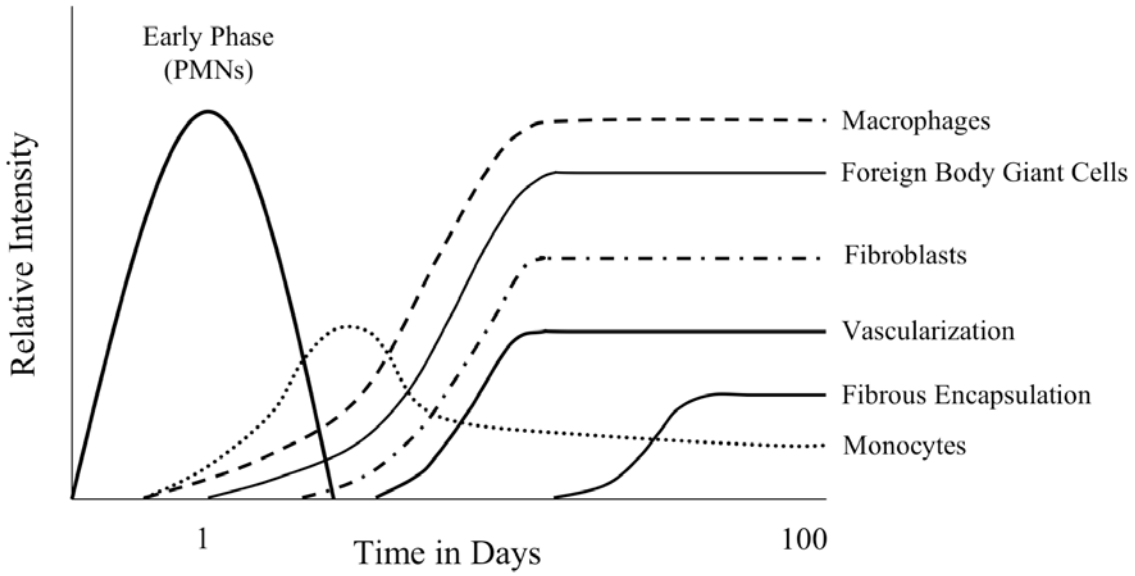

Figure 1.2 The presence of biomedical implants alters the normal healing response, and leads to chronic inflammation and the formation of a fibrous capsule (Adapted from Anderson, 1988).

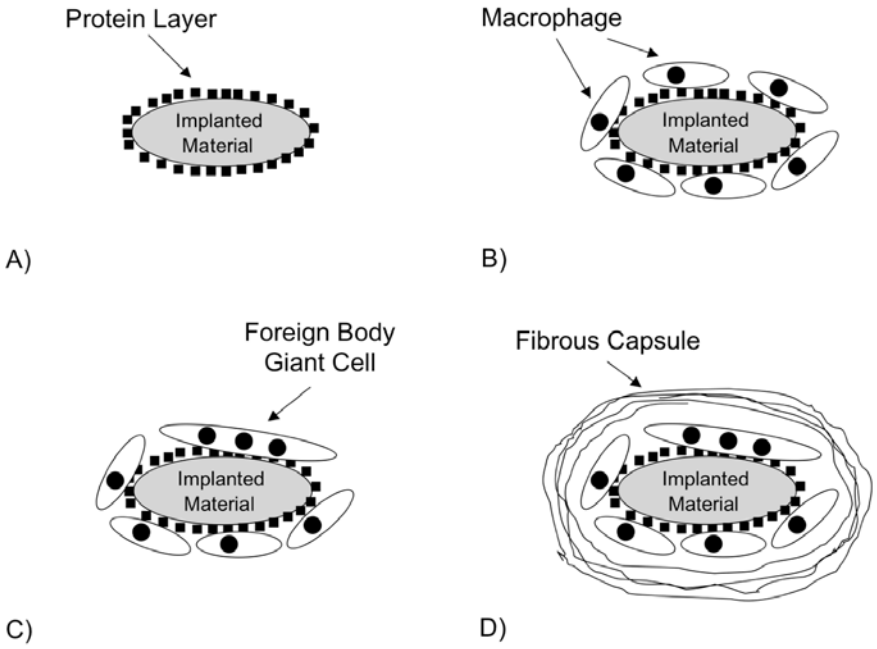

Figure 1.3 Graphic representation of the foreign body response. A) Adsorption of proteins; B) Attachment of macrophages; C) Fusion of macrophages to form foreign body giant cells; D) Synthesis of collagen forming the avascular, fibrous capsule.

Cellular Response

As part of the immune response, helper T cells secrete cytokines that assist in nearly all aspects of the immune response (Sherwood 1997). Helper T cells develop from pluripotent hemopoietic stem cells of bone marrow, and are further processed in the thymus. The helper T cells that leave the thymus are in a naïve state (Th0), and remain as such until they are activated. Antigen presenting cells (APC's) present sequences of the foreign body or bacteria to the Th0 cells, which bind to specific receptors on the Th0 cell surface, thereby activating the helper T cell. Activation of Th0 cells depends on the antigen presented to the T cell and can lead to two functionally distinct subclasses of helper T cells: Th1 and Th2 (Alberts 1994). The Th1 activation pathway leads to a cellular based immunity and directs Killer T cells and macrophages to attack abnormal cells and microorganisms, whereas the Th2 activation leads to humoral immunity, resulting in the production of antibodies that are used to neutralize foreign invaders and substances outside the cell.

These subclasses (Th1 and Th2) are distinguished by the cytokines they produce, with Th1 cells secreting interferon-γ and interleukin-2, while Th2 cells secrete interleukin-4, interleukin-5, and interleukin-13(Gordon 2003; Lu et al. 2004) (Figure 1.4). The Th1 pathway is induced by both the binding of specific antigens, as well as interleukin-12 (IL-12) that is secreted by phagocytic cells. The Th2 pathway induction is promoted by the secretion of interleukin-4 (IL-4) from mast cells and a subset of T cells (Al-Saffar et al. 1998). Binding of IL-12 to its receptor on the surface of a Th1 cell acts through the STAT4 transcription factor, causing Th1 cells to produce interferon-γ, while

the signal transduction that takes place as a result of IL-4 binding is carried out through the STAT6 transcription factor and leads to the production of more IL-4 (Kotanides et al. 1996) (Figure 1.4). T cell activation plays an important role in subsequent healing processes, especially in the activation of the macrophage.

The macrophage has been called the "orchestrator" of the wound healing response (Ratner 2002). Macrophages arise from bone marrow derived monocytes and when activated act both as the first line of defense and as accessory cells in the immune response (Sherwood 1997; Ma et al. 2003). For years, activated macrophages were identified simply as cells that secrete inflammatory cytokines and kill various pathogens (Mosser 2003). However, research of the past decade has illustrated that macrophage activation and behavior is much more diverse and is highly dependent upon the cytokines released by Th1 and Th2 activated cells, to the point that two macrophage activation states are now recognized: classical and alternative. Classical macrophage activation has been assigned to Th1 type responses where inactive macrophages are stimulated by the cytokine interferon-γ (IFN-γ) (Gordon 2003). IFN-γ activates the macrophage through the JAK1/2-STAT1 pathway (Ma et al. 2003). Classically activated macrophages appear with the presence of bacteria or other microorganisms, and secrete many pro-inflammatory cytokines such as TNF-α, IL-1, IL-6, and IL-12 (Mosser 2003). Some other processes attributed to this pathway are extracellular destruction and apoptosis in the form of NO production. The classsical activation state has been determined to be important in areas like cellular immunity, immunodeficiency disorders, and

hypersensitivity responses and tissue damage. Biological markers of classically activated macrophages have been identified as MHC class II and CD86.

The alternative activation pathway of macrophages takes place as the result of stimulation by cytokines secreted by Th2 type cells, those being predominately IL-4 and IL-13. The binding of IL-4 to its receptor appears to activate the transcription factor STAT6 (Hart et al. 1999). Alternatively activated macrophages as the result of IL-4 stimulation leads to a cell type that is phenotypically distinct from the classically activated macrophage (Gordon 2003). These macrophages have been shown to produce cytokines responsible for the synthesis of the extracellular matrix (e.g. fibronectin), suggesting they may be involved in tissue repair rather than the removal of microbial invaders (Mosser 2003). The alternatively activated macrophages also exhibit anti-inflammatory properties and are involved in the resolution of inflammation through the secretion of anti-inflammatory cytokines, for instance IL-10 (Porcheray et al. 2005). Macrophage mannose receptor has been determined to be a biological marker for alternatively activated macrophages, as its expression is increased on the surface of these macrophages with respect to classically activated macrophages.

During normal wound healing, the balance of these two macrophage activation states leads to final tissue repair, with the classically activated macrophages responsible for microbial destruction in early healing, and the alternatively activated macrophage decreasing inflammation and promoting angiogenesis (Porcheray et al. 2005). Cytokines released by both macrophage types are responsible for these processes, as well as recruiting other cell types to the wound area, such as keratinocytes, fibroblasts,

osteoblasts, etc. (Martin 1997) (Table 1.3). In response to implanted biomaterials, there is an apparent shift in the balance of Th1 and Th2, as cytokines released by macrophages in the peri-implant tissue favor a pro-inflammatory environment (Fournier et al. 2003) (Table 1.3).

It has been shown that macrophages adhered to implanted materials may undergo frustrated phagocytosis as the implant is too large for the macrophage to engulf it (Dadsetan et al. 2004). During frustrated phagocytosis, macrophages fuse to form multinucleated foreign body giant cells (FBGCs) that may consist of up to 200 nuclei (Anderson 2000). During *in vitro* studies, FBGC formation has been shown to be mediated by the Th2 production of interleukin-4 (IL-4) (McNally et al. 1995; DeFife et al. 1997). Interleukin-4 was also found to be involved in FBGC formation *in vivo* (Kao et al. 1995). There is support for the belief that FBGC formation results from alternatively activated macrophages as studies performed by McNally et al. and Stein et al. suggest that macrophage fusion takes place through the IL-4 induced up-regulation of the marker of alternatively activated macrophages, macrophage mannose receptor (MMR), as inhibition of MMR prevents the fusion of macrophages (Stein et al. 1992; McNally et al. 1996).

Foreign body giant cell formation has been implicated in implanted material cracking and degradation (Zhao et al. 1991). This undesired result was illustrated by Wiggins et al. who examined pacemaker leads that were explanted due to electrical dysfunction (Wiggins et al. 2001). The insulation of the pacemaker leads was cracked

and it was hypothesized that this damage was caused by high concentrations of hydrogen peroxide produced by inflammatory cells (Wiggins et al. 2001).

The role of FBGCs in inflammatory and wound healing responses is not well understood. Studies that aim to address the FBGC in inflammation often present conflicting results. For instance, Henandez-Pando et al. state that FBGCs produce inflammatory cytokines but also down-regulate inflammation (Hernandez-Pando et al. 2000). The Th2 production of IL-4, shown to induce FBGCs, has also been linked to the decrease in superoxide production and pro-inflammatory cytokine interleukin-1 activity (te Velde et al. 1988; Abramson et al. 1990). Mice deficient for the Th2 activation pathway die as a result of the inability to down-regulate the pro-inflammatory response of the Th1 pathway (Herbert et al. 2004). Also of interest, Th2 activated macrophages have been shown to produce the angiogenesis growth factor VEGF (Ragno et al. 2001).

From these studies, it can be suggested that the alternative activation of macrophages and formation of FBGCs is the body's attempt to attenuate the chronic inflammatory response associated with medical devices constructed with biomaterials. The negative impact of FBGC presence (i.e. material cracking and degradation) versus the positive influence (i.e. decrease in inflammation) makes it difficult to determine whether or not FBGCs are to be welcome participants of polymer associated healing when designing new implantable devices.

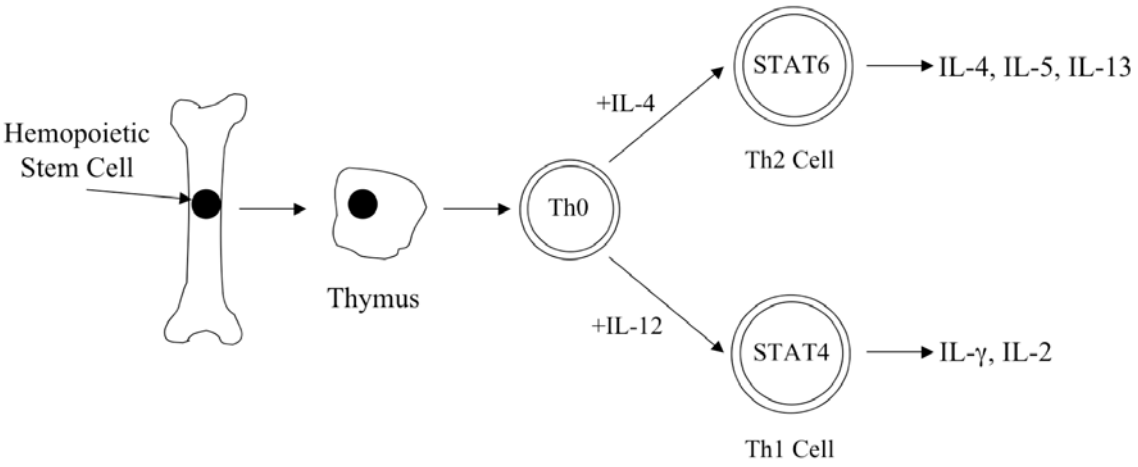

Figure 1.4 Progression of T cell maturation and activation. T cells begin as bone marrow derived stem cells and are further processed in the thymus. Cytokine signaling by IL-4 or Il-12 leads to two distinct pathways, the Th1 (bottom) and Th2 (top).

Molecular Response

Research investigating polymer associated healing has mainly focused on the cellular and tissue components of the healing response. As a result, efforts to choose implantable materials that promote desired peri-implant tissue morphology are essentially trial and error. Often, the biocompatibility of existing materials is determined by measuring the thickness of the fibrous capsule that surrounds the implanted device (Ward et al. 2002). Other methods of assessing biocompatibility rely on measuring protein adsorption and fibroblast adhesion to the implanted material (Lloyd et al. 1999). Likewise, cytokines involved in inflammatory reactions associated with implanted biomaterials are often presented, but are usually done so anecdotally with a relative lack of understanding to how or why they are expressed. These evaluations provide some measure of biocompatibility, but they reveal little about the pathways and mechanisms involved in the healing response. A comprehensive understanding of material-associated healing will necessitate the generation of molecular profiles of tissue undergoing altered healing.

Table 1.3 Macrophage secreted growth factors and cytokines

Growth Factor or Cytokine	Effect
PDGF	Chemotactic for fibroblasts; matrix production
Interleukin-1	Inflammation; elevated in polymer associated healing
Interleukin-6	Inflammation; elevated in polymer associated healing
Interleukin-8	Inflammation; elevated in polymer associated healing
TNF-α	Inflammation; elevated in polymer associated healing
VEGF	Angiogenesis

Improved Polymer-Associated Healing

The altered healing response generated upon implantation of polymer-based medical devices ultimately leads to decreased device function or complete failure. The avascular, fibrotic capsule has been implicated as the primary cause of this failure. Several groups have focused their attention and research on increasing the vascularity of the peri-implant tissue. These efforts include altering the surface of implanted polymer-based devices, either by modifying the polymer surface with biomolecules or by modifying the physical properties of the material. Expanding our understanding of the molecular components involved in the development of the avascular capsule may lead to new insights and methods of improving and enhancing the lifespan of the implanted device.

Improved Device Function by Vascularizing the Peri-Implant Tissue

Implanted medical devices fail due to being encapsulated by an avascular, fibrous capsule. Several groups have hypothesized that increasing the number of vessels in the tissue surrounding the implant will lead to improved and prolonged device function (Sharkawy et al. 1997; Cassell et al. 2002; Ratner 2002). The existence of the fibrous capsule is believed to be a barrier to diffusion of analytes such as glucose (Sharkawy et al. 1997). Promoting angiogenesis, the formation of new vessels from an existing vasculature, has been proposed as a mechanism for increasing the number of vessels in the surrounding tissue.

There have been published examples where the increase in peri-implant vessels has lead to improved device function. One such experiment was performed by Updike et al. who described a modification in the design of a glucose sensor that acts to promote angiogenesis (Updike et al. 2000). In this study, the group added a layer of ePTFE over the entire device to encourage capillary formation adjacent to the sensor. Performance of their new glucose sensor was demonstrated by day 7 and was shown to be functioning well after 5 months implantation, marked improvement over non-modified glucose sensors.

The most comprehensive study to date evaluating the diffusion barrier imposed by the formation of the avascular, fibrous capsule was performed by Sharkawy et al (Sharkawy et al. 1997). They implanted both porous materials and stainless steel cages, then peeled away the capsular tissue that formed around each. Sodium fluorescein was used as the analyte since it is similar in size to glucose. Diffusion coefficients were greater through the more vascularized tissue that formed around the porous material than the diffusion coefficients of the highly fibrous capsule surrounding the stainless steel cages. The results of this study are encouraging for the future of biomaterial-based medical devices. They suggest that engineering these devices to promote increased vessel formation in the tissue surrounding the device could greatly enhance long-term device function.

Strategies to Improve Vascularization of Peri-implant Tissue

Studies revealing improved device function resulting from increased peri-implant vasculature have inspired researchers to investigate methods of modifying implanted biomaterials to promote a vascularized capsule. Two primary classes of material modification have resulted from this effort: modification of the materials physical properties (structural modification or surface modification) and modification using biomolecules to induce angiogenesis and capillary formation. Each of these modification types has supporting evidence of peri-implant vascularization.

Many medical devices are constructed with porous biomaterials. Several studies have shown that adjusting the pore size of the material can alter the tissue response surrounding the implant. Rosengren et al., size when studying polypropylene mesh filters, determined that macrophages, angiogenesis, and fibrous capsule formation were influenced by the pore (Rosengren et al. 2003). Their results illustrated that smaller pore size (0.6 μm) inhibited inflammatory cell infiltration and lead to an avascular, fibrous capsule, whereas pore sizes of 10 and 30 μm resulted in early angiogenesis and decreased fibrous capsule. Similarly, Salzmann et al. examined the effects that pore size of ePTFE has on tissue response. This study looked at 3 pore sizes, defined as internodal distances, (30, 60, and 100 μm) and determined that the 60 μm internodal distance generated more vessels in the surrounding tissue as well as thinner fibrous capsule when compared to the other pore sizes (Salzmann et al. 1997).

Physical property modification is not limited to just changing the pore size. Boswell et al. removed the air that is trapped in the pores of ePTFE through a process

termed denucleation. They reported that at 5 weeks post-implantation there was a reduction in fibrous capsule formation, as well as an increase in vessel number in the tissue surrounding the implant (Boswell et al. 1999). Other groups have used processes such as photochemically modifying ePTFE that has been shown to increase the adhesion of endothelial cells (Gumpenberger et al. 2003).

Modification of porous materials with biomolecules has also become a major area of research for attempting to attenuate the formation of the fibrous capsule and stimulate the increase of a peri-implant vasculature. Kidd et al. demonstrated that modifying ePTFE with insoluble extracellular matrix (ECM) proteins leads to improved vascularity (Kidd et al. 2002). Cells from a tumorogenic cell line were sodded and cultured on ePTFE, during which time they deposited ECM proteins. Upon removal of the cells, ePTFE samples were implanted into rats, and after 5 weeks the tissue surrounding the material was found to contain more vessels than the tissue surrounding non-modified ePTFE (Kidd et al. 2002). As the understanding of angiogenesis and angiogenesis factors increases, groups are beginning to modify porous materials with specific proteins. The results of the Updike study that revealed increased capillary density surrounding their modified glucose sensor supported long-term glucose detection encouraged Ward et al. to determine whether or not capsule vascularity could be increased by using the potent angiogenesis factor vascular endothelial growth factor (VEGF). For this study, VEGF was infused through non-functional biosensors at the rate of 0.45 μg/day for 28 days. After the 28-day study, tissue surrounding the implant was evaluated for capillary density. It was determined that in the tissue that was 1 mm from the implantation site,

the capillary density was 200-300% higher than was the tissue surrounding saline infused biosensors. They also found that capillary density was 50-100% greater at 13 mm from the infusion site (Ward et al. 2003).

Molecular Role in Capsule Vascularization

The molecular mechanisms that prevent vascularization of the fibrotic capsule as a result of the foreign body response have not been well understood. In an experiment performed by Kyriakides et al., thrombospondin 2 (TSP2) was found to inhibit the proliferation of vessels in the fibrous capsule surrounding implanted materials (Kyriakides et al. 1999). When TSP2-null mice were given implants, the surrounding capsule was found to be highly vascularized. This is an encouraging discovery in terms of better understanding the mechanisms of the foreign body response. However, TSP2 is but one of many angiogenesis inhibitors and it is unknown what effect other inhibitors may have on the fibrous capsule. At the same time, numerous molecules exist that are pivotal to other processes of the foreign body response, e.g. collagen synthesis or inflammation.

Observed cellular and tissue responses are the result of activities that take place at the molecular level. Little is known about the molecular events that occur at the interface between host tissue and implanted material (Brauker 2001). Improved understanding of polymer associated healing will be gained when more emphasis is given to the molecular behavior in response to implanted materials.

Genomics

Our understanding of the molecular underpinnings responsible for the observed phenotype associated with implanted biomaterials will improve with the ability to measure changes in gene expression. Functional genomics is defined as the analysis of gene expression of a cell, tissue or organ under given conditions (Joos et al. 2003). Utilization of functional genomic tools allows the investigator to explore molecular behavior and interactions of a variety of biological processes (Fraser et al. 2004). The successful sequencing of the human genome in 2001, as well as the sequencing of the genomes of other species, has had an incredible impact on the field of functional genomics (Venter et al. 2001).

Functional genomics tools have been used to integrate gene expression datasets that contain large amounts of data. Integration of datasets usually requires that genes be clustered based on similar gene expression patterns over time (Eisen et al. 1998). Clustering genes based on expression pattern allows the investigator to more easily identify those genes that behave similarly and assign function to unknown genes based on the assumption that genes that cluster together share biological function (Marcotte et al. 1999).

For the studies of this dissertation, gene expression was primarily measured using microarrays constructed with mouse DNA libraries. Use of microarrays enable massive parallel analysis through hybridization-based expression monitoring (Schena et al. 1998). Microarrays are ideally suited for comparing gene expression of multiple samples, and

are attractive assays in the characterization, prognosis, and diagnosis of many tissue states.

The genomics approach used in this dissertation is similar to those studies that compared the genetic profiles of numerous cancer samples that did not present with obvious differences in tissue morphology, but each responded uniquely to the same treatment protocol (Alizadeh et al. 2001; Warner et al. 2004). By comparing the gene expression patterns of multiple samples that display similar tissue phenotypes, one can begin to pare down the number of genes that are responsible for similarities in observed tissue morphologies.

As will be discussed in more detail in subsequent chapters, studies performed for this dissertation analyzed the gene expression patterns for two modifications of ePTFE that have been shown to promote a more desirable material-associated healing response. The rationale for using a genomics approach is that it is unclear as to what genes are required for this improved healing response. Genes in tissue surrounding both ePTFE modifications were compared to identify those genes that were expressed in both treatment groups. This is a subtractive technique, as only those genes that were expressed in both modification groups were further analyzed, while the genes that were unique to each modification group were ignored. By doing this, a selection of genes was established that was more manageable to perform additional analysis. From this list, genes that shared expression patterns across time were the first to be examined, with the assumption that those genes were most significant in material-associated healing. Results using this method are detailed in Chapter 4.

Significance and Research Plan

Implantation of biomedical devices that are constructed from synthetic materials continues to rise. Presently, biomedical devices are packaged and shipped to hospitals while being labeled as "biocompatible". The current accepted definition of biocompatibility is "the ability of a material to perform with an appropriate host response in a specific application" (D.F. Williams, 1987). In reality, nearly all implanted materials illicit the foreign body response that leads to the formation of an avascular, fibrotic capsule; this is the body's attempt to isolate itself from the implanted material. As a result of this abnormal healing response, the long-term function of these devices are often severely compromised. Several strategies have been proposed to alter the abnormal healing response that is activated upon biomedical device implantation. Previous studies have shown that expanded polytetrafluoroethylene (ePTFE) that has been modified with extracellular matrix molecules and implanted subcutaneously leads to more vascular units surrounding the material. Additionally, the tissue that is in direct contact with the modified ePTFE is less dense and less fibrous when compared to non-modified ePTFE. These observations have led me to further investigate material-associated healing, with the goal being an improved understanding of biocompatibility through the following specific aims:

Specific Aim 1. Measure gene expression by cDNA microarray of tissue surrounding subcutaneously implanted ePTFE that is either non-modified or modified with extracellular matrix proteins. Previous studies from our laboratory

have shown at the cellular and tissue level that ePTFE that has been modified with conditioned media containing extracellular matrix proteins secreted by HaCaT cells leads to a phenotype of increased vascularity and a decrease in fibrous capsule formation in tissue surrounding the ePTFE, little is known of mechanism at the molecular level. To study the molecular component of ePTFE-associated healing, DNA microarrays have been implemented. We have constructed microarrays that consist of mouse DNA libraries. RNA from tissue surrounding ECM protein modified and non-modified at each timepoint (days 5, 7, 14, and 35) was isolated and amplified. This tissue was used to generate gene expression data for both modification groups.

Specific Aim 2. Measure gene expression by cDNA microarray of tissue surrounding subcutaneaously implanted ePTFE that is either non-modified or modified with purified laminin 5. Western blot analysis has verified that HaCaT conditioned media is laminin 5 enriched. Laminin 5 is a basement membrane protein that is synthesized by keratinocytes and is produced as a heterotrimer ($\alpha 3\beta 3\gamma 2$). Laminin 5 is present in this heterotrimer form in the HaCaT conditioned media (HCM). As laminin 5 is a predominate protein in the HCM, I hypothesize that laminin 5 is responsible for the observed altered tissue response. The methods to conduct the gene expression analysis for this aim were essentially the same as that of aim 1 except for the use of another ECM protein modification. Laminin 5 was purified from HCM using HPLC. Expanded ePTFE was either modified with purified laminin 5 or non-modified. Microarray data was analyzed and compared to results of the first aim.

Specific Aim 3. Use expression data from HCM and Ln-5 modified ePTFE to identify a molecular pathway responsible for the observed improvement of polymer-associated healing. As tissue responses are the result of molecular activities and regulation, it follows that similar tissue morphology is the result of shared molecular regulation. The hypothesis for this aim was that the comparison of gene expression of tissue surrounding both HCM and Ln-5 modified ePTFE will lead to a mechanism or pathway that is involved in the altered healing response. Knowledge of a specific mechanism or molecular pathway responsible for the observed altered healing response will advance understanding and improvement of implanted medical device biocompatibility.

2. GENE EXPRESSION IN TISSUE ASSOCIATED WITH EXTRACELLULAR MATRIX MODIFIED ePTFE

Introduction

The frequency that biomedical devices are implanted into the body, as well as the number of applications where biomaterials are being used continues to rise. Implanted materials commonly fail due to an abnormal healing mechanism and the foreign body response (Anderson 1988). Microdialysis studies have shown that the altered tissue morphology surrounding the implant is responsible for the device failure (Wisniewski et al. 2001). As a result, several approaches to improve synthetic material-associated healing are being explored, including modifying materials with biomolecules (Tassiopoulos et al. 2000; van Bilsen et al. 2004) and manipulating the material's physical properties (surface morphology, porosity, etc.) (Golden et al. 1990). One proposed suggestion for improved material-host compatibility is to promote increased nutrient movement within the implant by vascularizing the material (Cassell et al. 2002). We have established methods to modify expanded polytetrafluoroethylene (ePTFE) with pro-vascular extracellular matrix proteins in an attempt to promote increased vascularity around and within the porous material. Matrix proteins secreted by a cell line shown to elicit an angiogenic response were deposited into the interstices of the porous ePTFE prior to implantation (Kidd et al. 2002; Kidd et al. 2003). The tissue surrounding the modified implant was less fibrous and highly vascularized when compared to bare, non-

modified ePTFE. Current views of improved biocompatibility suggest this modification would lead to improved device longevity and efficiency (Ganta et al. 2003).

While the tissue response to ePTFE is well characterized at the morphology level, little is known as to what is happening at the molecular level during this process. By using cDNA microarray technology, we aimed to characterize the increased vascularity, at the molecular level, in the tissue surrounding extracellular-modified and non-modified ePTFE.

Materials and Methods

Modification of ePTFE

Cells from the spontaneously immortalized keratinocyte cell line, HaCaT, were grown to 70% confluency in 175cm^2 flasks and then fed serum free DMEM (20ml per flask) for 48hours. The serum free, HaCaT conditioned medium (HCM) was collected and centrifuged to remove cell debris. Tubular ePTFE (C. R. Bard, Inc., Tempe, AZ) with an inner diameter of 4-mm was used either non-modified (controls), or HCM modified. Prior to HCM modification, ePTFE was denucleated by soaking in a graded ethanol series (Boswell et al. 1999). HCM modification of ePTFE was performed as described by previously (Kidd et al. 2005). Briefly, the ePTFE was coated with HCM by capping the distal end of the denucleated graft and placing it into a bioreactor filled with 55ml HCM that was re-circulated through the bioreactor assembly at a rate of 15ml/min for 1 hour, thereby coating both surfaces and the interstices of the material.

In vivo Study Design

NIH guidelines for the care and use of laboratory animals (NIH Publication #85-23 Rev. 1985) have been observed. The tubular ePTFE, modified or non-modified, was cut into 2 cm length sections, then segmented longitudinally and implanted into adult male mice (129-SVJ; 18-22 g). Each mouse was anesthetized with 2.5% Avertin (0.1 mL/10 g), and four small incisions were made to create two subcutaneous tunnels extending from haunch to shoulder. One strip of polymer was inserted into each tunnel

and closed with 7.5mm wound clips. At four timepoints, the ePTFE and associated tissue was removed, cut into strips, and immersed in RNA*later* solution (Ambion, Austin, TX).

Microarray Manufacture

NaOH-cleaned microscope slides (75mm x 25mm) were coated by submersion in a 2% 3-Aminopropyltrimethoxysilane solution for 10 minutes. Slides were then rinsed twice in 95% EtOH for 5 minutes each before a final 5 minute rinse in 100% EtOH. A mouse cDNA library from the National Institute on Aging (http://lgsun.grc.nia.nih.gov) containing approximately 15,000 unique cDNA clones was printed in duplicate using a VersArray ChipWriter (Bio-Rad, Hercules, CA).

RNA Isolation

To isolate RNA from ePTFE-associated tissue, explants were removed from RNA*later* and immediately frozen in liquid nitrogen. Sections were ground to a fine powder using a mortar and pestle. Ground samples were transferred to a pre-weighed 6 ml round bottom tube and RNA Bee isolation reagent (Tel-Test, Inc., Friendswood, TX) was added at 2 mL per 100 μg of tissue. Samples were placed on ice and homogenized using a Tissue Tearor (Biospec Products, Inc., Bartlesville, OK) at maximum setting for 1 minute. The homogenate was transferred to Phase Lock Gel tubes (Eppendorf, Westbury, NY) and centrifuged at 14,000 rpm for 15 minutes at 4°C. RNA was isolated from the aqueous layer following the provided protocol.

RNA Amplification

RNA was amplified using the MessageAmp™ aRNA kit (Ambion, Austin, TX) that is based on a linear amplification protocol(Van Gelder et al. 1990). During the cDNA purification step, Ambion's clean-up columns were replaced with MinElute™ PCR purification columns (Qiagen, Valencia, CA) that permit the elution of cDNA in as little as 9 μl of nuclease-free H_2O, eliminating the need for further concentration. This amplification protocol generates a linear 1000-2000 fold increase in aRNA from mRNA contained within the starting material.

cDNA Labeling

Quantity and quality of RNA was determined by spectrophotometry. RNA was used at a concentration ≥ 2 μg/μL and a 260/280 ratio ≥ 1.6. Reverse transcription reactions were performed using EndoFree RT (Ambion) during which amino allyl dUTPs (2 mM) and dNTP's (10 mM dATP, dGTP, dCTP, and 3 mM dTTP) were incorporated. RNA was primed using random hexamers (http://www.idtdna.com). To increase signal, reactions were run for 2 hours at 42°C, contrary to the 48°C recommended for the RT enzyme. After 2 hours, samples were denatured at 95°C for 5 minutes and immediately transferred to ice. Base hydrolysis of remaining RNA was performed by addition of 8.6 μL of 1M NaOH and 8.6 μL of 0.5M EDTA, pH 8.0, and incubated at 65°C for 15 minutes. The solution was neutralized by adding 8.6 μL of 1M HCl.

Hybridization of cDNA

After cDNA purification, samples were dried to 1-2 μL by vacuum centrifugation. Samples were then resuspended in 3 μL of Sodium bicarbonate ($NaHCO_3$)(25 mg/mL) and 5 μL of Alexa 546 or 647 (Molecular Probes, Eugene, OR) and placed in the dark for 1 hour. The solutions were pooled and purified as described above, the only exception being that one extra wash with 75% EtOH was administered.

An equal volume of 2X hybridization buffer (8X SSC, 60% Formamide, 0.2% SDS), 10 μg of Cot-1 DNA, and 10 μg of poly dA were added to the pooled cDNA. This solution was hybridized overnight to a microarray slide using a GeneTac hybridization station (Genomic Solutions, Inc., Ann Arbor, MI) at 47°C. Hybridized arrays were washed twice with 1X SSC, 0.1% SDS and 0.1X SSC, 0.01% SDS while in the GeneTac hybridization station (Genomic Solutions, Inc., Ann Arbor, MI) and rinsed in 0.1X SSC before being dried.

Scanning of Array

Hybridized slides were scanned using an epifluorescence/CCD based scanner (ArrayWoRx^{e}™, Applied Precision, Issaquah, WA). Random areas of the slide were examined to determine proper exposure for each channel prior to scanning the data. Using bundled spot finding analysis software (MolecularWare, Irvine, CA), signal intensities for each spot were determined and analyzed using an in-house, ANOVA-based custom analysis package called CARMA.

Quantitative PCR

To verify gene expression from the microarray data, quantitative real-time PCR was used. Primers were designed using the Primer3 program (http://frodo.wi.mit.edu/cgi-bin/primer3/primer3.cgi), and were designed to be within approximately 300 bp from the 3' end of the gene, and generated products of approximately 100-200 bp in length. All primers were ordered from Integrated DNA Technologies. Three micrograms of amplified RNA was reverse transcribed with random hexamers using the Ambion Endofree RT kit. Two microliters of cDNA was run in duplicate for each sample. The total reaction volumes for each tube was 10 μL and included 0.4 μL 25 mM $MgCl_2$, 0.25 μL 1X Sybr Green, 0.35 μL RNase free water, 2 μL forward and reverse primers and 5 μL of Sybr Green master mix from Qiagen's Quantitect Sybr Green PCR Kit. The reactions were detected by the Rotor-Gene RG-3000 (Corbett Research, Sydney, Australia) in a 72-well rotor. The reactions were denatured at 95ºC for 15 minutes, followed by 45 cycles of 15 seconds at 95ºC, 15 seconds at 58ºC, and 20 seconds at 72ºC.

Results

At 4 timepoints (days 5, 7, 14, and 35), ePTFE implants were removed retaining tightly associated tissue. These timepoints were chosen based upon relevant physiological events, those being: acute inflammation, angiogenesis, vascular maturity, and tissue remodeling. The amount of tissue associated with ePTFE increased with time (data not shown). Though associated tissue consists of cells both surrounding the implant and within the pores of the ePTFE, the majority of tissue was outside the implant. A small section of each implant from both treatment groups was stained with hematoxylin and eosin to visualize gross tissue morphology (Figure 2.1). Consistent with a previous study (Kidd et al. 2005), tissue surrounding HCM-modified ePTFE implanted for 35 days was less dense than tissue surrounding non-modified ePTFE. It was also observed that more cells were present within the pores of the material. These cells were identified as primarily vascular cells by GS-1 staining (Kidd et al. 2005).

All samples were hybridized to a microarray consisting of approximately 15,000 unique clones. For this microarray experiment, 16 hybridizations were performed with each sample being independently hybridized 4 times according to the hybridization scheme displayed in Figure 2.2. Following data analysis by ANOVA (Kerr et al. 2000), 3590 of the 15,000 unique clones on the array were measured as expressed. Of these 3590 genes, 789 were determined to undergo significant differential expression ($p < 0.05$) during at least one time-point in the study regardless of modification or between treatments. The expression data was mean-centered, unit-normalized, and clustered based on similar patterns of expression across the time-course for both treatments. This

clustering method generated 14 unique clusters of expression (Figure 2.3), which were further condensed to seven general super-patterns based on the observed similarity of expression (Figure 2.4).

The clustered data revealed that there are fewer unique patterns of expression in the non-modified ePTFE group when compared to HCM-modified ePTFE. In fact, of the 14 clusters in Figure 3, there are only 3 general expression patterns unique to tissue surrounding the non-modified ePTFE (panel B, Figure 2.5). In contrast, a unique pattern of expression existed for 6 of the clusters that was associated with the HCM-modified ePTFE (panel A, Figure 2.5). Clusters 6 and 13 (Figure 2.3) show that the expression patterns of both treatment groups was essentially the same.

Because much of the gene expression data observed in the 14 clusters overlapped, those that displayed the most similarity in expression over time were condensed further to obtain the 7 super-patterns of expression seen in Figure 2.4. For instance, clusters 1, 2, and 3 were combined to generate super-pattern 1 (Figure 2.4). An example of a gene assigned to this super-pattern is the glycolytic enzyme α-enolase, which catalyzes a high-energy intermediate necessary for the generation of ATP during glycolysis (Subramanian et al. 2000; Saulot et al. 2002). The genes of super-pattern 1 were progressively down-regulated in the non-modified group, while the same genes in the HCM-modified group were slightly down-regulated at day 7 when compared to the non-modified group. The same genes were then significantly up-regulated at day 35 in the HCM-modified group when in comparison to the non-modified group. Super-pattern 2 was formed by combining the data from clusters 4, 5, and 6. Little change was observed in gene

expression over time between the two treatments leading to the belief that their expression is independent of polymer modification. One gene present in this super-pattern is tropomyosin 2, which acts to regulate actin-myosin interactions as well as stabilize actin filament structure (Lehman et al. 2000). Clusters 7 and 8 were sufficiently unique and became super-patterns 3 and 4, respectively. Again, the gene expression in the non-modified group was down over time in both of these super-patterns, however the genes of the HCM-modified group of super-pattern 3 was down-regulated at day 14 and was significantly up-regulated at day 35. Cyclin c is a gene that is contained in super-pattern 3 and is involved in the G1/S transition of the cell cycle (Naldini et al. 1999). Genes of the HCM-modified group in super-pattern 4 underwent up-regulation at day 5 when compared to the non-modified sample. The expression of these genes was then down-regulated at day 14 comparatively. Super-pattern 4 contains numerous hemoglobin related genes. Super-pattern 5 is comprised of clusters 10, 11, and 12 and whose non-modified group is up-regulated at days 14 and 35. The HCM-modified group of genes in super-pattern 5 are up-regulated by day 7 before being down-regulated at later timepoints. Super-pattern 6 is comprised solely of those genes grouped in cluster 9. The only difference separating expression patterns of the two treatment groups is that the HCM-modified group is up-regulated at day 7. A gene of interest found within this super-pattern is PECAM. Expression of PECAM is limited to vascular endothelial cells (Ilan et al. 2003). As a result, it is often used as an endothelial cell marker. Finally, the mean expression data of clusters 13 and 14 were pooled to give super-pattern 7. Like super-pattern 2, super-pattern 7 displayed little difference in expression between both

treatments. However, instead of a progressive down-regulation, the genes of super-pattern 7 tended to be progressively up-regulated. The gene for the matricellular protein SPARC is located within super-pattern 7. SPARC has been shown to be involved in the foreign body response upon implantation of biomaterials (Kyriakides et al. 2003).

Paired t-tests were used to directly compare the mean expression data of both treatments at each timepoint. A statistical difference ($p<0.001$) at day 5 was observed only in super-pattern 4, whereas a difference was calculated at day 7 in super-patterns 1, 5, and 6. Genes in super-patterns 3, 4, and 5 were differentially expressed with respect to treatment at day 14, while super-patterns 1, 3, and 5 contained genes that were differentially expressed at day 35. Based on the statistical data, genes of super-pattern 5 were most responsive to ePTFE modification as three timepoints were found to be significantly different (days 7, 14, and 35).

Of the 789 genes measured as significantly expressed, there were 279 genes that were characterized and had known gene function (Tables 2.2-2.10). Several genes were printed on the array more than once. The remainder of the genes were either expressed sequence tags (EST's) or clones with unknown function. Four gene function classifications were used to categorize the 279 genes. General cell activity (including cell signaling, cytoskeleton, etc.), inflammation/immunity, matrix associated genes, and proliferation were chosen as the functional classes. Table 2.1 shows how these genes were organized into the four categories. Relative expression of the HCM-modified ePTFE group with respect to the non-modified ePTFE group was signified as up- or down-regulated at days 7 and 35. Column 5 of Table 2.1 lists the cluster numbers that

contain at least one gene of the corresponding functional category. Since each functional category contained genes for many different genes from different clusters, the predominate expression pattern was used to signify the up- or down-regulation at the 2 timepoints. The abundance of clusters assigned to each functional class illustrates the fact that the expression is complex and no one functional class can be assigned to just one cluster.

Quantitative real-time PCR was performed to verify the microarray results. Figure 2.6 displays the expression patterns generated through microarray analysis and quantitative PCR for PECAM and α-Enolase. Both techniques agreed with the general pattern of expression seen in each treatment group for both genes.

Discussion

Previous studies within our laboratory have established a method for coating a porous material (ePTFE) with extracellular matrix molecules from an immortalized human keratinocyte cell line (HaCaT). It was observed that this coating process caused an increase in vessel-specific cells surrounding the ePTFE and within the pores of the ePTFE as well as a change in tissue phenotype (Kidd et al. 2002; Kidd et al. 2004). The aim of the current study was to use gene expression data to describe the increased vascularity and altered tissue morphology. A microarray consisting of 15,000 mouse cDNA's was implemented to measure the relative gene expression in tissue associated with both HCM-modified ePTFE and non-modified ePTFE over 5 weeks of time. Using an ANOVA model, the gene expression data was analyzed and organized into discrete patterns of expression to identify both amplitude and temporal differences in transcript steady-state levels either within a treatment or between treatments.

The clustering data revealed variation in gene expression data between the non-modified and HCM-modified ePTFE. As is displayed in Figure 2.5, there are 6 unique temporal expression patterns related to the HCM-modified ePTFE, while there are only 3 patterns unique to the non-modified ePTFE group. These results suggest that the cells of the tissue surrounding the non-modified ePTFE are less dynamic with respect to transcription activity. A collagen-rich fibrous capsule eventually surrounds the non-modified ePTFE. This fibrous capsule is known to decrease the function of implantable devices by reducing material-tissue interactions and has limited ability to remodel and adapt to the local environment (Sharkawy et al. 1997).

The experimental design of this study differs from other microarray studies. Historically, results from microarray studies have been reported as an up or down regulation in gene expression of one treatment group in relation to another at only one timepoint. From our data, it can be observed that one timepoint is not sufficient to describe the transcriptional behavior throughout the course of the study. If we were to limit our study to day 35 for instance, our interpretation of the data would be considerably different and would omit significant differences in gene expression at earlier timepoints. An example of this can be seen in cluster 8. At day 35 of this cluster, there is no significant difference in gene expression between treatment groups. However, the genes of the HCM-modified group are significantly up-regulated at day 5 and down-regulated at day 14 when compared to the non-modified group.

The temporal nature of this study over a 5-week timecourse allows for a more reliable description of gene expression because of the ability to follow trends across time. To illustrate, Table 2.1 displays that the majority of inflammation-related genes have been segregated into clusters 1 and 2, where the genes of the HCM-modified tissue group are down-regulated at day 7 as compared to the non-modified group, before being up-regulated at day 35. However, there is one gene in the inflammation category, Nuclear Factor of Activated T-cells, whose gene expression pattern falls within cluster 7. This cluster is similar to clusters 1 and 2 in that the genes associated with the HCM-modified group are up-regulated at day 35, but the gene expression is down-regulated at day 14 as opposed to day 7 in clusters 1 and 2. This example suggests that temporal analysis is

discriminatory and is able to differentiate between genes that share a similar function but may be involved in distinct pathways.

The clustered data also suggests that the healing response has yet to reach steady state, as the gene expression appears to still be undergoing significant regulation at day 35. Previous studies examining the response to implanted ePTFE had an endpoint at day 35, but it may be necessary to extend the length of the study to ensure that the healing response and related gene expression has reached steady state (Kidd et al. 2002). It is possible, however, that the system may never reach steady-state due to a chronic healing response and constant remodeling of the surrounding tissue and presence of inflammatory cells (Hagerty et al. 2000).

Several approaches have been suggested to improve synthetic material-related healing. They include modifying the materials with biomolecules as well as manipulating the physical properties of the material (Tassiopoulos et al. 2000; van Bilsen et al. 2004). Two criteria have been hypothesized to improve the biocompatibility of synthetic devices: increasing peri- and intra-implant vascularity, and reduction of fibrous capsule formation (Sharkawy et al. 1997; Updike et al. 2000; Ratner 2002). Wisniewski et al. have argued that modulating the tissue response is critical for long-term functionality of implanted porous devices such as glucose sensors (Wisniewski et al. 2001). Our HaCaT-conditioned media modification of ePTFE has been histologically shown to alter the healing response in the surrounding tissue by increasing vascularity and decreasing the presence of a fibrous capsule (Kidd et al. 2005). In essence, this modification attempts to recreate the dynamic tissue phenotype normally present during

normal wound healing that progresses through inflammation, tissue formation, and tissue remodeling.

The goal of this study was to use microarray technology to characterize and segregate genes involved in processes such as general cell activity, inflammation, matrix regulation, and cell proliferation into distinct expression patterns. It was hypothesized that by doing this, patterns would be generated that would correspond to specific processes and could be used to assess the current state of the surrounding tissue. For instance, it would be expected that the early occurrence of angiogenesis would lead to a cluster containing angiogenesis-related genes that would display up-regulation of expression at early timepoints before being down-regulated at the end of the timecourse. This data could then be used as a diagnostic to measure the ability of a specific material modification to promote increased vascularity. The results indicate that the system is much more complex, and no one process can be assigned to one exclusive pattern. For example, those genes that are involved in general cell activity such as transcription factors and energy metabolism are present within all clusters. The majority of inflammation genes are present in several clusters that share a similar expression pattern, but there are also 5 inflammatory genes on the array that display unique gene expression and are contained in different clusters. These genes are cyclophilin, lymphocyte antigen 6 complex, lipocalin 2, nuclear factor of activated T-cells, and SPARC-like 1. Because of the complexity in gene transcription, molecular pathways to describe the observed increase in vascularity in tissue surrounding HCM-modified ePTFE were not obvious based on the clustered expression data. What can be concluded from this data is that the

tissue surrounding the HaCaT conditioned media-modified ePTFE is more dynamic in terms of transcriptional activity than that of the tissue surrounding the non-modified ePTFE. This is evidenced by the formation of 6 distinct expression patterns for the HCM-modified group and only 3 patterns generated by the non-modified group.

Another conclusion is that all of the clusters taken together are essentially a "genetic fingerprint" that can be assigned to tissue healing in response to a specific material or material modification. The gene expression fingerprinting or profiling permits for the creation of a database that links the morphologic data to the expression data of a specific material and/or material modification. When used in conjunction with pattern recognition/comparison software, this database will act as a diagnostic tool to assess the tissue response of biopsies at various times after biomedical device implantation. It will also aid in improving biocompatibility and material modification by expanding upon known tissue-material interactions and corresponding gene expression profiles.

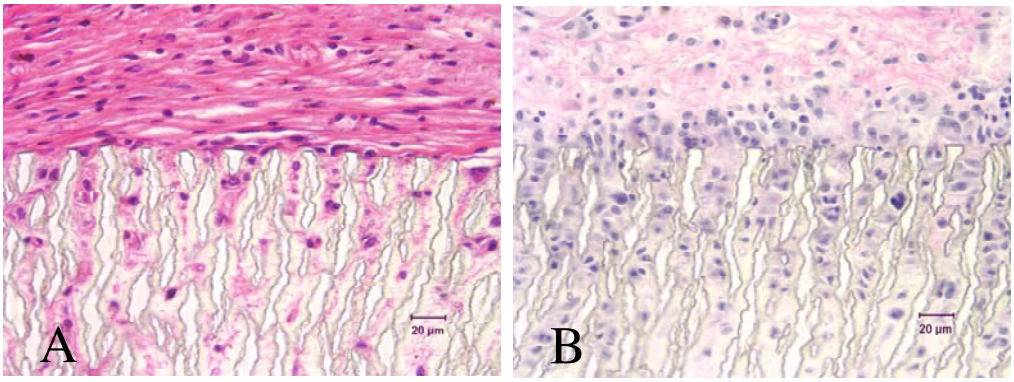

Figure 2.1 Light micrographs of sections stained with hematoxylin and eosin. Tissue surrounding non-modified ePTFE (A) is more dense compared to HCM modified ePTFE (B). There is also increased density of cells within the pores of the HCM modified ePTFE.

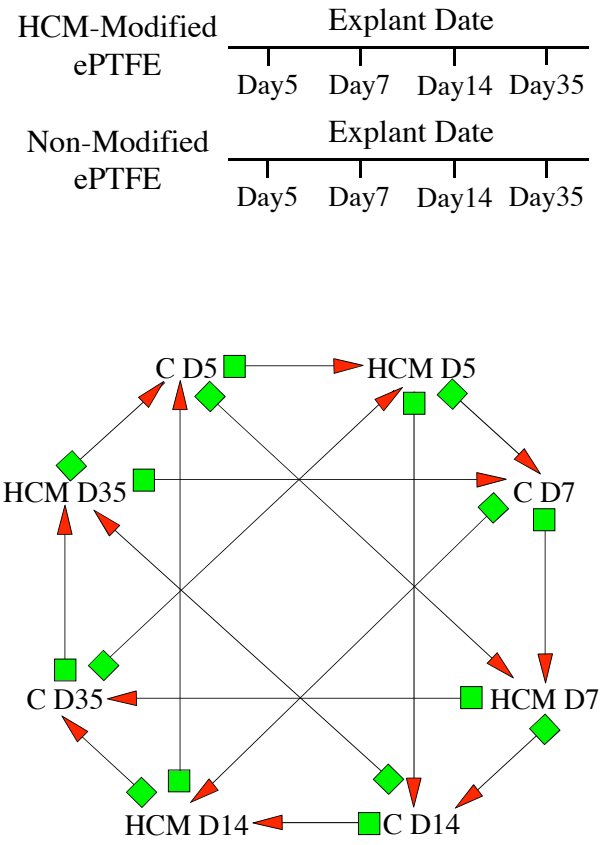

Figure 2.2 Diagram of the experimental design and hybridization scheme. Time course of the experiments and the specific days at which samples were explanted for microarray analysis (above). Below is the hybridization scheme used to perform the hybridizations for the ANOVA analysis. One hybridization (arrow) consists of two samples labeled with two dyes. In the hyb scheme, the sample shown at the box end of the arrow was labeled with Alexa 546 and combined with the sample at the head of the arrow that was labeled with Alexa 647.

Figure 2.3 The fourteen clusters of genes expressed during polymer-associated healing. Genes that undergo similar patterns of expression were grouped by hierarchical clustering. Values are the mean (± SEM) of all relative expression for all genes in the cluster at each time point. * significantly different at the $p < 0.05$ level by unpaired Student t-test.

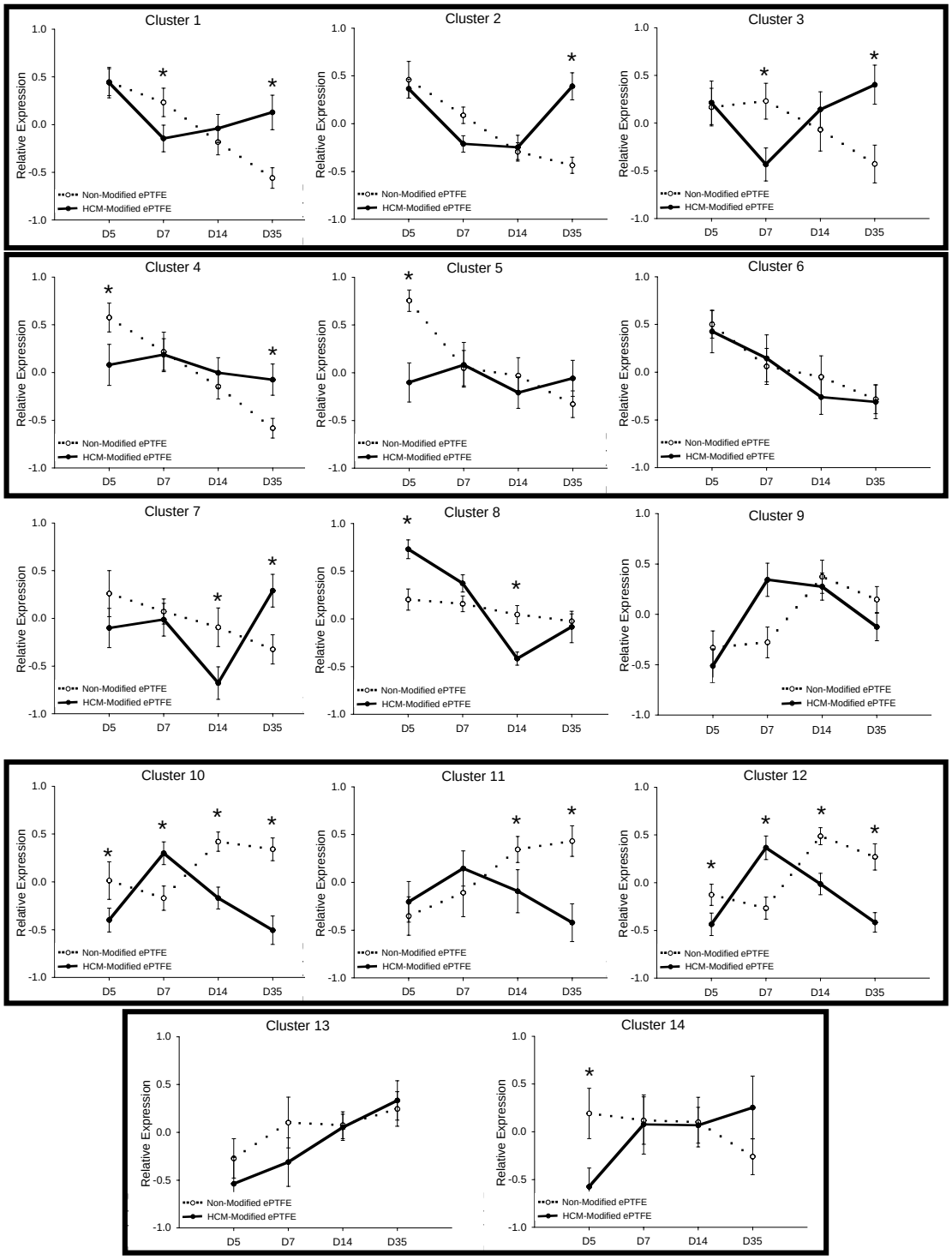
Cluster 1
Cluster 2
Cluster 3
Cluster 4
Cluster 5
Cluster 6
Cluster 7
Cluster 8
Cluster 9
Cluster 10
Cluster 11
Cluster 12
Cluster 13
Cluster 14
Relative Expression
1.0
0.5
0.0
-0.5
-1.0
D5
D7
D14
D35
Non-Modified ePTFE
HCM-Modified ePTFE
*

Figure 2.4 Seven super-patterns of gene expression following the combining of mean expression data of similar clusters (contained within boxes) from figure 3. Values are the mean (± SEM) of all relative expression for all genes in the cluster at each time point. * Significantly different at the $p < 0.05$ level by unpaired Student t-test.

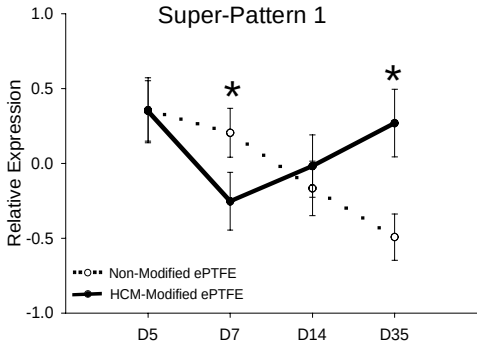
Super-Pattern 1
Relative Expression
1.0
0.5
0.0
-0.5
-1.0
*
*
Non-Modified ePTFE
HCM-Modified ePTFE
D5
D7
D14
D35

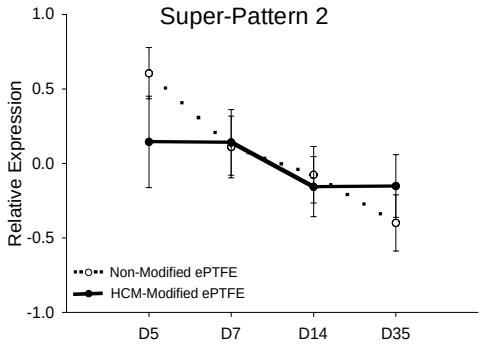
Super-Pattern 2
Relative Expression
1.0
0.5
0.0
-0.5
-1.0
Non-Modified ePTFE
HCM-Modified ePTFE
D5
D7
D14
D35

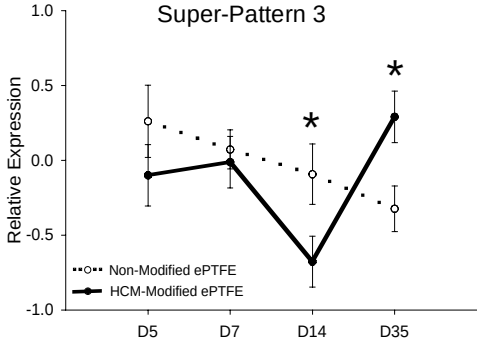
Super-Pattern 3
Relative Expression
1.0
0.5
0.0
-0.5
-1.0
*
*
Non-Modified ePTFE
HCM-Modified ePTFE
D5
D7
D14
D35

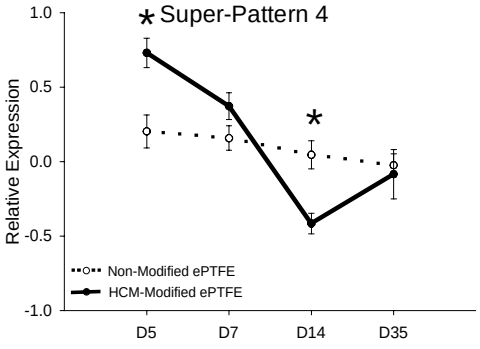
* Super-Pattern 4
Relative Expression
1.0
0.5
0.0
-0.5
-1.0
*
Non-Modified ePTFE
HCM-Modified ePTFE
D5
D7
D14
D35

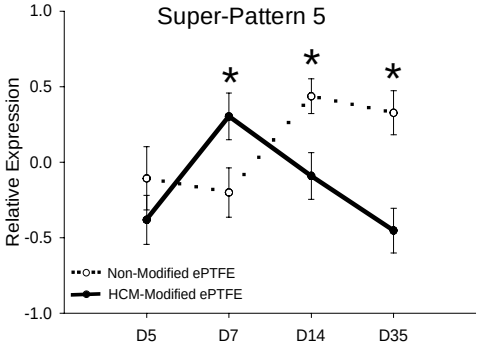
Super-Pattern 5
Relative Expression
1.0
0.5
0.0
-0.5
-1.0
*
*
*
Non-Modified ePTFE
HCM-Modified ePTFE
D5
D7
D14
D35

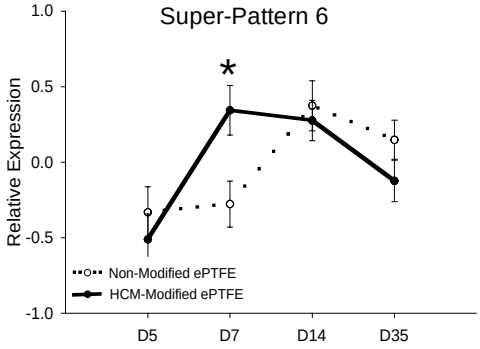
Super-Pattern 6
Relative Expression
1.0
0.5
0.0
-0.5
-1.0
*
Non-Modified ePTFE
HCM-Modified ePTFE
D5
D7
D14
D35

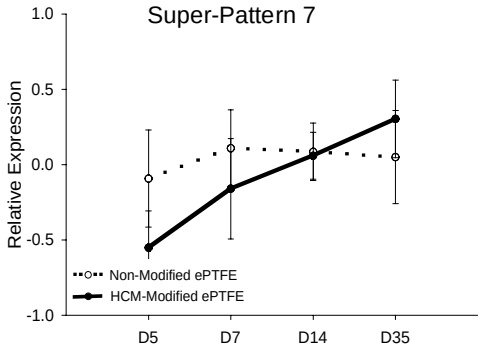
Super-Pattern 7
Relative Expression
1.0
0.5
0.0
-0.5
-1.0
Non-Modified ePTFE
HCM-Modified ePTFE
D5
D7
D14
D35

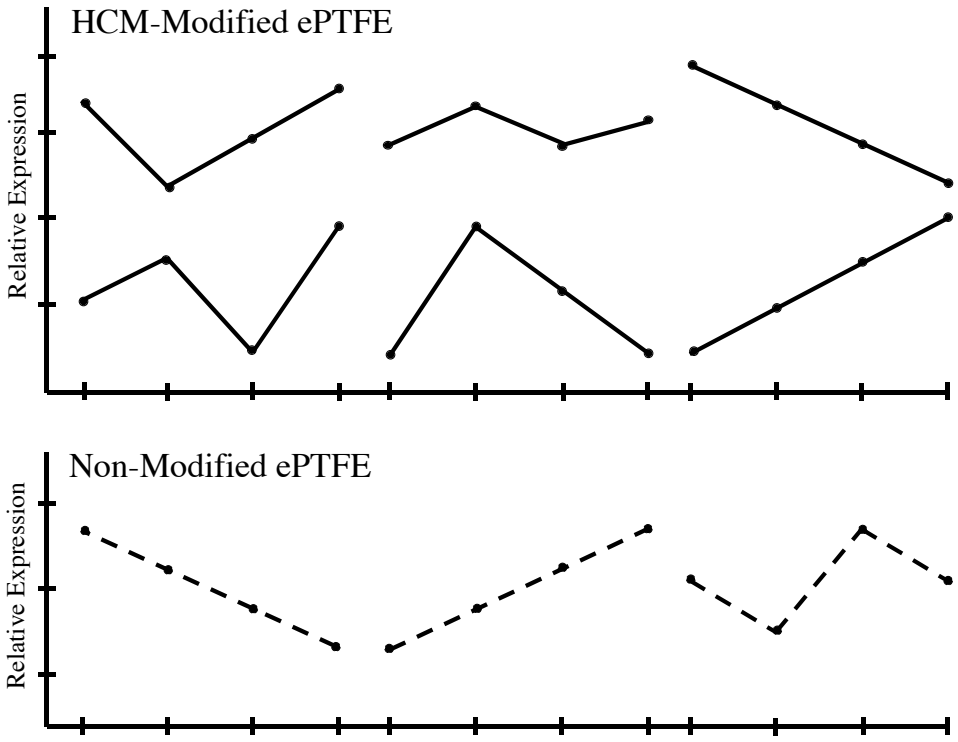

Figure 2.5 Diagram of overall patterns of expression for both treatment groups. There were 6 general patterns of expression for the HCM-modified ePTFE and 3 general gene expression patterns in the tissue surrounding the non-modified ePTFE.

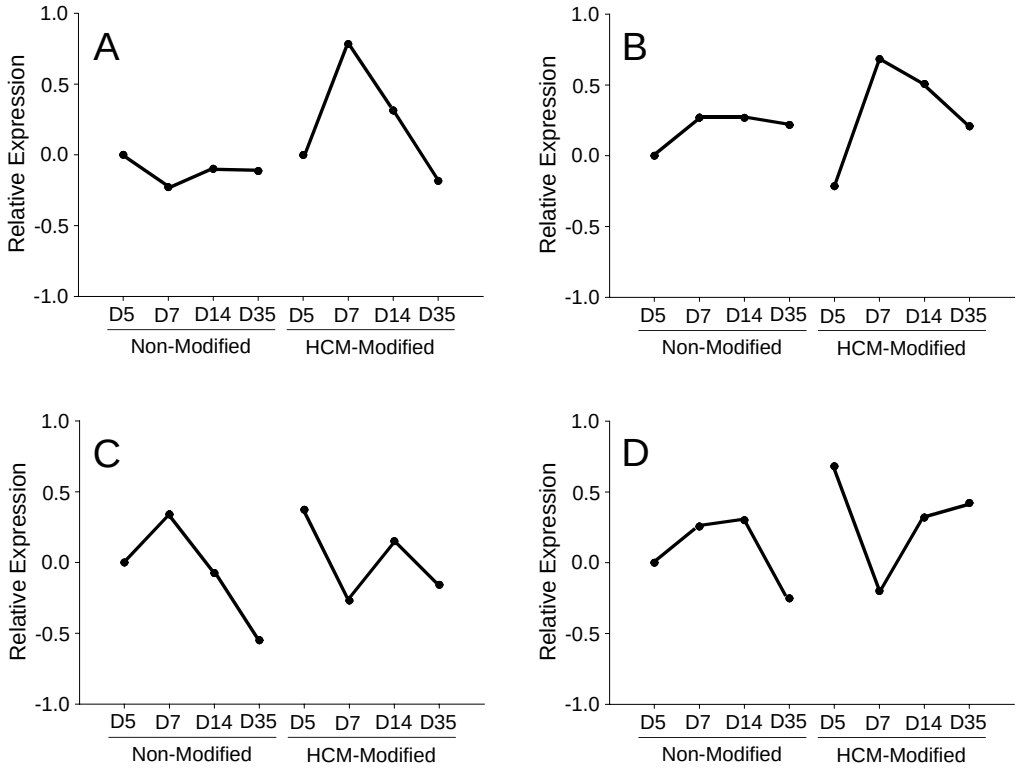

Figure 2.6 Comparison of microarray and quantitative real-time PCR. A) Output from ANOVA of the gene expression pattern for PECAM. B) Quantitative real-time PCR data for PECAM. Each method confirms that the expression of PECAM is up-regulated at day 7 of the HCM-modified ePTFE group and is down-regulated thereafter. Gene expression for α-Enolase as measured by C) ANOVA and D) real-time PCR. Expression values were normalized to day 5 non-modified values (which was set to 0.0).

Table 2.1. Classification of Expressed Known Genes

Gene Function	# of Genes	Day 7†	Day 35†	Clusters*
Cell Activity	233	Cluster Dependent	Cluster Dependent	All
Inflammation/Immunity	18	Down	Up	1,3,6,12
Matrix Associated	16	Down	Up	1,2,4,6,10,12,13
Proliferation	12	Cluster Dependent	Cluster Dependent	1,2,3,4,6,10,11,12

† The predominate expression of each gene class is given for days 7 and 35.
* Cluster numbers that contain at least one gene for each class

Table 2.2 Cluster 1

Gene	Funtional Category
Rattus norvegicus protein tyrosine phosphatase type IVA	Cellular Activity
Mus musculus tyrosine 3-monooxygenase	Cellular Activity
Mus musculus S100 calcium binding protein A6 (calcyclin)	Cellular Activity
Mus musculus guanine nucleotide binding protein	Cellular Activity
Mus musculus histocompatibility 2	Cellular Activity
Mus musculus tubulin, beta 5 (Tubb5)	Cellular Activity
Mus mus. glyceraldehyde-3-phosphate dehydrogenase (GAPDH)	Cellular Activity
Mus musculus hemoglobin alpha	Cellular Activity
Mus musculus ferritin heavy chain (Fth)	Cellular Activity
Mus musculus integral membrane protein 3	Cellular Activity
Mus musculus domesticus mitochondrial DNA	Cellular Activity
Mus musculus core promoter element binding protein	Cellular Activity
UNKNOWN: Similar to Mus musculus ribosomal protein S2	Cellular Activity
Mus musculus, eukaryotic translation elongation factor 1 alpha 1	Cellular Activity
Mus musculus similar to hypothetical protein 2	Cellular Activity
Mus musculus ribosomal protein, large, P1	Cellular Activity
Mus musculus ribosomal protein S5	Cellular Activity
Mus musculus ribosomal protein S4	Cellular Activity
Mus musculus ribosomal protein S3	Cellular Activity
Mus musculus ribosomal protein S28	Cellular Activity
Mus musculus ribosomal protein S27a	Cellular Activity
Mus musculus ribosomal protein S2	Cellular Activity
Mus musculus ribosomal protein S18	Cellular Activity
Mus musculus ribosomal protein L9	Cellular Activity
Mus musculus ribosomal protein L6	Cellular Activity
Mus musculus ribosomal protein L5	Cellular Activity
Mus musculus ribosomal protein L27a	Cellular Activity
Mus musculus ribosomal protein L13a	Cellular Activity
Mus musculus acidic ribosomal phosphoprotein PO	Cellular Activity
Mus musculus suppressor of initiator codon mutations	Cellular Activity
Mus musculus secreted acidic cysteine rich glycoprotein (Sparc)	Inflammation/Immunity
Mus musculus peptidylprolyl isomerase B	Inflammation/Immunity
Mus musculus peptidylprolyl isomerase A	Inflammation/Immunity
Mus musculus lymphocyte antigen 6 complex	Inflammation/Immunity
Mus musculus cathepsin L	Matrix
Mus musculus prothymosin alpha	Proliferation
Mus musculus tumor protein (Tpt1)	Proliferation

Table 2.3 Cluster 2

Gene	Functional Category
Mus musculus, Similar to transgelin 2	Cellular Activity
Mus musculus thioredoxin 1 (Txn1)	Cellular Activity
Mus musculus selenoprotein P, plasma, 1 (Sepp1)	Cellular Activity
Mus musculus peroxiredoxin 1 (Prdx1)	Cellular Activity
Mus musculus annexin A2 (Anxa2)	Cellular Activity
Mus musculus Nedd4 WW binding protein 5	Cellular Activity
Mus musculus protein phosphatase 1	Cellular Activity
Mus musculus ATPase, H+ transporting, lysosomal 9kD	Cellular Activity
Mus musculus ATPase, H+ transporting, lysosomal 38kDa	Cellular Activity
Mus musculus ATPase, H+ transporting, lysosomal 16kD	Cellular Activity
Mus musculus FK506 binding protein 1a	Cellular Activity
Mus musculus ferritin light chain 1 (Ftl1)	Cellular Activity
Mus musculus CD9 antigen (Cd9)	Cellular Activity
Mus musculus, Similar to cytochrome b-245	Cellular Activity
Mus musculus ninjurin 1 (Ninj1)	Cellular Activity
Mus musculus, FBJ osteosarcoma oncogene	Cellular Activity
Mus musculus Cd63 antigen (Cd63)	Cellular Activity
Mus musculus spermidine/spermine N1-acetyl transferase	Cellular Activity
Mus musculus proteasome (prosome, macropain) subunit	Cellular Activity
Mus musculus splicing factor Sc35	Cellular Activity
Mus musculus ribosomal protein L7	Cellular Activity
Mus musculus ribosomal protein L35	Cellular Activity
Mus musculus ribosomal protein L3	Cellular Activity
Mus musculus ribosomal protein L23	Cellular Activity
Mus musculus ribosomal protein 10	Cellular Activity
UNKNOWN: Similar to Mus musculus Fc receptor, IgG	Inflammation/Immunity
UNKNOWN: Similar to Mus musculus beta-2 microglobulin	Inflammation/Immunity
Mus musculus secreted phosphoprotein 1	Inflammation/Immunity
Mus musculus peptidylprolyl isomerase A	Inflammation/Immunity
Mus musculus protein (peptidyl-prolyl cis/trans isomerase)	Inflammation/Immunity
Mus musculus, Similar to lysozyme	Inflammation/Immunity
Mus musculus, interleukin 2 receptor	Inflammation/Immunity
Mus musculus cysteine rich intestinal protein	Inflammation/Immunity
Mus musculus cathepsin L	Matrix
Mus musculus Niemann Pick type C2	Matrix
Mus musculus cell division cycle 42 homolog	Proliferation

Table 2.4 Cluster 3

Gene	Functional Category
UNKNOWN: Similar to Mus musculus actinin, alpha 1 (Actn1)	Cellular Activity
Mus musculus actin related protein 2/3 complex	Cellular Activity
Mus musculus breast cancer 2 (Brca2)	Cellular Activity
Mus musculus glutathione S-transferase, mu 2 (Gstm2)	Cellular Activity
Mus musculus cyclin ania-6a gene	Cellular Activity
Mus musculus tight junction protein 1 (Tjp1)	Cellular Activity
Mus musculus, Similar to protein phosphatase 2	Cellular Activity
Mus musculus tumor-associated calcium signal transducer 1	Cellular Activity
Mus musculus similar to Absent in melanoma 1 protein	Cellular Activity
Mus musculus tripartite motif protein 27	Cellular Activity
UNKNOWN: Similar to Mus musculus anti-Mullerian hormone	Cellular Activity
Mus musculus teratocarcinoma-derived growth factor	Cellular Activity
Mus musculus bromodomain-containing protein BRD4	Cellular Activity
Mus musculus UDP-Gal:betaGlcNAc beta	Cellular Activity
Mus musculus similar to transmembrane protein (63kD)	Cellular Activity
UNKNOWN: Similar to Mus musculus, SEC61, alpha subunit 2	Cellular Activity
Mus musculus vacuolar protein sorting 35	Cellular Activity
Mus musculus hippocampus abundant gene transcript 1	Cellular Activity
Mus musculus, Similar to Rab geranylgeranyl transferase	Cellular Activity
Mus musculus, peptidylprolyl isomerase (cyclophilin)	Inflammation/Immunity
Mus musculus chondroitin sulfate proteoglycan 6	Matrix
Mus musculus, Similar to TOB3	Matrix
Mus musculus procollagen C-proteinase enhancer	Matrix
Mus musculus protein regulator of cytokinesis 1-like	Proliferation
UNKNOWN: Similar to Homo sapiens Kruppel-like factor 5	Proliferation

Table 2.5 Cluster 4

Gene	Functional Category
Mus musculus actin, beta, cytoplasmic	Cellular Activity
UNKNOWN: Similar to Rattus sp. cytochrome oxidase	Cellular Activity
Mus musculus, Similar to cytochrome c oxidase III	Cellular Activity
Mus musculus cytochrome c oxidase subunit II (Cox2)	Cellular Activity
Mus musculus, similar to ribosomal protein S27	Cellular Activity
Mus musculus ribosomal protein L7	Cellular Activity
Mus musculus ribosomal protein L22	Cellular Activity
Mus musculus fibulin 2 (Fbln2)	Matrix
Mus musculus bone morphogenetic protein 1 (Bmp1)	Matrix
Mus musculus sarcoglycan	Matrix

Cluster 5

Gene	Functional Category
Mus musculus hemoglobin alpha, adult chain 1	Cellular Activity
Mus musculus putative homeodomain transcription factor	Cellular Activity

Table 2.6 Cluster 6

Gene	Functional Category
Mus musculus epimorphin (Epim)	Cellular Activity
Mus musculus BCL2-associated athanogene 4	Cellular Activity
Mus musculus Ca2+-dependent activator for secretion	Cellular Activity
Mus musculus sorbitol dehydrogenase 1 (Sdh1)	Cellular Activity
Mus musculus WD repeat domain 5 (Wdr5)	Cellular Activity
Mus musculus Unc-51 like kinase 2	Cellular Activity
Mus musculus similar to Diacylglycerol kinase	Cellular Activity
Mus musculus neural-salient serine/arginine-rich (Nssr)	Cellular Activity
Mus musculus, solute carrier family 2	Cellular Activity
Mus musculus L-3-hydroxyacyl-Coenzyme A dehydrogenase	Cellular Activity
Mus musculus ZAP3 protein	Cellular Activity
Mus musculus adaptor-related protein complex AP-3	Cellular Activity
Mus musculus, lysosomal-associated protein transmembrane	Cellular Activity
Mus musculus Swi/SNF related matrix associated	Cellular Activity
Mus musculus RuvB-like protein 2 (Ruvbl2)	Cellular Activity
Mus musculus growth hormone receptor (Ghr)	Cellular Activity
Mus musculus solute carrier family 1	Cellular Activity
Mus musculus hypermethylated in cancer 1	Cellular Activity
Similar to M.musculus mRNA for zinc finger protein	Cellular Activity
Mus musculus, Similar to zinc finger protein 143	Cellular Activity
Mus musculus makorin, ring finger protein, 1 (Mkrn1)	Cellular Activity
Mus musculus tuftelin interacting protein 11 (Tfip11)	Matrix
Similar to Homo sapiens Ras-GTPase activating protein SH3	Proliferation
Mus musculus topoisomerase (DNA) III beta (Top3b)	Proliferation

Table 2.7 Cluster 7

Gene	Functional Category
Mus musculus actinin alpha 3 (Actn3)	Cellular Activity
Mus musculus actin, beta, cytoplasmic (Actb)	Cellular Activity
Mus musculus cytochrome c oxidase, subunit IVa (Cox4a)	Cellular Activity
Mus musculus glucosamine-6-phosphate deaminase (Gnpi)	Cellular Activity
Mus musculus WD repeat domain 1 (Wdr1)	Cellular Activity
Mus musculus fatty acid binding protein 3, muscle and heart	Cellular Activity
Mus musculus pyruvate kinase 3 (Pk3)	Cellular Activity
Mus musculus, Similar to tubulin alpha 1	Cellular Activity
Mus musculus carbonyl reductase 2 (Cbr2)	Cellular Activity
Mus musculus tropomyosin 2, beta (Tpm2)	Cellular Activity
Mus musculus myosin light chain	Cellular Activity
Mouse tropomyosin isoform 2 mRNA	Cellular Activity
Mus musculus heat shock protein, 70 kDa	Cellular Activity
Mus musculus cold shock domain protein A (Csda)	Cellular Activity
Mus musculus, ADP-ribosylation factor 1	Cellular Activity
Mus musculus similar to Collagen alpha 1	Matrix
Mus musculus prothymosin alpha (Ptma)	Proliferation

Table 2.8 Cluster 8

Gene	Functional Category
Mus musculus myristoylated alanine rich protein kinase C	Cellular Activity
Mus musculus growth arrest specific 1 (Gas1)	Cellular Activity
Mus musculus, platelet/endothelial cell adhesion molecule	Cellular Activity
Mus musculus, eukaryotic translation initiation factor 2	Cellular Activity
Mus musculus similar to 60S RIBOSOMAL PROTEIN L17	Cellular Activity

Cluster 9

Gene	Functional Category
Mus musculus, profilin 1	Cellular Activity
Mus musculus GRO1 oncogene (Gro1)	Cellular Activity
Mus musculus amino levulinate synthase mRNA	Cellular Activity
Mus musculus ganglioside-induced differentiation-associated-1	Cellular Activity
Mus musculus MARCKS-like protein (Mlp)	Cellular Activity
Mus musculus, Similar to guanine nucleotide binding protein	Cellular Activity
Mus musculus stearoyl-Coenzyme A desaturase 2 (Scd2)	Cellular Activity
Mus musculus domesticus mitochondrial DNA	Cellular Activity
Mus musculus ring finger protein 10 (Rnf10)	Cellular Activity
Mus musculus immediate early response 3 (Ier3)	Cellular Activity
Mus musculus heme oxygenase (decycling) 1 (Hmox1)	Cellular Activity
Mus musculus pericentriolar material gene 1 protein (Pcm1)	Cellular Activity
Mus musculus ribosomal protein S14 (Rps14)	Cellular Activity
Mus musculus ribosomal protein L29 (Rpl29)	Cellular Activity
Mus musculus lymphocyte antigen 6 complex, locus E (Ly6e)	Inflammation/Immunity
Mus musculus lipocalin 2 (Lcn2)	Inflammation/Immunity
Mus musculus ubiquitin-conjugating enzyme E2L 3 (Ube2l3)	Matrix
Mus musculus expressed in non-metastatic cells 1	Proliferation

Table 2.9 Cluster 10

Gene	Functional Category
Mus musculus cytochrome c oxidase, subunit VIc (Cox6c)	Cellular Activity
Mus musculus ATP synthase, H+ transporting mitochondrial F1	Cellular Activity
Similar to Mus musculus NADH dehydrogenase	Cellular Activity
Mus musculus NADH dehydrogenase flavoprotein 1 (Ndufv1)	Cellular Activity
Mus musculus N-myc downstream regulated 2 (Ndr2)	Cellular Activity
Mus musculus hepatoma-derived growth factor (Hdgf)	Cellular Activity
Similar to Mus musculus aldolase 1, A isoform (Aldo1)	Cellular Activity
Mus musculus voltage-dependent anion channel 1 (Vdac1)	Cellular Activity
Mus musculus platelet-activating factor acetylhydrolase	Cellular Activity
Mus musculus lysosomal-associated protein transmembrane 4A	Cellular Activity
Mus musculus binding protein suppressor of hairless	Cellular Activity
Mus musculus erythroid derived 2,-like 1 (Nfe2l1)	Cellular Activity
Mus musculus cartilage associated protein (Crtap)	Matrix
Mus musculus ubiquitin B (Ubb)	Matrix

Table 2.10 Cluster 11

Gene	Functional Category
Mus musculus cyclin C (Ccnc)	Cellular Activity
Similar to Mus musculus domesticus mitochondrial DNA	Cellular Activity
Mus musculus tetratricopeptide repeat domain (Ttc3)	Cellular Activity
Mus musculus syntrophin, acidic 1 (Snta1)	Cellular Activity
Mus musculus, ribosomal protein L23a	Cellular Activity
Similar to Rattus norvegicus golgi SNAP receptor complex	Cellular Activity
Similar to Mus musculus nuclear factor of activated T-cells	Inflammation/Immunity
Mus musculus replication factor C, 140 kDa (Recc1)	Proliferation

Cluster 12

Gene	Functional Category
Rattus norvegicus ornithine decarboxylase antizyme inhibitor	Cellular Activity
Mus musculus lipidosis-related protein lipidosin (lpd)	Cellular Activity
Mus musculus epidermal growth factor receptor	Cellular Activity
Mus musculus sorting nexin 2 (Snx2)	Cellular Activity
Mus musculus ATP-binding cassette, sub-family E (OABP)	Cellular Activity
Mus musc. UDP-Gal:betaGlcNAc beta 1,4- galactosyltransferase	Cellular Activity
Mus musculus RAS-related protein-1a (Rap1a)	Cellular Activity
Mus musculus nucleophosmin 1 (Npm1)	Cellular Activity
Mus musculus heat shock protein, 86 kDa 1 (Hsp86-1)	Cellular Activity
Mus musculus ubiquitin-conjugating enzyme E2D 2 (Ube2d2)	Matrix
Mus musculus B-cell translocation gene 4 (Btg4)	Proliferation

Table 2.11 Cluster 13

Gene	Functional Category
UNKNOWN: Similar to insulin-like growth factor I (exon 6)	Cellular Activity
Similar to tyrosine 3monooxgenase/tryptophan 5	Cellular Activity
Mus musculus acid phosphatase 5, tartrate resistant (Acp5)	Cellular Activity
Similar to Mus musculus implantation-related RGS2-like protein	Cellular Activity
Mus musculus apolipoprotein B editing complex 1 (Apobec1)	Cellular Activity
Mus musculus, Similar to transmembrane 7 superfamily	Cellular Activity
Mus musculus lysosomal membrane glycoprotein 2 (Lamp2)	Cellular Activity
Mus musculus SPARC-like 1 (mast9, hevin) (Sparcl1)	Inflammation/Immunity
Mus musculus syndecan 2 (Sdc2)	Matrix

Cluster 14

Gene	Functional Category
Mus musculus, ATPase, H+ transporting, lysosomal 70kD	Cellular Activity
Mus musculus G1 to phase transition 1 (Gspt1)	Cellular Activity
Mus musculus microtubule-associated protein 1 (Map1lc3)	Cellular Activity
Mus musculus serine (or cysteine) proteinase inhibitor	Cellular Activity

3. COMPARISON OF GENE EXPRESSION BETWEEN TWO ePTFE MODIFICATIONS THAT PROMOTE SIMILAR ALTERED HEALING RESPONSES

Introduction

The long-term viability of implanted devices is often prevented by the formation of a fibrous capsule as part of the foreign body response. As a result, efforts have been focused on modifying biomaterials that are used to construct implanted medical devices with the goal being to engineer the tissue surrounding the implanted device (Sharkawy et al. 1997). Stimulation of vessel formation in the surrounding tissue has been proposed as an approach to alter the healing response and improve the function of indwelling devices such as glucose sensors, vascular grafts, and immunoisolation devices (Trivedi et al. 2000; Updike et al. 2000; Wisniewski et al. 2000; Merzkirch et al. 2001). Prior studies have shown that modification of ePTFE, a porous material often used to construct biomedical devices, with conditioned media of an immortalized cell line (HaCaT) leads to both a decrease in capsular thickness and an increase in the number of vessels present in the surrounding tissue (Kidd et al. 2005). Western blotting revealed the extracellular matrix molecule laminin-5 (Ln-5) as being a predominant protein in the HaCaT conditioned media (HCM). Purified Ln-5 modification of ePTFE was also shown to illicit a tissue response similar to that of HCM-modified ePTFE (Kidd et al. 2005).

A lack of understanding as to the molecular mechanisms involved during HCM-modified ePTFE associated healing lead us to perform large-scale gene analysis of the

tissue surrounding both modified and non-modified ePTFE. From that analysis, it was determined that HCM-modification promotes the existence of tissue that is more dynamic with regard to transcriptional activity (Schwartz et al. 2005). These results offered new insights into mechanisms at the molecular level of altered ePTFE associated healing. However, gene expression patterns generated by comparing HCM-modified ePTFE associated tissue to non-modified ePTFE associated tissue is insufficient to suggest molecular targets or mechanisms that should be considered when designing new devices. Gene expression analysis of tissue surrounding Ln-5 modified ePTFE that has similar tissue morphology to HCM-modified ePTFE may better define those molecular pathways central to the altered healing response seen with extracellular matrix modified ePTFE.

The molecules involved in any biological process are based on what genes are expressed, as well as the level of their expression. With this in mind, we have performed a large-scale analysis of the temporal gene expression patterns of the tissue associated with HCM and Ln-5 modified ePTFE. By comparing the genes expressed in the tissue surrounding both modification types, we can better define the molecular systems and pathways present during ePTFE-associated healing that may be serve as the basis for developing novel polymer modifications to manipulate the healing response.

Materials and Methods

Purification of Laminin-5

Using the ÄKTA FPLC system (Amersham Pharmacia Biotech), harvested HaCaT conditioned medium was passed over an affinity column prepared by coupling Sepharose 4B (Amersham Pharmacia Biotech) to the anti–Ln 5 β3 chain antibodies. Laminin-5 was eluted from the column with 1M acetic acid and fractions were neutralized, dialyzed, and quantitated using a Bradford Protein Assay.

Ln-5 Modification of ePTFE

Prior to surface modification, grafts are denucleated by placing them in a series of ten EtOH grades from 100% to 10%, 15 minutes in each, during which the ePTFE becomes transparent. The material was then washed in denucleated water and then PBS. Laminin-5 (20 μg/μl) was forced repeatedly through the graft and its interstices using a syringe.

Implantation of ePTFE

Laminin 5 modified ePTFE was implanted subcutaneously as previously described (Schwartz et al. 2005). Briefly, tubular Ln-5 modified, or non-modified ePTFE was cut into 2 cm length sections, then sliced longitudinally and implanted into adult male mice (129-SVJ; 18-22 g). The implanted ePTFE was removed at 3 timepoints. One-quarter of each implant was retained for tissue processing, while the remainder was placed in RNA*later* solution (Ambion, Austin, TX).

Evaluation of Tissue Morpholgy

Tissue samples that were fixed in Histochoice (AMRESCO Inc., Solon, Ohio), paraffin embedded, sectioned to a 6 μm thickness, and stained with hematoxylin and eosin (H&E) to visualize gross tissue histology. Sections were also stained with *Griffonia simplicifolia-1* (GS-1) to identify vascular cells.

RNA Isolation

Samples were removed from RNA*later* solution (Ambion, Austin, TX) and RNA was isolated from tissue associated with the ePTFE implants as previously reported (Schwartz et al. 2005).

Microarray

Microarray slides were prepared by first coating NaOH-cleaned microscope slides (75 mm x 25 mm) in a solution of 2% 3-aminopropyltrimethoxysilane and 2% (1,4-Phenylene-diisothiocyanate) for 10 minutes. After a 5 minute rinse in 100% EtOH, a mouse oligo (70-mer) library from Qiagen (Valencia, CA) containing approximately 32,000 elements was spotted onto the slides using a VersArray ChipWriter (Bio-Rad, Hercules, CA). After spotting, slides were baked for 90 minutes at 90ºC and stored in a dessicator (15% relative humidity) until used. The advantages of using an oligo library over a cDNA library include more complete annotation of the gene sequences and more uniform hybidization kinetics.

aRNA Amplification

RNA amplification was performed using the Amino Allyl MessageAmp™aRNA kit from Ambion (Austin, TX) that is based on a linear amplification protocol (Van Gelder et al. 1990). Briefly, 2.5 µg of total RNA from each sample was amplified following the provided protocol. During the in vitro transcription section of the protocol, amino allyl modified UTP's were incorporated into the synthesized aRNA. The aRNA was purified using the supplied clean-up columns before dye incorporation.

aRNA Labeling

Alexa Fluor® 555 and Alexa Fluor® 647 (Molecular Probes, Eugene, OR) were resuspended in 6.6 µl of DMSO. Appropriate dyes (1 µl) were added to 2.5 µg of aRNA in 3.3 µl nuclease-free H_2O, 1.6 µl 0.3 M $NaHCO_3$, and 4 µl DMSO. The labeled aRNA samples were then mixed with the corresponding sample. Labeled aRNA was purified using the RNeasy® Kit and following the provided purification protocol. The labeled aRNA was eluted from the columns with 50 µl of nuclease-free H_2O.

aRNA Hybridization

To the 50 µl of labeled aRNA, 10 µl of Cot-1 DNA (1 µg/µl) and 60 µl of 2X Hybridization Buffer (8X SSC, 60% formamide, 0.2% SDS) were added. Printed slides were washed in 1% SDS solution at 50-60ºC and rinsed in nuclease-free H_2O at room temperature. The washed slides were then placed in a clean hybridization station cartridge assembly and positioned on the GeneTac hybridization station (Genomic

Solutions, Inc., Ann Arbor, MI). Each sample was injected onto the slide and allowed to hybridize at 42ºC for 12-16 hours, afterwhich the slide was removed and rinsed with 0.1X SSC. DyeSaver™was then applied to the dried slides.

Scanning of Microarray

Hybridized slides were scanned as previously described (Schwartz et al. 2005). Briefly, an epifluorescence/CCD-based scanner (ArrayWoRx$_e$™, Applied Precision, Issaquah, WA) was used along with spot finding software (MolecularWare, Irvine, CA) to measure individual spot intensities. The data collected was analyzed using an ANOVA-based custom analysis package.

Quantitative PCR

Quantitative PCR was also used to measure gene expression of those genes contained within the oligo library, as well as for genes that were not represented in the library. All primers were designed using the Primer3 program (http://genome.wi.mit.edu/cgi-bin/primer3/primer3.cgi). The primers were designed against the 3' end of the gene, and were constructed to generate products of approximately 100-200 bp in length.

Results

Laminin-5 that was purified from HaCaT conditioned media and the 3 subunits of the Ln-5 molecule were positively identified by western blot analysis (Figure 3.1A). The purified Ln-5 was successfully used to coat ePTFE by repeatedly passing the protein through the pores of the material. This was confirmed by using an antibody against the β3 subunit after application of Ln-5 onto the ePTFE (Figure 3.1B).

Samples of ePTFE that were either non-modified or modified with Ln-5 were removed from the subcutaneous position at days 5, 14, and 35 while retaining all associated tissue. To visualize gross tissue morphology, tissue sections were stained with hematoxylin and eosin. Vessels were also stained using GS-1 to identify vascular elements. Consistent with previous studies evaluating HCM-modified ePTFE (Schwartz et al. 2005), tissue surrounding Ln-5 modified ePTFE was less dense and contained more vessels than non-modified ePTFE. Figure 3.2 illustrates the difference in tissue response from the day 5 time point to the final day 35 time point for Ln-5 modified and non-modified ePTFE.

The HCM-modified ePTFE study used a cDNA microarray, whereas the samples from this study were hybridized to an oligo array consisting of approximately 32,000 elements, with each element being a unique 70-mer sequence. Amino allyl modified UTP's were incorporated into the RNA during the *in vitro* transcription step of RNA amplification. This step was necessary because the strand that is printed onto the array is complementary to the amplified RNA (aRNA) product, thus it is essential that the aRNA is labeled and amplified. To retain consistency, total RNA from tissue associated with

the HCM-modified ePTFE was also amplified and hybridized in the same fashion as the Ln-5 modified ePTFE. The hybridization scheme used for both modification groups is shown in Figure 3.3. After hybridization, slides were scanned and intensity values were generated and analyzed by ANOVA (Kerr et al. 2000).

Each modification group expressed a set of genes that were different in number and content. Of the approximate 32,000 elements on the array, the tissue associated with the Ln-5 modified ePTFE expressed 8201 genes, of which 523 genes possessed significant differential expression for at least one timepoint ($p < 0.05$). From the HCM-modified group, 5779 genes were measured as expressed and 595 genes were measured as having differential expression for at least one timepoint. Expression data was then mean-centered and unit normalized to assist in comparative analysis between the two modification types.

Comparing the two sets of significant expression data yielded 178 genes that were co-expressed in tissue surrounding both the HCM-modified ePTFE and Ln-5 modified ePTFE (Tables 3.1-3.4). These genes can be categorized into four main functions: cell activity, inflammation/immunity, matrix associated, and proliferation. Genes involved in general cellular activity comprised the largest functional category of those genes that were shared. These genes made up 40% of the 178 genes shared between the two groups (Table 3.1). The next largest functional category contained genes related to inflammation/immunity. Inflammation/immune response related genes comprised 21% of the shared genes (Table 3.2). A quarter of the inflammation/immune response related genes were related to specific macrophage function, such as the macrophage

inflammatory protein 2 (MIP-2), a cytokine that has been shown to possess chemotactic activity for many inflammatory and immune cells (Driscoll 1994).

Expression patterns for the 178 common genes had two possible outcomes. 1) Similar expression between HCM-modification and Ln-5 or 2) different expression between the modification groups. One gene that displayed similar gene expression between the modification groups was CXCL5 that is involved in neutrophil activation (Bisset et al. 2005) (Figure 3.4A). This gene exhibits down-regulation over the duration of the experiment. An example of a gene that is also involved in the inflammatory response, but is differentially regulated as a result of the proteins used to modify the ePTFE is CCL12, which is involved in directing the migration of monocytes into inflammatory sites (Huang et al. 2001) (Fig. 3.4B). This gene is up-regulated at days 5 and 14 in tissue associated with HCM-modified ePTFE, while it is down-regulated at day 35. Expression data illustrates that in tissue surrounding Ln-5 modified ePTFE, CCL12 is up-regulated at day 5, but down-regulated and days 14 and 35. Another macrophage related gene that was regulated in tissue surrounding all ePTFE modification groups as measured by microarray analysis is interleukin 4 receptor (IL-4R) (Figure 3.5A). Expression of IL-4R was verified using quantitative PCR (Q-PCR), establishing that this gene is up-regulated at day 5, before being down-regulated at days 14 and 35. Interleukin-4 receptor has been shown to be presented on the surface of alternatively activated macrophages (Herbert et al. 2004).

Discussion

It has been shown that modifying ePTFE with media conditioned with extracellular matrix proteins secreted by the immortalized keritinocyte cell line HaCaT, stimulates vascularity and a less fibrous capsule in the tissue surrounding the implanted material (Kidd et al. 2005). The current lack of understanding concerning the molecular mechanism underlying polymer-associated healing prompted us to measure gene expression patterns associated with HCM-modified ePTFE and non-modified ePTFE (Chapter 2). Results from that study illustrate that there is more active and dynamic transcriptional activity in the tissue surrounding the HCM modified ePTFE, as evidenced by there being more unique patterns of expression than compared to the non-modified associated tissue. The use of one ECM modification type produced a dataset that was complex in nature, making it difficult to assign specific genes to specific processes.

Subsequent analysis of the HaCaT conditioned media found that it was enriched with the extracellular matrix protein laminin-5 (Ln-5). When ePTFE was modified with purified Ln-5, a tissue response based on histologic evaluation, similar to that observed surrounding the HaCaT conditioned media modified ePTFE was elicited. The aim of the current study was to compare gene expression patterns of tissue surrounding HCM and Ln-5 modified ePTFE. Having two modification groups that generate similar tissue morphologies is thought to focus and condense the number of genes that are directly involved in the altered healing response associated with extracellular modified ePTFE.

All samples were hybridized to a microarray consisting of approximately 32,000 70-mer oligo sequences. This was a departure from the prior gene expression study that

used a microarray that was constructed with 15,000 mouse cDNAs. The reason for the change in microarray type is twofold. The first reason is that the oligo library used is more thoroughly characterized and there are fewer genes present with unknown function. Often cDNA libraries are constructed based on expressed sequence tag (EST) presence, many of which have yet to be characterized. The second reason for choosing an oligo-based array over a cDNA array is that the increased probe length of the cDNA also increases the possibility of cross-hybridization due to repetitive or common sequence. Oligo sequences are designed to eliminate the existence of similar sequence, making oligo-based arrays more specific.

Gene expression data was analyzed by ANOVA, identifying 595 genes found in tissue surrounding HCM-modified ePTFE where there was differential gene expression for at least one timepoint over the course of the experiment. Analysis generated 523 genes in the tissue surrounding Ln-5 modified ePTFE where there was at least one timepoint that displayed differential gene expression ($p < 0.05$). From these genes, 178 were shared between modification groups. Although these 178 genes were commonly expressed, their expression patterns were not necessarily similar. In fact, analysis of these genes provides examples where expression of a gene is expressed similarly between modification groups, while another gene may be expressed differently depending on the modification used. An example of a gene that is similarly expressed in both modification groups is CXCL5, a gene involved in neutrophil activation. This gene exhibited progressive down-regulation over the course of the experiment. CCL12, a gene that participates in monocyte migration, displays a different expression pattern between

groups. These examples suggest that while the same genes are being affected by both HCM and Ln-5 modification, they are regulated by each modification differently.

This finding, along with the fact that many genes expressed were unique to either HCM or Ln-5 modification, suggests that laminin-5 is not the sole protein constituent of the HCM. There may be other molecules present in the conditioned media responsible for the difference in expression patterns. These molecules may be inhibitors or promoters of Ln-5, or they may influence different molecular pathways apart from the purified Ln-5.

The expression data and comparison of the genes that are shared between the HCM and Ln-5 modification leads to another observation that may have implications when revealing the molecular basis for the apparent, altered healing response. Of the 178 shared genes, the predominate functional category was that of general cell function. This result is not surprising as the cells surrounding the implanted material undergo normal cellular activities, and because of the presence of the ePTFE, cellular behavior is likely to be altered and detected in the gene expression data. However, the prospect of using differences in gene expression of basic cellular function to explain the altered healing in response to implanted ePTFE, while important, is challenging due to the breadth of genes involved as well as the uncertainty of what cell type or types are contributing to the observed expression. Focusing on the second most prevalent functional class, inflammation/immunity, appears to be a more reasonable approach for two reasons. 1) The number of genes contained within this group is smaller, making it easier to examine the role of each, and 2) the gene expression data suggests that the macrophage may be the

cell type that should be investigated as a quarter of the genes found within this category are macrophage related (Table 3.2).

The original aim of this study was to compare the gene expression data generated by tissue surrounding ePTFE that was modified with either HaCaT conditioned media or purified Ln-5, two modifications that stimulate similar tissue morphology. The altered healing response leads to a tissue that is less cellular and dense, with a higher vascular density. Results of this comparison suggest that future considerations and research be directed toward the regulation and activation of the macrophage as an explanation for the altered tissue response. Comparison of gene expression data associated with these two material modifications that lead to a similar tissue response furthers our understanding of the molecular processes involved in ePTFE associated healing. The findings presented in this study may lead to molecular targets that could be used to improve medical device biocompatibility.

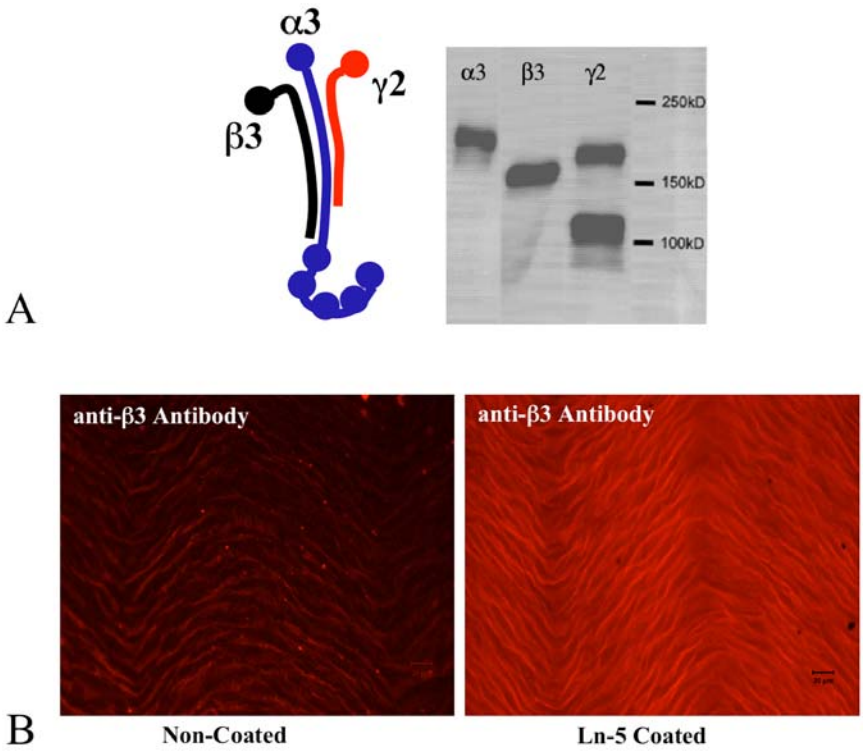

Figure 3.1 Purified Ln-5 modification of ePTFE. A) Western blot analysis illustrating the 3 chains of laminin-5. B) Laminin-5 is adhered to ePTFE following the passage of Ln-5 solution through the interstices of the material.

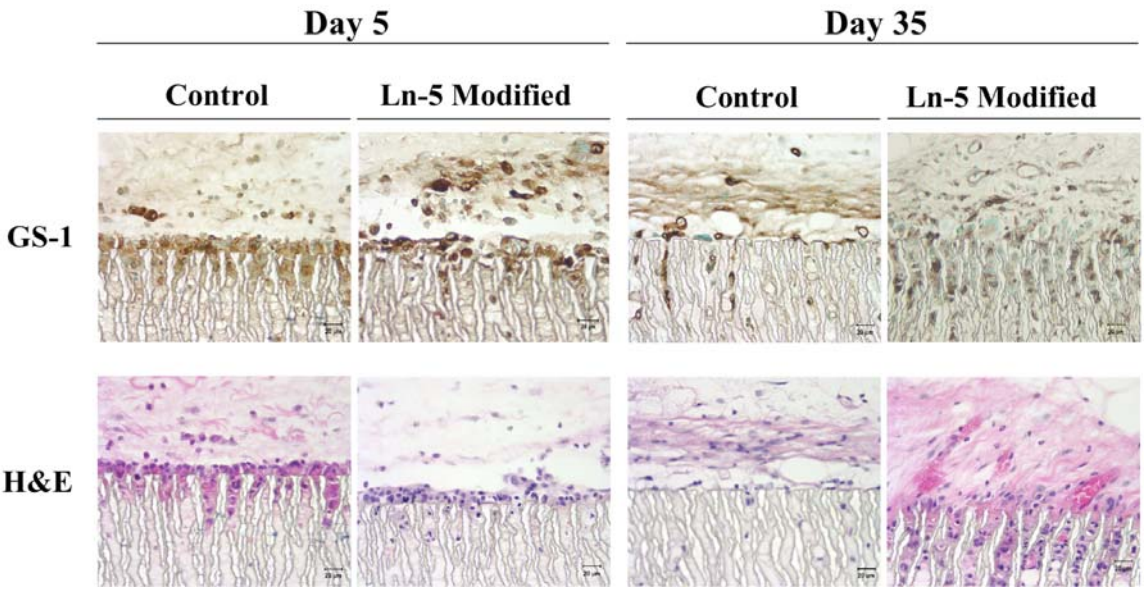

Figure 3.2 Light micrographs of day 5 and 35 sections stained with GS-1 and hematoxylin and eosin. Positively stained GS-1 cells demonstrate that there are more vascular elements at both timepoints surrounding Ln-5 ePTFE. Hematoxylin and eosin staining illustrates that tissue surrounding non-modified ePTFE is more dense than tissue surrounding the Ln-5 modified ePTFE.

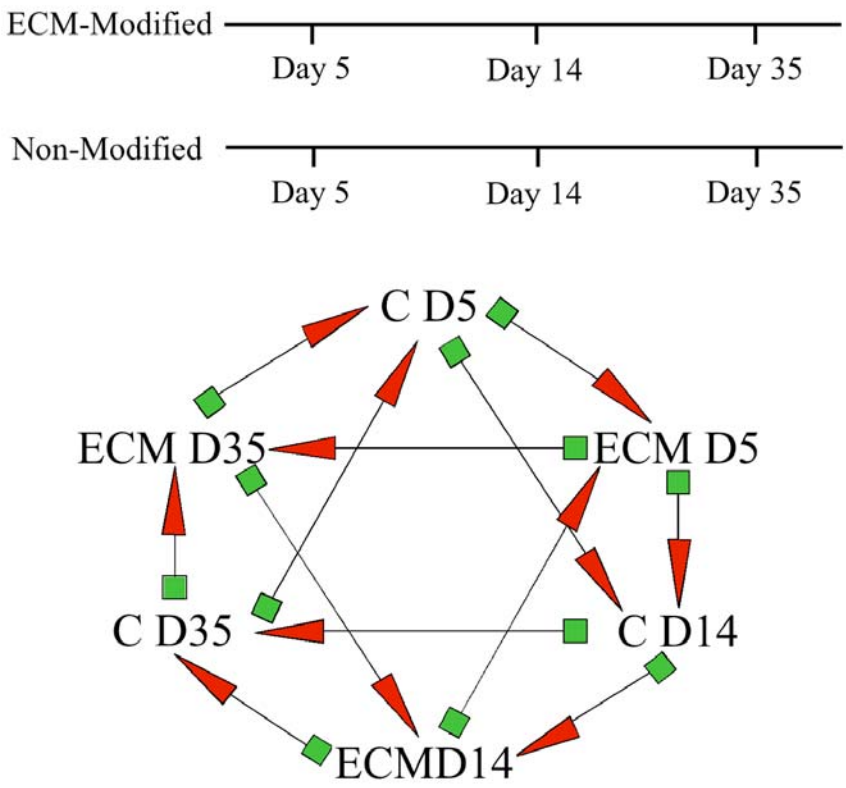

Figure 3.3 Experimental design and hybridization scheme. Samples were explanted at days 5, 14, and 35 for both HCM and LN-5 based experiments. The hybridization scheme (below) shows how samples were compared for ANOVA. This scheme was used for all modification groups.

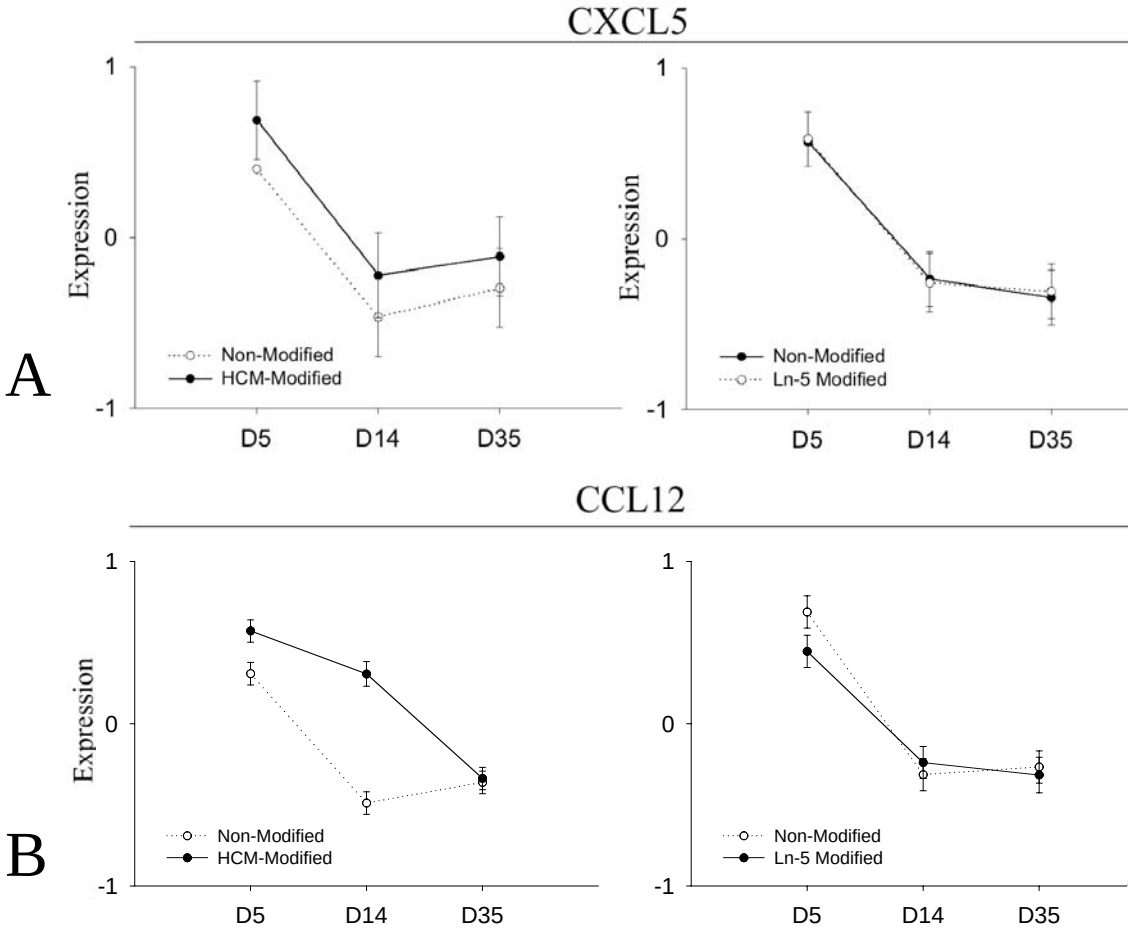

Figure 3.4 Gene Expression comparison of two inflammatory related genes between HCM and Ln-5 modification. A) Expression of CXCL5 differs little between modification groups. B) There is a difference in expression of CCL12 among HCM and Ln-5 modified ePTFE, as CCL12 was up-regulated with respect to non-modifed ePTFE at day 14. There was no change in expression of CCL12 between Ln-5 modified and non-modified ePTFE.

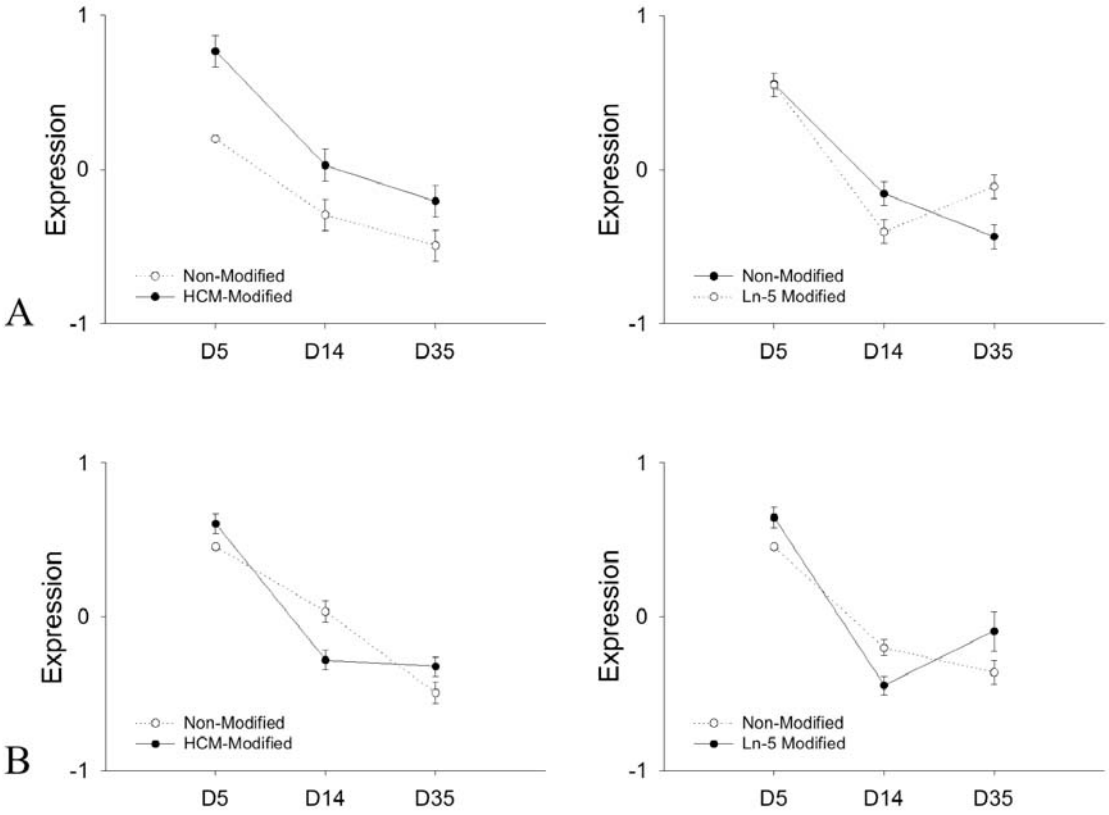

Figure 3.5 Gene expression of IL-4R in tissue surrounding HCM and Ln-5 modified ePTFE as measured by A) microarray and B) quantitative PCR. In all cases, IL-4R expression is up-regulated at day 5, and down-regulated at days 14 and 35.

Table 3.1 Cellular activity related genes

Gene
40S RIBOSOMAL PROTEIN SA (P40)
KRUEPPEL-LIKE FACTOR 13
RNA-BINDING PROTEIN RALY
SPECTRIN BETA CHAIN, BRAIN 1
TRB-2
NEURONAL MEMBRANE GLYCOPROTEIN M6-B (M6B)
SYNTENIN 2
NEUROMEDIN B-32
NEURONATIN
7S NERVE GROWTH FACTOR ALPHA CHAIN PRECURSOR
BCL2/ADENOVIRUS E1B 19-KDA PROTEIN-INTERACTING PROTEIN 3
DESMIN
MYOSIN-BINDING PROTEIN H (MYBP-H)
ACTIN, GAMMA-ENTERIC SMOOTH MUSCLE (ALPHA-ACTIN 3)
TROPONIN I
TROPOMYOSIN BETA CHAIN (TROPOMYOSIN 2)
TROPONIN I, SKELETAL, SLOW 1
MYOSIN, HEAVY POLYPEPTIDE 2
MYOSIN REGULATORY LIGHT CHAIN 2
ACTIN, ALPHA CARDIAC
MYOSIN, HEAVY POLYPEPTIDE 2
MYOZENIN; CALSARCIN-2
TROPONIN C
TROPONIN T3
ALPHA-ACTININ 3
TROPOMYOSIN ALPHA 3 CHAIN (TROPOMYOSIN 3)
TUBULIN ALPHA-4
CARBOXYPEPTIDASE H PRECURSOR
ACYL-COA DESATURASE 1
C-TYPE (CALCIUM DEPENDENT
28 KDA INTERFERON RESPONSIVE PROTEIN
LIVER CARBOXYLESTERASE 22
GELSOLIN PRECURSOR
GLYCOPROTEIN
CATALASE (EC 1.11.1.6)

Table 3.1-*Continued*

Gene
EPOXIDE HYDROLASE 1 (EC 3.3.2.3)
CARBONIC ANHYDRASE 13
CARBONIC ANHYDRASE III
PROBABLE C->U EDITING ENZYME APOBEC-2
NUCLEOSIDE DIPHOSPHATE KINASE
NUCLEOSOME ASSEMBLY PROTEIN 1-LIKE 1
C-4 METHYL STEROL OXIDASE
IMMUNOGLOBULIN SUPERFAMILY, MEMBER 4
REGULATOR OF G-PROTEIN SIGNALING 2
PROTEIN-TYROSINE SULFOTRANSFERASE 1
DEATH ASSOCIATED PROTEIN KINASE 1
SORBIN AND SH3 DOMAIN CONTAINING 1
MEMBRANE-SPANNING 4-DOMAINS
MYC BOX DEPENDENT INTERACTING PROTEIN 1
UROKINASE PLASMINOGEN ACTIVATOR SURFACE RECEPTOR
ARYL SULFOTRANSFERASE (EC 2.8.2.1)
INTEGRIN ALPHA X
GROWTH ARREST SPECIFIC 6
HOMEOBOX PROTEIN HOX-C6 (HOX-3.3)
CENTROMERE PROTEIN A (CENP-A)
CALSYNTENIN-1 PRECURSOR
PROGRESSIVE ANKYLOSIS PROTEIN
G2/MITOTIC-SPECIFIC CYCLIN B1
CYCLIN-DEPENDENT KINASES REGULATORY SUBUNIT 2 (CKS-2)
PLATELET GLYCOPROTEIN IV (GPIV)
PROTEIN TYROSINE PHOSPHATASE, RECEPTOR TYPE, S
THROMBOSPONDIN 4
SUPEROXIDE DISMUTASE
LEPTIN PRECURSOR (OBESITY FACTOR)
LIPOPROTEIN LIPASE PRECURSOR (EC 3.1.1.34)

Table 3.2 Inflammation/Immunity related genes

Gene
SMALL INDUCIBLE CYTOKINE B5 PRECURSOR (CXCL5)
C-C CHEMOKINE RECEPTOR TYPE 2 (C-C CKR-2)
SMALL INDUCIBLE CYTOKINE A8 PRECURSOR (CCL8)
SMALL INDUCIBLE CYTOKINE A2 PRECURSOR (CCL2)
SMALL INDUCIBLE CYTOKINE A12 PRECURSOR (CCL12)
GRANULOCYTE COLONY STIMULATING FACTOR RECEPTOR (G-CSF-R)
INTERLEUKIN-4 RECEPTOR ALPHA
Z-DNA BINDING PROTEIN 1
PLASMINOGEN ACTIVATOR INHIBITOR-2
ALLOGRAFT INFLAMMATORY FACTOR 1
RESISTIN-LIKE ALPHA PRECURSOR (RELMALPHA)
MACROPHAGE INFLAMMATORY PROTEIN 2
MACROPHAGE METALLOELASTASE
MACROPHAGE RECEPTOR MARCO
BETA-HEXOSAMINIDASE BETA CHAIN PRECURSOR
DEDICATOR OF CYTO-KINESIS 2
MEMBRANE COPPER AMINE OXIDASE (EC 1.4.3.6)
MEMBRANE-SPANNING 4-DOMAINS
GROWTH REGULATED PROTEIN (CXCL1)
SIMILAR TO INTEGRIN, BETA-LIKE 1
CALGRANULIN A
SERUM AMYLOID A-1
INTERLEUKIN-1 BETA
T-CELL SURFACE GLYCOPROTEIN CD1D1
COMPLEMENT FACTOR B
COMPLEMENT FACTOR D
INTERFERON-ACTIVATABLE PROTEIN 202B
ARGINASE 1 (EC 3.5.3.1)
EOSINOPHIL-ASSOCIATED RIBONUCLEASE 11
CHITINASE 3-LIKE 3
CHITINASE-3 LIKE PROTEIN 1
ADIPONECTIN
B-CELL LINKER
SIMILAR TO BONE MARROW STROMAL CELL ANTIGEN 2
B-CELL DIFFERENTIATION ANTIGEN LYB-2
NEUTROPHIL GELATINASE-ASSOCIATED LIPOCALIN

Macrophage related genes are in bold.

Table 3.3 Matrix Related Genes

Gene
SERINE (OR CYSTEINE) PROTEINASE INHIBITOR
STEFIN 2
STEFIN 3
ALPHA-1-ANTITRYPSIN 1-1
STEFIN 2-LIKE
GLANDULAR KALLIKREIN K1
COLLAGENASE 3
CATHEPSIN K
STROMELYSIN-1
COLLAGEN ALPHA 2(VI)
COLLAGEN ALPHA 1(IV)
EXTRACELLULAR MATRIX PROTEIN 1
SECRETED MODULAR CALCIUM-BINDING PROTEIN 2
LATENT TRANSFORMING GROWTH FACTOR BETA BINDING PROTEIN 3
COLLAGENOUS REPEAT-CONTAINING
LAMININ ALPHA-2 CHAIN
MATRIX GLA-PROTEIN

Table 3.4 Proliferation Related Genes

Gene
VASCULAR ENDOTHELIAL GROWTH FACTOR RECEPTOR 1 (FLT-1)
CD9 ANTIGEN
BETA PLATELET-DERIVED GROWTH FACTOR RECEPTOR

4. EXTRACELLULAR MATRIX PROTEIN MODIFICATION OF EPTFE PROMOTES FORMATION OF FOREIGN BODY GIANT CELLS AT THE TISSUE-MATERIAL INTERFACE

Introduction

Implantation of medical devices initiates a foreign body response that leads to a coordinated, temporal series of molecular and cellular events ultimately resulting in an avascular, fibrous capsule (Ratner 2002). The formation of this capsule is particularly detrimental to devices such as indwelling sensors that depend on free diffusion of analytes between the surrounding tissue and the sensor (Gerritsen 2000). It has been hypothesized that to increase long-term viability and function of implanted synthetic medical devices, material surfaces should be modified either chemically, biologically, or physically to alter the foreign body response and decrease the chronic inflammatory response (Golden et al. 1990; van Bilsen et al. 2004). One strategy that has been proposed to improve device function is to increase the vascularity in the surrounding tissue as well as decrease the occurrence of capsule formation around the device. Kidd et al. have demonstrated that modification of expanded polytetrafluoroethylene (ePTFE) with extracellular matrix proteins secreted by the human squamous epithelial cell line HaCaT leads to more vessels in the tissue surrounding the material (Kidd et al. 2002; Kidd et al. 2004). Since HaCaT is known to produce an extracellular matrix that is enriched with laminin-5 (Ln-5), Kidd et al. showed that modification of ePTFE with laminin-5 also promotes peri-implant tissue that is more vascularized and is less dense in

structure (Kidd et al. 2005). While this result has prompted the hypothesis that the deposited Ln-5 is acting directly upon endothelial cells (EC) in the surrounding tissue by stimulating EC adhesion, little is known as to mechanisms at the molecular level and whether or not Ln-5 is stimulating an alternative mechanism that leads to improved ePTFE-associated healing.

Previous work comparing the gene expression of tissue surrounding both HaCaT modified-ePTFE and purified Ln-5 ePTFE produced a number of common genes, many of which respond with similar expression patterns (see Chapter 2). These include a collection of genes that are associated with macrophage activation, in particular interleukin-4 receptor (IL-4R) that is expressed on macrophages. These gene expression results suggest a focus toward the macrophage and it's behavior in response to ECM-modified and non-modified ePTFE.

The macrophage has been implicated in having a central role in the tissue response to biomaterials and is a principal cell type of the normal foreign body response (Anderson 1988). It is believed that the presence of synthetic materials often results in the fusion of adhered macrophages into multinucleated foreign body giant cells (FBGCs) as a consequence of the inability of the macrophage to phagocytose the large biomaterial (Ratner 2002). However, the specific role of FBGCs with respect to synthetic biomaterial associated healing remains unclear, with evidence suggesting that FBGCs may play a more active role in the healing response than previously thought. While the prevailing belief that FBGC formation is responsible for the ultimate deposition of a collagenous, fibrous capsule leading to device failure (Sharkawy et al. 1997; Ratner

2002), other studies indicate that FBGC formation may be a means to diminish the chronic inflammatory response (te Velde et al. 1988).

In the present study we used the results of previous gene expression analysis to evaluate whether ECM-modification of ePTFE using both HaCaT conditioned medium and purified Ln-5 influenced macrophage activity when compared to non-modified ePTFE. Our results suggest that ECM modification of ePTFE regulates and promotes FBGC formation at the tissue-material interface through the modulation of the ligand interleukin-4 (IL-4), and the prolonged presence of FBGCs may create an environment conducive to both increased vasculature and improved healing.

Materials and Methods

FBGC Evaluation

Tissue samples that were fixed in Histochoice (AMRESCO Inc., Solon, Ohio) and paraffin embedded were stained with hematoxylin and eosin (H&E) to visualize foreign body giant cells. Using a 40x objective on a Nikon microscope, multinucleated cells at the tissue-material interface were counted over a total length of 1 mm.

RNA Isolation

Samples were removed from RNA*later* solution (Ambion, Austin, TX) and RNA was isolated from tissue associated with the ePTFE implants as previously reported (Schwartz et al. 2005).

Microarray

Microarray manufacture was performed by first coating NaOH-cleaned microscope slides (75 mm x 25 mm) in a solution of 2% 3-aminopropyltrimethoxysilane and 2% (1,4-Phenylene-diisothiocyanate) conversion coating for 10 minutes. After a 5 minute rinse in 100% EtOH, a mouse oligo (70-mer) library from Qiagen (Valencia, CA) containing approximately 32,000 elements was spotted onto the slides using a VersArray ChipWriter (Bio-Rad, Hercules, CA). After spotting, slides are baked for 90 minutes at 90ºC and stored in a dessicator (15% relative humidity) until used. The advantages of

using an oligo library over a cDNA library include more complete annotation of the gene sequences and more uniform hybidization kinetics.

aRNA Amplification

RNA amplification was performed using the Amino Allyl MessageAmp™aRNA kit from Ambion (Austin, TX) that is based on a linear amplification protocol (Van Gelder et al. 1990). Briefly, 2.5 µg of total RNA from each sample was amplified following the provided protocol. During the in vitro transcription section of the protocol, amino allyl modified UTP's were incorporated into the synthesized aRNA. The aRNA was purified using the supplied clean-up columns before dye incorporation.

aRNA Labeling

Alexa Fluor® 555 and Alexa Fluor® 647 (Molecular Probes, Eugene, OR) were resuspended in 6.6 µl of DMSO. Appropriate dyes (1 µl) were added to 2.5 µg of aRNA in 3.3 µl nuclease-free H_2O, 1.6 µl 0.3 M $NaHCO_3$, and 4 µl DMSO. The labeled aRNA samples were then mixed with the corresponding sample. Labeled aRNA was purified using the RNeasy® Kit and following the provided purification protocol. The labeled aRNA was eluted from the columns with 50 µl of nuclease-free H_2O.

aRNA Hybridization

To the 50 µl of labeled aRNA, 10 µl of Cot-1 DNA (1 µg/µl) and 60 µl of 2X Hybridization Buffer (8X SSC, 60% formamide, 0.2% SDS) were added. Printed slides

were washed in 1% SDS solution at 50-60ºC and rinsed in nuclease-free H_2O at room temperature. The washed slides were then placed in a clean hybridization station cartridge assembly and positioned on the GeneTac hybridization station (Genomic Solutions, Inc., Ann Arbor, MI). Each sample was injected onto the slide and allowed to hybridize at 42ºC for 12-16 hours, afterwhich the slide was removed and rinsed with 0.1X SSC. DyeSaver™was then applied to the dried slides.

Scanning of Microarray

Hybridized slides were scanned as previously described (Schwartz et al. 2005). Briefly, an epifluorescence/CCD-based scanner (ArrayWoRx$_e$™, Applied Precision, Issaquah, WA) was used along with spot finding software (MolecularWare, Irvine, CA) to measure individual spot intensities. The data collected was analyzed using an ANOVA-based custom analysis package.

Quantitative PCR

Quantitative PCR was also used to measure gene expression of those genes contained within the oligo library, as well as for genes that were not represented in the library. All primers were designed using the Primer3 program (http://genome.wi.mit.edu/cgi-bin/primer3/primer3.cgi). The primers were designed against the 3' end of the gene, and were constructed to generate products of approximately 100-200 bp in length. Primers were designed to measure the expression of interleukin-4 receptor, interleukin-4, and interleukin-13. Primer sequences for each were:

interleukin-4 receptor (forward: 5'-ctggctgtctcctcttccac-3'; reverse: 5'-cccaggacttaggaacgtca-3'), and interleukin-4 (forward: 5'-tcaacccccagctagttgtc-3'; reverse: 5'-tgttcttcgttgctgtgagg-3'). Primers were purchased from Integrated DNA Technologies (http://www.idtdna.com, Coralville, IA). RNA samples were reverse transcribed using 3 μg of aRNA and random hexamers. Two micrograms of cDNA were run in triplicate for each sample. Each reaction was performed using Qiagen's Quantitect Sybr Green PCR Kit. The reactions were detected by the Rotor-Gene RG-3000 (Corbett Research, Sydney, Australia) using a 72-well rotor. Reaction were first denatured at 95°C for 15 minutes followed by 45 cycles of 15 seconds at 95°C, 15 seconds at 60°C, and 20 seconds at 72°C.

Results

Gene Expression Data

At explant, ePTFE was removed along with all associated tissue. Using a previously described technique, total RNA was isolated from the tissue to be used in gene expression assays (Schwartz et al. 2005). The labeled RNA was hybridized to a microarray consisting of approximately 32,000 unique oligos. The oligos correspond to individual genes that are contained within the mouse genome, and the gene constituents of various pathways (i.e. inflammation) are well represented. Hybridization data was analyzed by ANOVA, and gene expression profiles were generated for all expressed genes. From this data, many genes related to the macrophage were detected as differentially expressed in tissue surrounding both HCM-modified and purified Ln-5 modified ePTFE. Examples of these macrophage related genes are Granulocyte-macrophage colony-stimulating factor receptor (GM-CSF-R), Macrophage inflammatory protein (MIP), and the macrophage receptor MARCO.

Included within the differentially expressed genes was the receptor for interleukin 4 (IL-4R). The gene expression pattern for this gene was similar for both modifications as well as for the non-modified ePTFE. There was an increase in IL-4R activity in the tissue at the day 5 timepoint for non-modified and ECM-modified ePTFE, before undergoing down-regulation at days 14 and 35 (Figure 4.1). The observation that IL-4 exhibited similar expression among all modification groups led to examination of whether or not the ligand to IL-4R changes according to ePTFE modification. As IL-4 interacts with receptor complexes containing the IL-4Rα chain, primers were designed to

measure IL-4 gene expression patterns using quantitative PCR (Q-PCR) (Kelly-Welch et al. 2003; Chatila 2004).

Q-PCR results for the primer sets specific to IL-4 suggest that its expression differs in response to the modification type. After unit normalizing and mean centering, the expression of IL-4 in the HCM-modified samples was up-regulated at days 5 and 14, while the expression at day 35 was down-regulated with respect to the other days (Figure 4.2A). Laminin-5 modified ePTFE showed that IL-4 expression is up-regulated at days 14 and 35 with respect to day 5 (Figure 4.2B). The IL-4 expression pattern of the non-modified ePTFE group was down-regulated at all timepoints when compared to the expression patterns of both HCM-modified ePTFE and purified Ln-5 modified ePTFE (Figure 4.2). These results show that both HCM-modification and purified Ln-5 modification result in modulation of IL-4 expression, however IL-4 expression differs based upon the modification type.

Further examination of the gene expression from the microarray data revealed two other inflammation/immunity related genes that displayed expression patterns similar to IL-4 in all treatment groups. The first of these genes was the VEGF receptor Flt-1. Like IL-4, this gene was up-regulated to the greatest extent at day 14 in tissue surrounding the HCM-modified ePTFE, and at day 35 in tissue surrounding Ln-5 modified ePTFE (Figure 4.3A). The second of these genes was the eosinophil associated ribonuclease 11, whose expression pattern over time was comparable to that of Flt-1 (Figure 4.3B).

FBGC Quantitation

The up-regulation of IL-4 at various timepoints for both ePTFE modification groups suggested that there might be a corresponding increase in FBGC presence (Kao et al. 1995). The differential IL-4 expression between the groups may also suggest that FBGCs appear at distinct timepoints. Tissue sections taken from days 5, 14, and 35 were stained with hematoxylin and eosin to identify FBGC's. Multinucleated cells were counted as FBGC's if the eosin stained nuclei of each section numbered greater than 5 and were arranged in a horseshoe configuration at the tissue-material interface (Figure 4.4). Counting of FBGC's was performed using a 40x water immersion objective, and data was collected for 1 mm along the length of the ePTFE surface. As FBGCs were rarely seen at the day 5 timepoint, FBGC counts are reported from days 14 and 35.

Results from the counting data demonstrate that the number of FBGCs at the interface of HCM-modified ePTFE was highest at the day 14 timepoint with an average of 5.5 ± 1.3 S.E.M. per millimeter of material (Figure 4.5A). The number of FBGCs was significantly higher at day 14 than at day 35 ($p < 0.05$) as performed by Student's t-test. By day 35, the number of FBGCs had dropped to an average of 2.6 ± 0.99 S.E.M. The number of FBGCs surrounding non-modified ePTFE at days 14 and 35 were 1.5 ± 0.66 and 1.1 ± 0.84, respectively. While the day 35 HCM-modified ePTFE sample was not statistically different than the two timepoints of the non-modified ePTFE, it was clear that there were more FBGCs at the interface of the day 35 HCM-modified ePTFE as compared to the non-modified samples.

FBGCs at the tissue-material interface of purified Ln-5 modified ePTFE were highest at the day 35 timepoint with an average of 6.63 ± 1.28 S.E.M. per millimeter of material (Figure 4.5B). The number of FBGCs at day 35 was significantly different when compared to day 14 (2.88 ± 1.13) Ln-5 modified as well as to the controls for each timepoint (1.5 ± 0.66 and 1.1 ± 0.84respectively). Similarly, the number of FBGCs at the interface of HCM-modified ePTFE was significantly higher at day 14 when compared to the same timepoint of purified Ln-5 modified ePTFE. FBGC number was significantly higher at day 35 for the purified Ln-5 modified ePTFE as compared to the number of FBGCs at the interface of day 35 HCM-modified ePTFE.

Discussion

Upon implantation of medical devices, a foreign body response (FBR) is initiated that leads to the eventual formation of an avascular, fibrous capsule and ultimately to device failure. This result has caused researchers to explore the feasibility of modifying implanted materials to increase the number of vessels while at the same time limiting the development of a fibrous capsule. Kidd et al. have demonstrated that culture medium enriched with laminin-5 (Ln-5) secreted from the HaCaT cell line, as well as purified Ln-5 used to modify ePTFE increases the number of peri-implant vessels and decrease the appearance of a dense, fibrous capsule. It is not clear what role the extracellular matrix (ECM) proteins play in this altered healing response. The goal of this study was to use gene expression data generated from tissue samples associated with HaCaT conditioned media (HCM)-modified ePTFE, purified Ln-5 modified ePTFE, and non-modified ePTFE to determine if the molecular foundation of the healing response could shed light on how these ECM proteins alter tissue morphology.

Results from the gene expression data revealed tissue associated with HCM-modified and Ln-5 modified ePTFE expressed common macrophage related genes. These results prompted the evaluation of the inflammatory response surrounding the modified ePTFE. There was a slight increase in macrophage numbers in the tissue surrounding the HCM-modified ePTFE, but no difference in macrophage number in tissue surrounding the Ln-5 modified ePTFE. One of the shared genes, IL-4R, exhibited an expression profile that warranted further examination.

Expression data for IL-4R displayed a similar expression pattern between both modification groups, including the non-modified ePTFE (Figure 4.1). This pattern consisted of an up-regulation of IL-4R at day 5 for all treatment groups, before being down-regulated at days 14 and 35. Similarities in expression pattern of IL-4R led us to measure the expression pattern of known ligands of this receptor. Q-PCR results demonstrated that the expression of IL-4R ligand interleukin-4 (IL-4) differed in response to the modification used (HCM or Ln-5). IL-4 was up-regulated at day 5 in the HCM-modified group, then down-regulated at days 14 and 35. In the tissue surrounding Ln-5 modified ePTFE, the ligand was up-regulated at days 14 and 35 when compared to day 5. Anderson et al. have performed numerous studies demonstrating that IL-4 is capable of inducing FBGC formation (DeFife et al. 1997; Dadsetan et al. 2004). Interleukin-4 is a T helper type 2 (Th-2) lymphocyte product, generated as a result of the alternative macrophage activation pathway.

Based on the fact that IL-4 can induce macrophage fusion and FBGC formation, we returned to the tissue samples to ascertain if there was a correlation between FBGC number and IL-4 expression. Because FBGCs do not stain with the pan-macrophage antibody F4/80, FBGCs were counted by observing their characteristic multinuclear cell morphology using hematoxylin and eosin staining. FBGC numbers correspond to changes in expression of IL-4, as up-regulation of IL-4 expression occurred at days 5 and 14 in tissue surrounding HCM-modified ePTFE and peak FBGC numbers was seen at day 14. Likewise, IL-4 expression and FBGC number were both at their greatest at day 35 of Ln-5 modified ePTFE.

Two statements can be made based on the IL-4R/IL-4 data. First, the similarity in gene expression of IL-4R between all modification groups suggests that IL-4R is up-regulated in response to material implant, and the expression of IL-4R is independent of ePTFE modification. The second statement is that FBGC formation is modulated by changes in expression of IL-4 as a result of ePTFE modification.

It has been hypothesized that HCM and Ln-5 modification of ePTFE promotes peri-implant vascularity due to direct interactions between the ECM proteins and endothelial cells (Kidd et al. 2005). The results of this study present an alternate mechanism through which HCM and Ln-5 alter ePTFE-associated healing, generating a new hypothesis that the stimulation of FBGC formation at the tissue-material interface decreases the formation of a fibrous capsule allowing for the establishment of tissue vascularity. Support of this hypothesis is provided by the fact that ePTFE modifications (HCM and Ln-5) that have been shown to increase vascularity and decrease fibrous capsule formation also generate more FBGCs at the material interface. The tissue-material interface of non-modified ePTFE contained few FBGCs and the surrounding tissue was characterized as being dense and fibrous. This hypothesis is also supported by gene expression analysis showing that expression of IL-4R ligand IL-4 correlates with the presence of FBGCs. Studies by van Luyn et al. have shown that macrophage recruitment, activation, and tissue incorparation to biomaterials is T cell dependent. The results of their studies detailed the fact that crosslinked collagen implanted into T cell wildtype mice had better tissue incorporation and the presence of FBGCs, while T cell

knockout mice lacked tissue incorporation, macrophage recruitment, and FBGC appearance at the site of implant (van Luyn et al. 1998).

There have been reports of deleterious effects on biomaterials as a result of FBGC formation, however the physiological significance of these multinuclear cell types is still unclear (Wiggins et al. 2001; McNally et al. 2003). Evidence exists that when taken together may help to explain how FBGCs create an improved healing response associated with ECM-modified ePTFE. Expression of IL-4 is known to have an inhibitory effect on pro-inflammatory cytokines like interleukin-1 (IL-1), interleukin-6 (IL-6), interleukin-10 (IL-10), and tumor necrosis factor-α (TNF-α) (te Velde et al. 1988; Schachtrupp et al. 2003). The result of the inhibition of these cytokines involved in the chronic inflammatory response is the ultimate decrease in fibrotic scar tissue. IL-4 also induces a state of alternative activation of macrophages through the Th2 pathway that leads to eventual formation of FBGCs (Anderson 2000). Alternatively activated macrophages have been proposed to have roles in angiogenesis and tissue remodeling (Kodelja et al. 1997; Mosser 2003). Vignery et al. reported that FBGCs are a differentiated cell type and the fusing macrophages undergo biochemical and morphological alterations to prepare them for specialized function, particularly that of wound healing, angiogenesis, and tissue remodeling (Vignery et al. 1989).

Two other genes that were categorized with IL-4R as being involved in inflammation/immunity further support the above claim that the appearance of FBGC's is the result of an alternative, Th2 pathway, and that foreign body giant cells are responsible for the promotion of an increase in vascularization. The first of these genes is the

vascular endothelial growth factor (VEGF) receptor, Flt-1. VEGF is a potent stimulator of angiogenesis, especially in wound healing, that binds to Flt-1 (Li et al. 2003). Gene expression data for Flt-1 reveals that it is up-regulated at day 14 in the HCM-modified ePTFE group, whereas its highest expression level was measured at day 35 in the Ln-5 modified group. The correlation between gene expression of Flt-1 and FBGC number suggests that FBGCs could be responsible for increased vascularity in peri-implant tissue. As was mentioned in the Cellular Response section of Chapter 1, as well as with reports from Vignery et al., FBGCs play a role in promoting angiogenesis.

The second gene examined was Eosinophil Associated Ribonuclease 11. Expression of this gene matched the expression pattern of Flt-1, and also corresponded to foreign body giant cell number. The presence of eosinophils supports the hypothesis that ECM-modification of ePTFE leads to an alternative activation pathway as eosinophils are recruited to the site of Th2 type responses (Rothenberg et al. 2006). It is unclear as to the role of this gene in the context of wound healing, however, the increased trancscript number of this eosinophil ribonuclease suggests that there are more eosinophils being recruited to tissue surrounding ECM-modified ePTFE.

The exact mechanism for the induction of the alternate activation pathway as a result of ECM modification of ePTFE is still unclear, however the results of this study can be used to make certain assumptions. Upon implantation, a layer of host proteins coats the implanted material, of which fibrinogen has been identified as the predominate protein of this layer (Vroman et al. 1980). As this protein layer is adsorbed to the surface of the material before any immune cells or macrophages, it is believed that interaction

between these cells is with the adsorbed protein layer rather than directly with the material. As such, when antigen-presenting cells encounter the implant they present a specific sequence to T cells that dictates the ultimate cellular response. It has been hypothesized by others that the nature of the protein layer is responsible for the subsequent cellular activity associated with implanted materials (Hu et al. 2001). Native adsorption of fibrinogen has been shown to illicit a pro-inflammatory response (Tang et al. 1995). I hypothesize that based on clear Th2, alternative activation responses elicited from the molecular data, adsorption of proteins from our ECM modification technique alters the sequence presented to naïve T cells such that a Th2 pathway is followed. As mentioned previously, this pathway is associated with attenuation of inflammation and tissue repair.

In conclusion, gene expression data from tissue surrounding ePTFE that was modified with either HaCaT conditioned media of purified laminin-5, shown to improve ePTFE associated healing, directed us to investigate the influence that multinuclear foreign body giant cells have on this altered healing response. FBGCs were found to exist to a higher extent at the tissue-material interface of ECM-modified ePTFE than at the interface of non-modified ePTFE (Figure 4.4). The presence of the FBGCs correlated with the expression of IL-4, a cytokine known to induce FBGC formation. Multiple studies suggest that fusion of macrophages into FBGCs create a cell type that has capabilities to direct a more normal healing response. Future considerations for the design of medical devices constructed from synthetic materials may involve creating conditions that favor FBGC formation.

Future Studies

To further strengthen the argument that ECM modification leads to an alternative activation pathway, more Q-PCR is required to measure expression of genes that were either not on the array or the transcript level was insufficient for detection on the microarray as was the case for IL-4. Initial genes selected for analysis would be those that were described in Chapter 1, especially the biological markers MMR and MHC class II to differentiate between classically and alternatively activated macrophages.

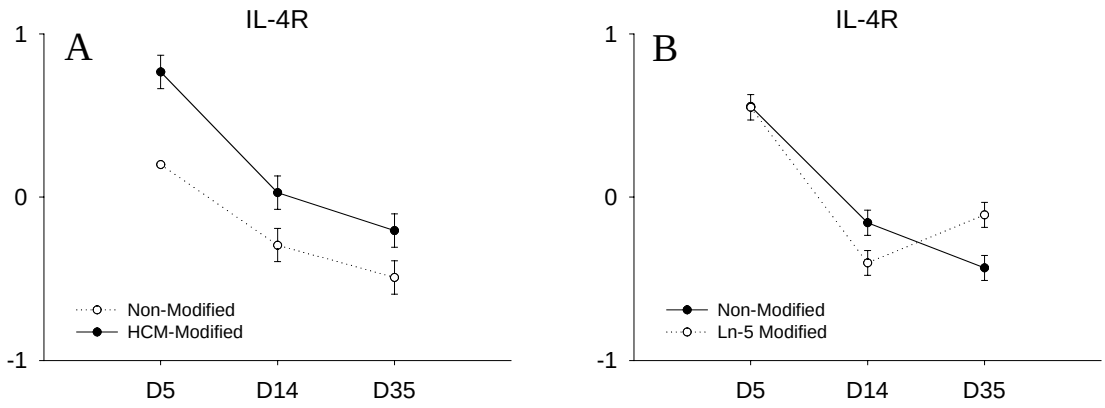

Figure 4.1 Gene expression profile of IL-4R from the microarray experiment, exhibiting an up-regulation at day 5 for the ECM-modified sample when compared to the non-modified ePTFE. Expression of IL-4R at days 14 and 35 were down-regulated in both A) HCM and B) Ln-5 modification with respect to expression at day 5.

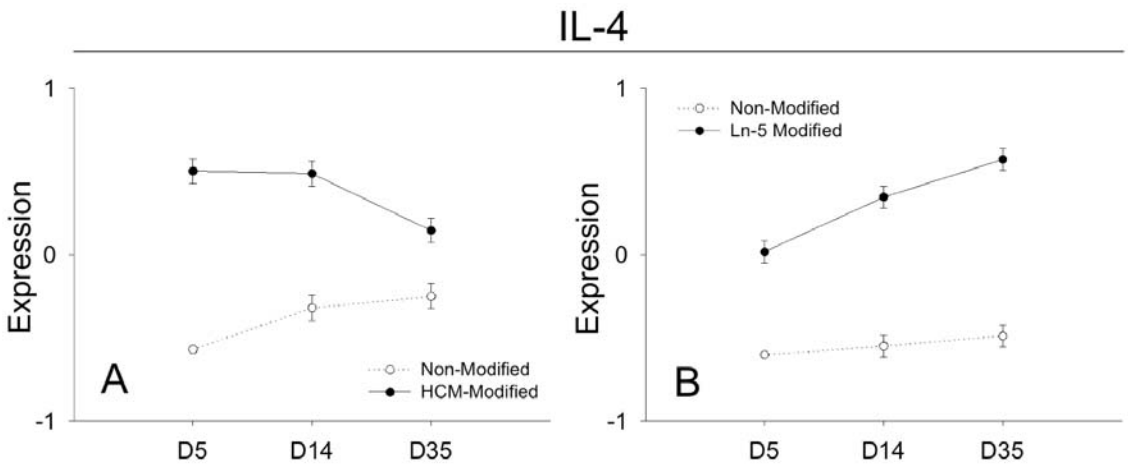

Figure 4.2 Q-PCR results for IL-4. A) Expression of IL-4 surrounding HCM-modified ePTFE was upregulated at day 5. B) IL-4 expression in tissue surrouding Ln-5 modified was up-regulated at days 14 and 35 as compared to day 5.

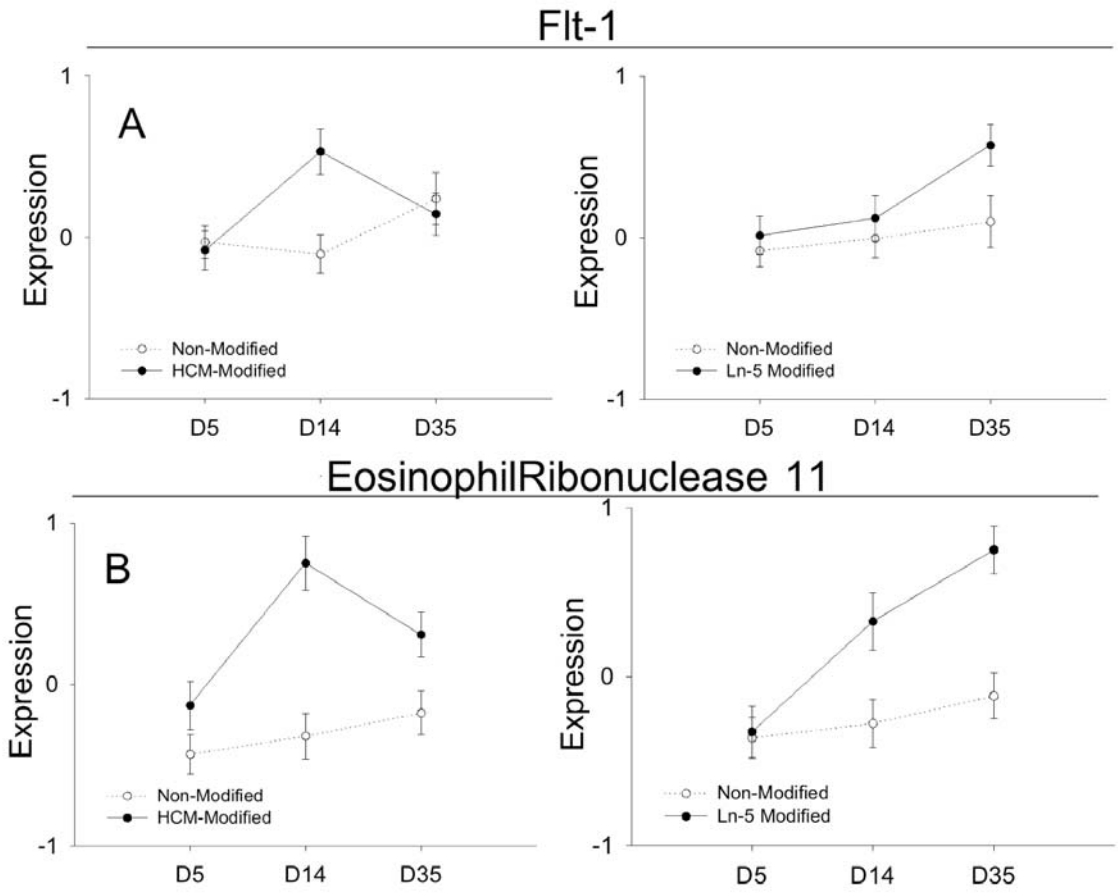

Figure 4.3 Gene expression profiles for A) Flt-1 and B) Eosinophil Associated Ribonuclease 11. Expression of both genes was up-regulated at day 14 in tissue surrounding HCM-modified ePTFE. The expression pattern for peri-implant tissue associated with Ln-5 illustrated that both genes are up-regulated at day 35.

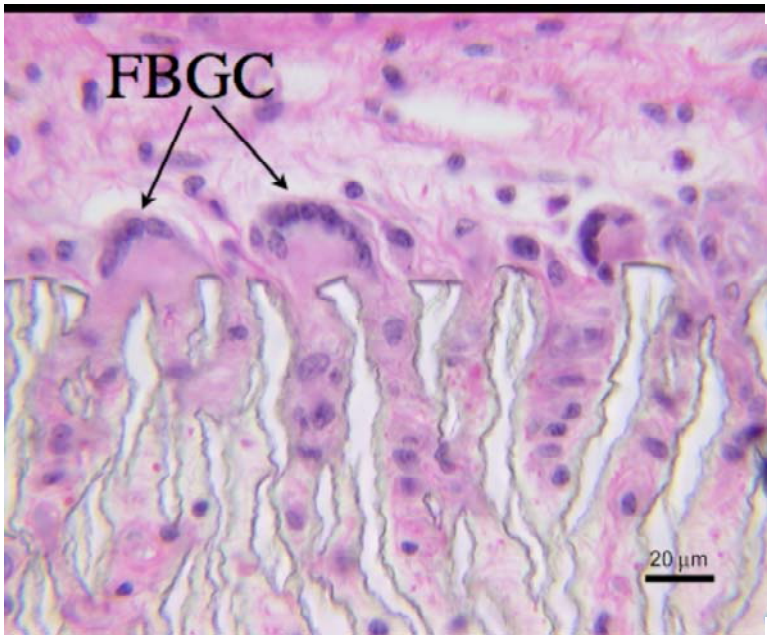

Figure 4.4 Light micrograph of tissue associated with HCM-modified ePTFE stained with hematoxylin and eosin. The multinucleated foreign body cells are apparent at the tissue-material interface and have a distinctive horseshoe appearance.

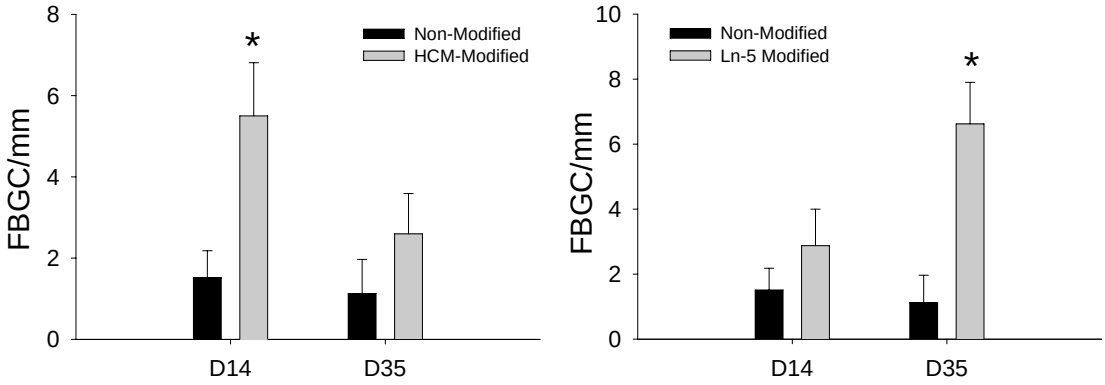

Figure 4.5 Average FBGC count at the tissue-material interface. A) Day 14 HCM-modified ePTFE had an average of 5.5 FBGC's at the interface. B) The tissue-material interface of Ln-5 modified ePTFE had an average of 6.63 FBGCs at day 35. Values are the mean number of FBGC's per 1 mm length of ePTFE (± SEM).

5. SUMMARY AND CONCLUSIONS

Millions of medical devices constructed with biomaterials are implanted into patients each year (Lysaght et al. 2000). The purpose for implanting medical devices is to recover, repair, or replace diseased or damaged tissue systems. Examples of these devices include vascular stents, indwelling glucose sensors, surgical sutures, and orthopedic replacements. Upon implantation, all synthetic biomaterials elicit an abnormal healing outcome that has come to be known as the foreign body response (FBR). The FBR is characterized by the establishment of a highly cellular, fibrous capsule, that is relatively devoid of blood vessels. Current dogma attributes this response to the deposition of a host protein layer upon the implant surface, thus confusing adhered macrophages that do not recognize the unnatural protein coating. As a result, macrophages that typically phagocytose foreign material attempt to ingest the entire device. Through a process called frustrated phagocytosis, the macrophages spread over the material surface, and fuse into multinuclear foreign body giant cells (FBGCs). Little is known about FBGC behavior in terms of life span and their relevance to wound healing, however there are reports of deleterious effects as a result of the presence of FBGCs, e.g. material degradation. Overall, the consequences of the FBR add up to decrease the long-term function and success of the implanted device.

Because of the negative results associated with FBR and the formation of the avascular fibrous capsule, several groups have proposed modifying biomaterials to improve the healing response. These include chemical, structural, and biomolecule modification of biomaterials. Modification of the materials is an attempt to increase

vessel number around the implant, thought to be essential for improved device performance, especially when analyte transport between device and tissue is necessary (Ratner 2002; Ward et al. 2003). Porosity has been shown to affect the level of vascularity in the tissue surrounding the implant (Salzmann et al. 1997).

Previous work done in our laboratory has investigated and demonstrated that modification of expanded polytetrafluoroethylene (ePTFE) with extracellular matrix proteins promotes an increase in vascularity and a reduced fibrous capsule in the surrounding tissue (Kidd et al. 2002; Kidd et al. 2003; Kidd et al. 2004). From these studies, laminin-5 enriched HaCaT conditioned media and purified laminin-5 were both found to stimulate a pro-vascular, less fibrous response in peri-implant tissue. The exact mechanism for this observation is unknown.

The goal of this dissertation was to examine the healing response associated with subcutaneously implanted ePTFE that was non-modified, HCM-modified, or purified Ln-5 modified at the molecular level. Three specific aims were developed to gain a better understanding of the altered healing response with the ultimate goal to reveal the underlying mechanisms that impact biocompatibility. The first aim was devised to measure the gene expression of tissue surrounding HCM-modified ePTFE and compare it to non-modified ePTFE using cDNA microarrays. The hypothesis driving this aim was that gene cohorts could be segregated based upon function, e.g. angiogenesis, inflammation, etc., thus providing new insights into how genetic pathways differ between the classic foreign body response and the altered response brought on by HCM modification. Aim #2 focused on the concept that modification of ePTFE with both

HCM and purified extracellular matrix protein laminin-5, a principal constituent of HaCaT conditioned media, stimulate peri-implant tissue that is more vascular in nature. The goal, then, of aim #2 was to measure gene expression patterns in tissue surrounding both HCM and laminin-5 modified ePTFE, with the hypothesis that laminin 5 is responsible for the observed tissue response. Aim #3 focused on utilizing the results of the first two aims to explain how regulation of gene activity is responsible for the altered healing response. It was hypothesized that the output from aims #1 and #2 would implicate a molecular pathway or cellular process that would shed light on how extracellular matrix protein modification improves ePTFE associated healing.

Use of gene expression assays to examine ePTFE associated healing

Within each cell is a full set of chromosomes, each containing identical genes. Of these genes, only a fraction are expressed at any given time. It is the subsets of genes that are being expressed that impart unique properties, giving rise to different cell types. The term gene expression defines the transcription of information from the DNA into mRNA. Translation of proteins from mRNA then takes place, and it is the proteins that are responsible for much of the cellular function. Regulation of gene expression is a tightly controlled process that can be modulated according to the needs of the cell, or through external stimuli. Gene expression analysis, particularly with the use of DNA microarrays, was chosen to measure the levels of mRNA that were transcribed from tissue surrounding implanted ePTFE to gain awareness of how cells respond to the presence of the ePTFE.

The gene expression experiment to address the hypothesis of aim #1 used a cDNA microarray that was constructed using a library consisting of approximately 15,000 unique elements purchased from the National Institutes of Aging. A time course study was established at days 5, 7, 14, and 35 with ePTFE that was either non-modified or HCM-modified. An ANOVA based analysis package, developed by Kevin Greer and adapted from Kerr et al., was used to generate gene expression data (Kerr et al. 2000). Aside from producing expression data, this analysis package accounts for sources of possible error inherent with microarray assays, for instance differences in hybridization kinetics and dye incorporation.

Expression data was clustered based on similar patterns of expression. Results outlined in Chapter 2 reveal that there were 6 overall patterns of expression associated with the HCM-modified ePTFE, while there were only 3 unique patterns of expression in tissue surrounding non-modified ePTFE. Concomitant with these results, a principal expression pattern related to the non-modified group displayed down-regulation across time, while those genes were varied in regulation in tissue related to the HCM-modified ePTFE. In the context of gene expression, two interpretations can be made to explain these observed results. The first interpretation is that the cells surrounding the HCM-modified ePTFE and associated with altered healing respond to the implantation of ePTFE by becoming more active and dynamic in terms of gene transcription. Alternatively, a second interpretation is that the predominate cell type or types present around the two modification groups are different, and that the tissue surrounding the non-modified ePTFE drifts toward an environment comprised of limited and less diverse cell

types that are only involved in one aspect of the healing response. A candidate cell type is the fibroblast, the cell responsible for synthesizing the characteristic collagenous capsule around implanted materials. It follows from this reasoning that the dynamic gene expression surrounding the HCM-modified is due to cells of multiple sorts participating in various aspects of the healing response such as angiogenesis and tissue remodeling.

As stated, the goal of aim #1 was to assign function to genes based on clustering and similar gene expression. It turned out that the expression of these genes was more complex than originally believed, and there was a tremendous amount of overlap among genes with known function and the clusters that they segregated into. This made it impossible to designate clusters to specific processes, however it provided a realistic outlook of what microarrays can and can't accomplish. As microarrays were beginning to be developed, they were touted as being the definitive assay for revealing molecular pathways. This is no longer the case, although by no means are microarrays are uninformative. To the contrary, microarray data can reveal vast amounts of valuable information if the investigator knows what to look for. This first experiment was a prime example that instead of focusing on specific genes and to what extent they are up or down-regulated at a particular time, what may be just as informative to assessing tissue states is the overall clustering and expression patterns associated with the tissue phenotype.

Another important realization that came about from the first study's results is that when performing microarray experiments, it is crucial to do so over a timecourse. There were numerous examples from study #1 where if a molecular assessment was made at

just one timepoint, it would appear as if there was no change in gene expression between modification groups. However, if the same gene was examined over the course of the experiment it became apparent that there was differential expression between the HCM and non-modified ePTFE.

It is also necessary to point out the importance of resolution of the timeline, that is, at what time points are the samples to be analyzed. For this group of studies, days 5, 14, and 35 were chosen based on the occurrence of relevant physiological events, those being: acute inflammation, vascular maturity, and tissue remodeling, respectively. Gene expression results are a reflection of the tissue and cellular state at the time of measurement. Important genetic transitions may be missed if there are wide gaps between time points. Ideally, samples would be analyzed as frequently as possible, so as to capture as much genetic information as possible that corresponds to tissue phenotype.

The experimental design of aim #2 provided an opportunity to use microarrays to their maximum potential. Because the tissue responses to ePTFE that had been modified with both HCM and Ln-5 was extremely similar, it was believed that those genes most responsible for the observed outcome would be evident. Microarray analysis has been shown to be highly discriminatory between tissues with like morphologies, and the degree of discrimination increases as the number of tissues with different genotypes but similar phenotypes increases. This has proved useful as a diagnostic tool, especially in the area of tumor diagnostics, where classification by histology is difficult and better classification may mean improved treatment regimens (Alizadeh et al. 2001).

Prior to the microarray experiment to address aim #2, the decision was made to use arrays that were constructed with 70-mer oligos. Oligo arrays are advantageous for two reasons. 1) They are more specific due to reduced common sequence with other oligos thus preventing cross-hybridization and 2) the oligos are better characterized and more is known about their function. After hybridization and analysis, it was determined that there were 595 differentially expressed genes for tissue around the HCM-modified ePTFE, while 523 genes were differentially expressed in tissue surrounding the Ln-5 modified ePTFE. When those two groups of genes were compared, 178 genes were shared. Although these genes were expressed in both modification groups, it did not necessarily mean that they were expressed similarly. In fact, there were numerous differences in gene expression over time between the same genes connected with both treatment groups.

Functional categories used for study #1 were again used and assigned to shared genes. The category containing the most genes was general cellular activity. Because of the complexity of these genes and the relative lack of obvious relationship to the healing response, attention was turned to the next most prevalent category, inflammation and immunity. This group consisted of 37 genes, with a quarter of the genes related specifically to macrophages. With the knowledge that macrophages are an integral part of the foreign body response, the possibility that macrophage activity and behavior is being regulated by both modification groups seemed like a path worthy of further investigation.

Study #3 began with the simple approach of counting the total number of macrophages surrounding the implanted ePTFE that was non-modified, HCM-modified, or Ln-5 modified. This method was taken because a significant number of genes related to the macrophage were revealed by the results of aim #2, and it was believed that macrophage gene regulation might be responsible for the altered healing response. Macrophage number associated with all treatment groups was uneventful, with little observed difference. There was a slight increase in macrophage presence associated with the HCM-modified ePTFE, a result consistent with prior reports by Kidd, et al. (Kidd et al. 2005). The imperceptible relationship between macrophage number and altered healing response was the motivation to further examine the expression data for a genetic explanation of the different tissue response.

Examination of the macrophage related genes uncovered a receptor and ligand pair has been implicated in the formation of foreign body giant cells (FBGCs), a multinuclear cell type. The receptor and ligand were interleukin-4R (IL-4R) and interleukin-4 (IL-4). The FBGCs were not initially examined in this study since our mouse macrophage anti-body, F4/80, does not stain FBGCs. To determine if FBGC presence was in some way related to the observed tissue response, sections stained with hematoxylin and eosin were used to identify the multinuclear configuration that is characteristic of FBGCs. Interestingly and unexpectedly, FBGC presence was highest in tissue associated with ECM-modified ePTFE, and there appeared to be a temporal component to peak FBGC levels. This result was unexpected because much of what is reported about FBGCs is that they have a negative impact on implanted materials.

However, recent reports are shedding new light on the role of FBGCs as part of the foreign body response, and these cells may be the body's attempt to modulate the chronic inflammatory response.

Returning to the gene expression data related to IL-4R and IL-4, the expression pattern of the IL-4R was similar regardless of treatment. IL-4R was up-regulated at day 5 and then down-regulated at days 14 and 35. This suggests that in response to implanted materials, macrophages turn on transcription of this receptor with the assumption that it is presented on the cell surface. An attempt to stain IL-4R to determine if it is expressed on the surface of resident macrophage was unsuccessful, most likely because the anti-body used was not optimized for immunohistological applications. Microarray generated IL-4R expression was confirmed by quantitative PCR.

Expression data for IL-4, predominately secreted by T cells of the alternatively activated Th-2 pathway, may explain the observed temporal appearance of peak FBGC values. At the tissue-material interface of HCM-modified ePTFE, FBGCs were highest at day 14. Expression of IL-4 was maximally expressed at days 5 and 14, while it's expression was down in comparison at day 35, corresponding to FBGC number. The interface of Ln-5 modified ePTFE exhibited the highest number of FBGCs at day 35. Correspondingly, IL-4 expression increased with time. I propose that regulation of IL-4 by the ePTFE treatments is responsible for the observed FBGC formation. Increased numbers of foreign body giant cells linked to tissue samples that are more vascular and less dense has interesting implications for how materials in general, and ePTFE specifically may be modified to promote improved healing.

Implications that the results of this dissertation have on future material modifications

Because the tissue response to implanted materials is the result of a highly coordinated and tightly regulated series of molecular events, design of new devices and material modifications must primarily address factors at the molecular level. The results of the three aims presented in this dissertation build upon each other to offer a molecular framework that can be used to improve polymer-associated healing. Although only two material modifications were examined here, the lessons learned should extend to many implanted materials.

At the very least, I propose that successful implanted materials or devices must stimulate a tissue response that is more dynamic at the transcription level. Results supporting this claim were presented in Chapter 2, and touched upon in the previous section. More transcriptional activity reflects a tissue that is able to participate in normal processes and is an attractive environment for those medical devices that need to be able to communicate with adjacent tissue or share in the exchange of various analytes. An example of a device that would benefit from this type of dynamic tissue is an indwelling glucose sensor. For proper device function, glucose must be able to pass from the tissue through the porous sensor membrane. Reichert et al. demonstrated that this process is significantly hindered by the presence of a fibrous capsule (Sharkawy et al. 1998). Results from Chapter 2 suggest that the formation of a fibrous capsule is characterized by austere gene expression.

The second implication that the work of this dissertation has on polymer associated healing stems from Chapters 3 and 4. These results have to do with inflammation, and in particular the modulation of macrophages. It appears that increased foreign body giant cell number is linked to a desired healing response. It is necessary to mention that this was an unforeseen finding, and was counter to what was believed would be observed prior to performing these experiments. Much of the commentary that is presented about material-associated healing treats FBGC presence as the endstage of the foreign body response and the principle cell type leading to device failure. Contrary to this position, the results of this research demonstrate that directing FBGC formation at the tissue-material interface may be a strategy to improve device-tissue interactions.

Promotion of foreign body giant cells at the tissue-material interface: a good idea?

With numerous reports of the deleterious impact that FBGC's have on implanted materials, it may seem foolish to propose a strategy that encourages the formation of FBGCs at the tissue-material interface. However, the data presented in this dissertation along with observations made by other studies suggest that FBGC presence may not be a simple indicator of the beginning-of-the-end of implanted device function, but instead is a complex, differentiated cell type capable of participating in beneficial wound healing processes. Even those reviews claiming that FBGCs are accepted to be a cell type that should be avoided at the tissue-material interface admit that little is known about the role they play in wound healing. The fact that more FBGCs were present at the interface of

ePTFE that was ECM modified, and that the surrounding tissue was more vascularized and less dense is reason enough to re-think the conventional position of FBGCs.

It has been proposed that FBGC formation may be the body's attempt to attenuate the chronic inflammatory response (Dadsetan et al. 2004). The chronic inflammatory response is characterized by the presence of macrophages, monocytes, and mononuclear cells. As with normal wound healing, the macrophage generates and secretes cytokines that signal fibroblasts to produce connective tissue. It is believed that during material-associated healing macrophages produce an abundance of these signaling molecules, causing fibroblasts to proliferate and synthesize collagen, leading to the formation of the fibrous capsule (Ratner 2002). Interleukin-4 has been shown to induce FBGC formation as well as inhibit pro-inflammatory cytokine secretion, many of which are produced by macrophages. Thus, increases in interleukin-4 expression and FBGC formation in tissue surrounding ECM-modified ePTFE are likely responsible for the prevention of fibrous capsule synthesis.

Future studies to prove that FBGC formation is responsible for the altered and improved ePTFE-associated healing response can be taken in one of two directions. One direction is to knock out or knock down IL-4 expression preventing the formation of foreign body giant cells. The other direction is to implant non-modified and ECM-modified ePTFE into SCID mice. Since IL-4 is predominately produced by T cells, performing these experiments in SCID mice will have the same effect as knocking out IL-4 activity.

Final thoughts on the role of HCM and Ln-5 modification in altered ePTFE-associated healing

It has previously been hypothesized that the extracellular matrix modification of ePTFE with HaCaT conditioned media or purified laminin-5 increases tissue vascularity through vessel stability (Kidd et al. 2005). This is a valid assumption as laminin-5 is a basement membrane protein that has been shown to promote adhesion complexes in endothelial cells, as well as interacting with vascular smooth muscle cells via the $\alpha_6\beta_4$ integrin pair (Homan et al. 1998). The findings presented in this body do not dispute this claim; rather they extend upon what can be inferred as a result of the altered tissue response because of protein modification.

From the results presented here, I propose that modification of the ePTFE with these extracellular matrix proteins acts to promote the alternative activation of macrophages that are in contact with the material. Alternatively activated macrophages, those associated with the Th-2 pathway, lack the ability to kill intracellular microbes as classically activated macrophages do, but have been found to mediate wound healing, angiogenesis, and extracellular matrix deposition (Mosser 2003). Support for differential macrophage activation comes from the expression data of interleukin-4, a characteristic cytokine of the alternative activation pathway. Interleukin-4 is dynamically expressed in the ECM-modified groups, but is down-regulated in the non-modified groups, highly suggestive of the different macrophage activation pathways. How ECM modification causes the shift in macrophage activation is unclear, however one explanation is that ECM protein deposition disrupts the adhesion of the host protein layer (fibrinogen) that is

typically formed on implanted materials. Macrophages that do not recognize the proteins associated with this layer become classically activated and participate in tissue destruction, leading to collagenous scar formation. ECM modification may influence the alternative activation pathway, causing macrophages to engage in normal wound healing and the establishment of healthy, active tissue.

Conclusions

The results presented in this dissertation provide new understanding into the molecular profile of tissue undergoing polymer-associated healing. Biomedical devices fail because of the formation of an avascular, fibrotic capsule due to an altered healing reaction termed the foreign body response. The goal of material modifications, whether physical, chemical, or biological, is to promote a wound healing event that produces a more natural tissue. This is critical to the long-term success and function of implanted devices. Often modifications are made on a trial and error basis, with incremental steps taken between major advances. An understanding of the molecular underpinnings of the foreign body response in comparison to normal healing will lead to more rapid advancement of successful material modifications and the accelerated realization of the ultimate objective of implanted medical devices; improved quality of life for the recipient.

A dramatic and unorthodox proposal for improving polymer-associated healing was made based on the results of the studies presented here. Molecular and cellular data suggest that the existence of foreign body giant cells at the tissue-material interface is associated with a desired tissue response. Although these studies were performed solely with ePTFE as the material model of implanted devices, it is believed that this proposal will extend to other materials used to construct medical devices.

Future studies will need to be performed to uncover the exact mechanism responsible for promoting foreign body giant cell formation. Also, these studies were only carried out to five weeks implantation. Experiments must be done to determine if

ECM-modification of ePTFE is able to sustain improved device function past the experimental endpoint utilized here. Regardless, the body of work presented as part of this dissertation will advance the field of biomaterials and lead to significantly improved implantable medical devices.

Appendices

Appendix A: Subcutaneous implantation of ePTFE

1) After ECM-modification, cut 2 cm length ePTFE lengthwise as shown.

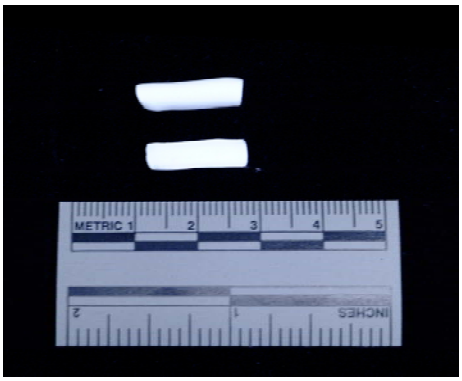

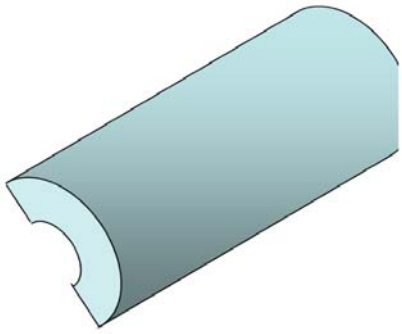

2) Sterile surgical instruments

- Sterile latex gloves
- Sterile saline in plastic Petri dish
- Michel suture clips
- Fine scissors, hemostats, forceps

3) Anesthetize mouse with 2.5% Avertin working solution (0.15ml/10g body wt.).

4) Remove hair on entire back of mouse with Nair cream depilatory.

5) Spray and wipe back of mouse with 70% EtOH.

6) Lift skin and make 2 small cuts on both sides of the spine near the tail, and 2 small cuts on both sides of spine near the neck.

7) Using the hemostats, create a tunnel underneath the skin from one opening to the other.

8) Grab the end of the modified ePTFE with the hemostat, and pull the ePTFE back under the skin. Make sure lumen side of ePTFE is positioned down.

9) Close cuts with Michel suture clips. Do not place clips too close to the implanted ePTFE. Final position should appear as shown below.

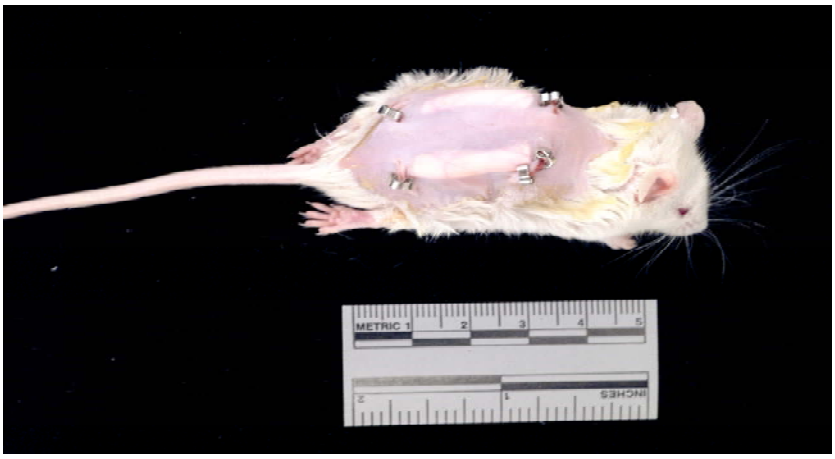

Appendix B: Processing explanted ePTFE for RNA isolation

1) Anesthetize mouse with 2.5% Avertin working solution (0.15ml/10g body wt.).

2) Remove Michel suture clips if they are still present.

3) Using scissors, trim skin away from ePTFE.

4) Remove ePTFE, taking only tissue that is closely associated with the material.

5) Cut the ePTFE into thin strips, placing them into RNA*later* solution.

6) Prior to the addition of liquid nitrogen, remove all RNA*later*.

7) Add liquid nitrogen and ePTFE-tissue in mortar and pestle.

8) Grind frozen ePTFE and tissue into as fine a powder as possible.

9) Mix ground material with RNA Bee solution.

10) Place solution into 15 ml round bottom tube.

11) Using a tissue tearer such as the one pictured below, further grind and mix the solution to lyse the cells.

12) Continue on with RNA isolation protocol.

Appendix C: Microarray aRNA hybridization protocol

Materials

Ambion, Amino Allyl MessageAmp™ aRNA Kit (product #1752)
2-5 μg Total RNA
2-4 RNase free beakers
0.3M $NaHCO_3$ (25 mg/ml)
Printed slides
RNeasy® Mini Kit (50) (Qiagen, product #74104)
Alexa Fluor® 555 and Alexa Fluor® 647 decapacks (Molecular Probes, product #A32755)
DMSO
RNase free 10%SDS
RNase free 20x SSC
RNase free H2O ~500 ml
Cot-1 DNA (10 μg/μl)
DyeSaver™ (Genisphere, product #Q500500)

Procedures

Note: first time users should read the Ambion instructions as they provide critical, detailed information regarding the procedure and heating methods.

RNA Amplification (each step performed for each RNA sample to be amplified)

A. First-Strand cDNA synthesis (RT)

1. Label 2 Tubes for each sample to be amplified.

   Tube 1 add:
   2.5 μg total RNA
   1 μl T7 Oligo(dT) Primer

   Adjust volume to 12 μl with Nuclease free water

2. Incubate for 10 min at 70˚C, then place on ice. While tube 1 is incubating, proceed to Tube 2 (prepare at room temperature, mix well, and place on ice).

   Tube 2 add:
   2 μl 10x First Strand Buffer

1 μl Ribonuclease Inhibitor
4 μl dNTP mix

3. Add Tube 2 (7 μl) to Tube 1 and incubate at 42˚C for 5min.

4. Add 1 μl Reverse Transcriptase to each reaction.

5. Incubate for 2hr at 42˚C, remove and place on ice.

B. Second-Strand cDNA Synthesis.

1. Mix the following reagents in order (on ice):
   (20 μl) cDNA sample (from step 5 above)
   63 μl Nuclease free water
   10 μl 10X Second Strand Buffer
   4 μl dNTP Mix
   2 μl DNA Polymerase
   1 μl RNase H

2. Incubate for 2hrs at 16˚C. (If using the thermal cycler, turn heated lid off)

3. Proceed to cDNA purification. Or you can stop at this point and freeze reactions at -20˚C.

C. cDNA Purification (requires portion of the kit stored at 4˚C).

1. Preheat Nuclease-free water to 50˚C.

2. Equilibrate each cDNA filter Cartridge by adding 50 μl of cDNA Binding Buffer and incubate for 5 minutes at room temperature.

3. Add 250 μl of cDNA Binding Buffer to each sample (step 2, sect. B).

4. Apply mixture to an equilibrated cDNA Filter Cartridge.

5. Centrifuge for 1 min at max speed.

6. Discard flow through.

7. Add 500 μl of cDNA Wash Buffer to each Filter Cartridge.

8. Centrifuge for 1 min at max speed.

9. Discard flow through.

10. Spin for an additional minute to remove residual ETOH.

11. Transfer cDNA Filter Cartridge to a new collection tube.

12. Add 9 µl warm nuclease free water (Elution).

13. Let stand 2 min at room temp.

14. Centrifuge for 1 min at max speed.

15. Repeat steps 12 – 14.

16. Volume should be 14-16 µl at this point, if not, adjust volume using nuclease free water and proceed to In Vitro Transcription. Or, procedure can be stopped and samples stored at -20˚C.

D. In Vitro Transcription to Synthesize aRNA

1. Assemble the following transcription reaction components (40µl total) in the following order at room temperature and mix well:
   - 14 µl double stranded cDNA (step 16, sect. E)
   - 3 µl aaUTP solution
   - 12 µl ATP, CTP, GTP mix
   - 3 µl UTP solution
   - 4µl T7 10X Reaction Buffer
   - 4µl T7 Enzyme Mix

2. Incubate the reaction in an oven for 6-14 hr at 37˚C.

3. Add 2 µl of DNase I to each reaction, mix, and incubate 30 min at 37˚C.

E. aRNA Purification (requires portion of the kit stored at 4˚C).

1. Preheat Nuclease-free water to 50˚C.

2. Prepare aRNA Filter Cartridge/Collection Tube assembly for each reaction

3. Add 58 µl of nuclease free water to each aRNA sample (step 4, sect. D).

4. Add 350 µl of aRNA Binding Buffer to each aRNA sample.

5. Add 250 μl of 100% ethanol to each aRNA sample
6. Apply mixture to an equilibrated aRNA Filter Cartridge.
7. Centrifuge for 1 min at max speed.
8. Discard flow through.
9. Add 650 μl of aRNA Wash Buffer to each Filter Cartridge.
10. Centrifuge for 1 min at max speed.
11. Discard flow through.
12. Spin for an additional minute to remove residual ETOH.
13. Transfer aRNA Filter Cartridge to a new collection tube.
14. Add 50 μl warm nuclease free water (Elution).
15. Let stand 2min at room temp.
16. Centrifuge for 1 min at max speed.
17. Repeat steps 15 – 17.
18. Proceed to Dye Coupling and Clean-up. Or, procedure can be stopped and samples stored at -80˚C.

<u>aRNA Hybridization</u>

A. Amino Allyl aRNA: Dye Coupling and Clean-up

1. Add 6.6 μl of DMSO to each tube of dye, mix well, and spin tubes.
2. In separate tube, add 2.5 μg of aRNA in 3.3 μl nuclease-free H_2O, 1.6 μl 0.3M $NaHCO_3$, 4 μl DMSO, and 1 μl of respective dye. It is critical not to mix the two aRNA samples together during this step. **Note:** Volume of aRNA can exceed 3.3 μl if concentration is low. If this is the case, it is necessary to adjust the final concentration of DMSO to 50%.
3. Incubate solution for 60min at room temp in the dark. **Note:** This is a good time to prepare the slides.

4. Optional Quenching step – Add 4.5 μl of 4M Hydroxylamine, mix, and incubate 15 min at room temp in the dark.

5. Combine respective aRNA samples for each hybridization and bring volume up to 100 μl using nuclease-free H_2O.

6. Proceed to labeled aRNA purification.

B. aRNA purification (RNeasy® Kit)

1. Add 10 μl of β-ME to 1 ml of Buffer RLT.

2. Add 350 μl Buffer RLT to each sample.

3. Add 250 μl 100 % EtOH and mix thoroughly.

4. Apply the sample (700 μl) to an RNeasy mini column in a 2 ml collection tube.

5. Centrifuge for 15 s at 10,000 rpm.

6. Discard flow through.

7. Transfer the RNeasy column into a new 2 ml collection tube.

8. Pipet 500 μl Buffer RPE onto the column.

9. Centrifuge for 15 s at 10,000 rpm.

10. Discard flow through.

11. Add another 500 μl Buffer RPE to column.

12. Centrifuge for 2 min at 10,000 rpm to dry the column.

13. Transfer the RNeasy column to a new 1.5 ml collection tube.

14. Pipet 25 μl Rnase-free water directly onto the membrane.

15. Centrifuge for 1 min at 10,000 rpm.

16. Repeat steps 14-15.

B. Preparing Labeled aRNA for Hybridization.

1. To 50 μl of labeled aRNA sample, add 10 μl of Cot-1 DNA (1 μg/μl) for a final volume of 60 μl.

2. Add 60 μl of 2X Hybridization Buffer.

Stock Solutions (**RNase free**)	Volume	2x Hyb buffer final concentration
20X SSC	40 μl	8x SSC
100% formamide	60 μl	60% formamide
10% SDS	2 μl	0.2% SDS

Note: Add in order listed, making sure that the SSC/formamide is at room temp before adding SDS. Makes ~ 100 μl, enough for 1 hybridization.

3. Store in aluminum foil until ready to hybridize.

C. Slide Preparation

1. Set up two 150ml, RNase free beakers for washing the slides. In one beaker, prepare 1%SDS (14 mls of RNase free 10%SDS and 126 mls DEPC H_2O), filter it, and heat to 50-60˚C in water bath. Fill a second beaker with 150mls DEPC H_2O. Place both beakers in flow hood.

2. Rinse slide in the 1%SDS first by moving back and forth for about 1.5 min.

3. Transfer slide to the beaker filled with H_2O and also wash for about 1min. Remove the slide slowly so that it dries as it is removed from the H_2O.

D. Hybridization

1. Place slide into clean hybridization station cartridge assembly, and place on hybridization station. Insert port plugs.

2. Select the desired hybridization program (typically 42 degree program).

3. Once prompted by the hybridization station, remove plug, and inject sample and hybridize 12-16 hrs.

E. Washing Slides

1. Abort hybridization program

2. Select desired wash program. **Note:** RNase free wash solutions should be used for this.

3. Remove slide and rinse in 150ml 0.1X SSC solution (150ml beaker, 750µl of RNase free 20xSSC to 150mls DEPC H_2O and filter). Remove slowly to dry.

4. Apply DyeSaver™ to each slide by dipping slide into a vial filled with the DyeSaver™.

Appendix D: Use of an anti-fade reagent in conjunction with cDNA microarrays to inhibit loss of fluorescence caused by photobleaching and oxidation

Introduction

Successful microarray data acquisition requires that the intensity and integrity of fluorescent dyes remain high throughout the course of the scan. In two color microarray analyses, Alexa 546 and 647 or Cy3 and Cy 5 are commonly used. However, the red dyes (Alexa 647 or Cy5) tend to rapidly lose fluorescence upon exposure to excitation light. This is of particular importance when using epifluorescence/CCD based scanners, as large regions at any one time of the array are exposed to excitation light during the scan. Consequently, fluorescence gradually diminishes during the scan producing an intensity gradient. Unfortunately this gradient can become so severe that adequate data for nearly half of the slide can be difficult to obtain. The creation of this gradient appears to be independent of the elements on the array as the gradient forms in the exact orientation when the slide is scanned from the opposite direction (Fig 1). If there were any gene or location specific properties, one would expect to see the intensity gradient flip as the array was scanned in reverse.

This occurrence is better explained with two processes, photobleaching and oxidation. Photobleaching results in the formation of a non-fluorescent molecule from a fluorescent one. Briefly, when a fluorescent molecule is illuminated with excitation light, its electronic state is converted to a higher level where it eventually emits a photon to return to its ground state. However, the molecule can enter the triplet state where energy is also dissipated. Generally, when a molecule is at the triplet state and at room

temperature, it can decay through chemical reactions, and it is during these chemical reactions with oxygen that the fluorescent molecule is bleached (Doornbos et al. 1997). Multiple excitation events lead to repeated decay and eventual loss of fluorescence. It has also been shown that molecular oxygen is capable of quenching signal from fluorescent dyes (Singh et al. 1992; Corbett et al. 1994). Since the microarrays are exposed to air during post-processing, transfer to scanner, and during the scan, it is highly likely that this process is also contributing to the loss of fluorescent signal.

Many products have been developed to circumvent the loss of fluorescence, typically referred to as anti-fade reagents because they aid in reducing signal loss caused by the factors previously described. Nearly all of these were developed as mounting media for fluorescent microscopy, examples include *N*-propyl galate and *p*-phenylenediamine (Longin et al. 1993; Florijn et al. 1995; Ono et al. 2001). In addition to these reagents, various companies produce anti-fade kits.

The intent of this study was to utilize a commercially available anti-fade kit and evaluate its potential to reduce the photobleaching and oxidation encountered during our microarray experiments.

Materials and Methods

RNA Isolation

Kidneys were excised, minced, and submerged in RNA*later*™ (Ambion, Austin, TX). Prior to RNA isolation, tissue was removed from RNA*later*™. RNA isolation was performed according to the protocol provided with RNA Bee™ (Tel-Test, Inc., Friendswood, TX). Briefly, the tissue was placed in a 6 ml round-bottom tube and RNA Bee was added at 2 ml per 100 mg. Using a tissue homogenizer, tissue was ground in RNA Bee™ to free RNA from cells. The homogenized mixture was then added to a 2 ml Phase Lock Gel™ (Eppendorf, Hamburg, Germany) tube to provide a stable barrier between the organic phase and the nucleic-acid aqueous phase. Chloroform was added at 200 μl per 2 ml of RNA Bee™ solution. The tube was shaken for 15 seconds and centrifuged at 12,000 x g for 15 minutes at 4 °C. Upon completion of centrifugation, the aqueous layer was decanted and placed in a fresh tube. An equal volume of 100% isopropanol was added and mixed by inverting the tube several times. The tube was again placed in the centrifuge and spun for 15 minutes to pellet the RNA. The pellet was briefly washed with a 70% EtOH solution. EtOH was removed and the pellet was allowed to air dry during which time any residual EtOH evaporated. The pellets were then resuspended in nuclease-free water to a final concentration of 2-2.5 μg/μl.

cDNA Synthesis

Quantity and quality of RNA was determined by spectrophotometry. RNA was used if it had a concentration ≥ 2 μg/μl and a 260/280 ratio ≥ 1.6. Reverse transcription

reactions were performed using EndoFree RT™ (Ambion) during which amino allyl dUTPs (2 mM) and dNTP's (10 mM dATP, dGTP, dCTP, and 3 mM dTTP) were incorporated. RNA was primed using oligo dT. To increase signal, reactions were run for 2 hours at 42 °C, contrary to the 48 °C recommended for the RT enzyme. After 2 hours, samples were denatured at 95 °C for 5 minutes and immediately transferred to ice. Base hydrolysis of remaining RNA was performed by addition of 8.6 μl of 1M NaOH and 8.6 μl of 0.5M EDTA, pH 8, and incubated at 65 °C for 15 minutes. The solution was neutralized by adding 8.6 μl of 1M HCl.

cDNA Purification

Amino allyl modified cDNA was purified using PCR purification columns (Qiagen, Valencia, CA). cDNA samples were brought up to 100 μl with Milli-Q H_2O to which 500 μl of Buffer PB was added. The PCR purification protocol was followed exactly, with the exception of substituting 75% EtOH for Buffer PE as a wash solution. cDNA was eluted off the column by using Milli-Q H_2O at a pH of 8.0.

Labeling and Hybridization of cDNA

After cDNA purification, samples were dried to 1-2 μl by vacuum centrifugation. Samples were then resuspended in 3 μl of Sodium bicarbonate ($NaHCO_3$)(25 mg/ml). Lyophilized Alexa Fluor® dyes 546 and 647 (Molecular Probes, Eugene, OR) were diluted in 250 μl of DMSO, of which 5 μl of the appropriate dye were added to the cDNA/$NaHCO_3$ solution. In this study, identical RNA was labeled with each dye, a

technique referred to as a self-self hybridization. This is done to account for any dye-specific effects that may exist. The solution was allowed to sit in the dark for 1 hour. After 1 hour the samples were brought up to 50 μl with H_2O, after which the samples labeled with 546 and 647 were combined and purified as described above, the only exception being that one extra wash with 75% EtOH was administered. To the eluate, an equal volume of 2X hybridization buffer (8X SSC, 60% Formamide, 0.2% SDS) was added along with 10 μg of Cot-1 DNA (Invitrogen, Carlsbad, CA) and 10 μg of poly dA (18-mer)(Integrated DNA Technologies, Coralville, IA). This solution was applied to a microarray slide using a GeneTac™ hybridization station (Genomic Solutions, Inc., Ann Arbor, MI) and hybridized at 47°C overnight. The slides were washed using two wash solutions (1X SSC, 0.1% SDS and 0.1X SSC, 0.01% SDS) by first passing the solutions over the slide for 20 seconds and then holding them on the slide for 30 seconds. Slides were rinsed in 0.1X SSC and dried.

Application of ProLong Anti-Fade

ProLong™ anti-fade (Molecular Probes, Eugene, OR) was prepared per supplied protocol. To component A, 1 ml of glycerol stock solution was added and the tube was vortexed for resuspension. After vortexing, the tube was spun to eliminate any bubbles that may have formed. To a prepared array, 65μl of ProLong was added in a continuous stream down the center of the slide. A cover slip cleaned with 2M NaOH and rinsed in H_20 was placed over the array and the ProLong™ was allowed to evenly spread under the cover slip. ProLong™ was cured 4 hours to overnight before the slide was scanned.

Scanning of Array

Hybridized slides were scanned using an epifluorescence/CCD based scanner (Applied Precision, Inc., Issaquah, WA). Random areas (2.25 mm^2) of the slide were examined to determine proper exposure for each channel. Once exposure times were established, the printed region was scanned and the data was collected. Using the spot finding analysis software (MolecularWare, Inc., Cambridge, MA), signal intensities for each spot were calculated. From that data, location specific signal intensities across the slide were generated by calculating the average intensities of each column.

Results and Discussion

The propensity of fluorescent dyes to bleach after being exposed to excitation light, as well as their ability to be quenched by molecular oxygen has motivated us to explore a new approach to limit reduction of fluorescence during cDNA microarray scanning. Arrays scanned in our laboratory using an epifluorescence/CCD based scanner occasionally experience fluorescence degradation caused by multiple exposures to excitation light. This process led to the establishment of a signal intensity gradient across the array, as the spots farthest from the scan origin endured the longest periods of excitation (Fig. 1). At the same time, processed arrays waiting to be scanned, while kept in the dark, were being exposed to oxygen that may contribute to loss of signal.

In contrast, when ProLong™ was applied to the microarray slide containing cDNA generated from identical RNA samples immediately after post-processing, signal intensity appeared to be more consistent across the slide (Fig. 1). Furthermore, the reduction in signal gradient resulted in the inclusion of 440 more spots that could be analyzed. Although a gradient was still seen after the application of ProLong™ in the Alexa Fluor® 647 channel, total fluorescence signal increased 2-fold over arrays with no anti-fade. Analysis of Alexa Fluor® 546 with and without anti-fade did not show a gradient as Alexa Fluor® 647 did, but there was an overall increase of approximately 30% when anti-fade reagent was used (Fig. 2). The loss of fluorescence of Alexa Fluor® 647 was in the range of 30-50% from one side of the array to the other. By increasing the number of spots successfully detected, the data can be analyzed and presented with more

confidence. Although the signal of Alexa Fluor® 647 still decreased across the slide, the overall increase in signal made it possible for those spots to be detected.

This study has shown that use of ProLong™ anti-fade reagent with cDNA microarrays greatly increases the number of spots that can be reliably detected. Ono et al. compared several anti-fade mounting media using fluorescence on a confocal microscope (Ono et al. 2001). They showed that ProLong™ maintained the highest level of fluorescence over time. Although we chose to use ProLong™, we think that most anti-fade reagents, commercially available or homemade, will significantly increase the amount of signal obtained. In addition, use of anti-fade has proved to be effective in long-term storage of hybridized microarray slides, as robust signals were obtained several weeks after initial use. While the data presented here were collected using an epifluorescent scanner, treatment of slides should prove useful when laser-based scanners are also used. Results of this study suggest that an anti-fade reagent should be used in conjunction with cDNA microarray hybridization.

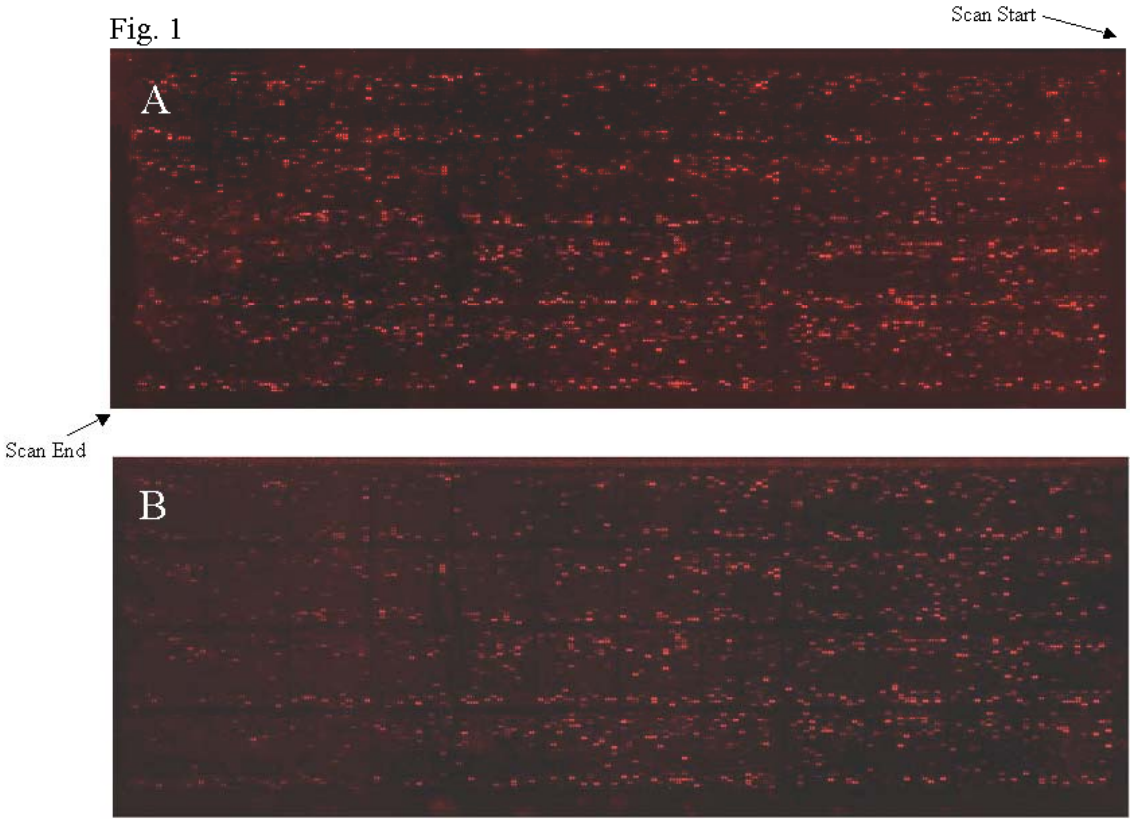

Figure 1 Scanned image of microarray hybridized with kidney cDNA that was labeled with Alexa Fluor® 647 and treated with A) ProLong™ or not treated B) with ProLong™.

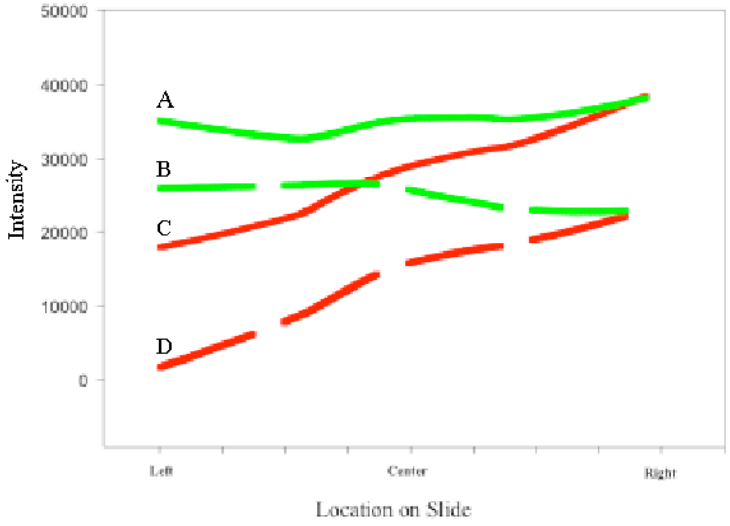

Figure 2 Plot of spot intensity of each dye with respect to location on microarray slide. Right side of graph represents location on slide where scan initiates, while left side of graph indicates location last to be scanned. A) Intensity data for Alexa Fluor® 546 treated with ProLong™. B) Across slide intensity values from Alexa 546 on slide not treated with ProLong™. C) Intensity data for Alexa Fluor® 647 on slide treated with ProLong™, illustrating intensity gradient from right to left and the overall increase in signal when compared to intensity of D) Alexa Fluor® 647 on slide not treated with ProLong™.

REFERENCES

Abramson, S. L. and J. I. Gallin (1990). "IL-4 inhibits superoxide production by human mononuclear phagocytes." J Immunol **144**(2): 625-30.

Al-Saffar, N., et al. (1998). "Direct activation of mast cells by prosthetic biomaterial particles." J Mater Sci Mater Med **9**(12): 849-53.

Alberts, B. (1994). Molecular biology of the cell. New York, Garland Pub.

Alizadeh, A. A., et al. (2001). "Towards a novel classification of human malignancies based on gene expression patterns." J Pathol **195**(1): 41-52.

Anderson, J. M. (1988). "Inflammatory response to implants." ASAIO Trans **34**(2): 101-7.

Anderson, J. M. (2000). "Multinucleated giant cells." Curr Opin Hematol **7**(1): 40-7.

Bauer, J. J., et al. (1999). "Twelve-year experience with expanded polytetrafluoroethylene in the repair of abdominal wall defects." Mt Sinai J Med **66**(1): 20-5.

Bier, J. (2000). "History of facial prostheses." September 28, 2005, from http://www.gesichtsepithetik.de/eng/history.html.

Bisset, L. R. and P. Schmid-Grendelmeier (2005). "Chemokines and their receptors in the pathogenesis of allergic asthma: progress and perspective." Curr Opin Pulm Med **11**(1): 35-42.

Boswell, C. A., et al. (1999). "Evaluation of an aqueous drainage glaucoma device constructed of ePTFE." J Biomed Mater Res **48**(5): 591-5.

Boswell, C. A. and S. K. Williams (1999). "Denucleation promotes neovascularization of ePTFE in vivo." J Biomater Sci Polym Ed **10**(3): 319-29.

Branemark, P. I. (1983). "Osseointegration and its experimental background." J Prosthet Dent **50**(3): 399-410.

Brauker, J. (2001). "Unraveling mysteries at the biointerface: molecular mediator of inhibition of blood vessel formation in the foreign body capsule revealed." SurFACTS in Biomaterials **6**(3): 1-5.

Butany, J., et al. (2002). "Hufnagel valve: the first prosthetic mechanical valve." Cardiovasc Pathol **11**(6): 351-3.

Cassell, O. C., et al. (2002). "Vascularisation of tissue-engineered grafts: the regulation of angiogenesis in reconstructive surgery and in disease states." Br J Plast Surg **55**(8): 603-10.

Chatila, T. A. (2004). "Interleukin-4 receptor signaling pathways in asthma pathogenesis." Trends Mol Med **10**(10): 493-9.

Clark, R. A. F. (1996). The Molecular and Cellular Biology of Wound Repair. New York, Plenum Press.

Corbett, J. D., et al. (1994). "Deoxygenation affects fluorescence photobleaching recovery measurements of red cell membrane protein lateral mobility." Biophys J **66**(1): 25-30.

Dadsetan, M., et al. (2004). "Surface chemistry mediates adhesive structure, cytoskeletal organization, and fusion of macrophages." J Biomed Mater Res **71A**(3): 439-48.

Davis, J. R. and ASM International. (2003). Handbook of materials for medical devices. Materials Park, OH, ASM International.

DeFife, K. M., et al. (1997). "Interleukin-13 induces human monocyte/macrophage fusion and macrophage mannose receptor expression." J Immunol **158**(7): 3385-90.

Diegelmann, R. F. and M. C. Evans (2004). "Wound healing: an overview of acute, fibrotic and delayed healing." Front Biosci **9**: 283-9.

Doornbos, R. M., et al. (1997). "Experimental and model investigations of bleaching and saturation of fluorescence in flow cytometry." Cytometry **29**(3): 204-14.

Driscoll, K. E. (1994). "Macrophage inflammatory proteins: biology and role in pulmonary inflammation." Exp Lung Res **20**(6): 473-90.

DuPont. "History of Teflon." Retrieved September 30, 2005, from http://www.teflon.com/NASApp/Teflon/TeflonPageServlet?pageId=/consumer/na/eng/news/news_detail.teflon_history.html.

Eisen, M. B., et al. (1998). "Cluster analysis and display of genome-wide expression patterns." Proc Natl Acad Sci U S A **95**(25): 14863-8.

Florijn, R. J., et al. (1995). "Analysis of antifading reagents for fluorescence microscopy." Cytometry **19**(2): 177-82.

Fournier, E., et al. (2003). "Biocompatibility of implantable synthetic polymeric drug carriers: focus on brain biocompatibility." Biomaterials **24**(19): 3311-31.

Fraser, A. G. and E. M. Marcotte (2004). "Development through the eyes of functional genomics." Curr Opin Genet Dev **14**(4): 336-42.

Ganta, S. R., et al. (2003). "Vascularization and tissue infiltration of a biodegradable polyurethane matrix." J Biomed Mater Res **64A**(2): 242-8.

Gerritsen, M. (2000). "Problems associated with subcutaneously implanted glucose sensors." Diabetes Care **23**(2): 143-5.

Golden, M. A., et al. (1990). "Healing of polytetrafluoroethylene arterial grafts is influenced by graft porosity." J Vasc Surg **11**(6): 838-44; discussion 845.

Gordon, S. (2003). "Alternative activation of macrophages." Nat Rev Immunol **3**(1): 23-35.

Gore, W. L. (2005). "About Gore: Timeline." Retrieved September 30, 2005, from http://www.gore.com/en_xx/aboutus/timeline/.

Gumpenberger, T., et al. (2003). "Adhesion and proliferation of human endothelial cells on photochemically modified polytetrafluoroethylene." Biomaterials **24**(28): 5139-44.

Hagerty, R. D., et al. (2000). "Cellular proliferation and macrophage populations associated with implanted expanded polytetrafluoroethylene and polyethyleneterephthalate." J Biomed Mater Res **49**(4): 489-97.

Hanke, C. W. (2002). "A new ePTFE soft tissue implant for natural-looking augmentation of lips and wrinkles." Dermatol Surg **28**(10): 901-8.

Hannouche, D., et al. (2005). "Ceramics in total hip replacement." Clin Orthop Relat Res(430): 62-71.

Hart, P. H., et al. (1999). "Differential responses of human monocytes and macrophages to IL-4 and IL-13." J Leukoc Biol **66**(4): 575-8.

Herbert, D. R., et al. (2004). "Alternative macrophage activation is essential for survival during schistosomiasis and downmodulates T helper 1 responses and immunopathology." Immunity **20**(5): 623-35.

Hernandez-Pando, R., et al. (2000). "Inflammatory cytokine production by immunological and foreign body multinucleated giant cells." Immunology **100**(3): 352-8.

Homan, S. M., et al. (1998). "Endothelial cells assemble two distinct alpha6beta4-containing vimentin-associated structures: roles for ligand binding and the beta4 cytoplasmic tail." J Cell Sci **111 (Pt 18)**: 2717-28.

Hu, W. J., et al. (2001). "Molecular basis of biomaterial-mediated foreign body reactions." Blood **98**(4): 1231-8.

Huang, D. R., et al. (2001). "Absence of monocyte chemoattractant protein 1 in mice leads to decreased local macrophage recruitment and antigen-specific T helper cell type 1 immune response in experimental autoimmune encephalomyelitis." J Exp Med **193**(6): 713-26.

Ilan, N. and J. A. Madri (2003). "PECAM-1: old friend, new partners." Curr Opin Cell Biol **15**(5): 515-24.

Izhar, U., et al. (2001). "Novel synthetic selectively degradable vascular prostheses: a preliminary implantation study." J Surg Res **95**(2): 152-60.

Joos, L., et al. (2003). "Functional genomics and gene microarrays--the use in research and clinical medicine." Swiss Med Wkly **133**(3-4): 31-8.

Kakisis, J. D., et al. (2005). "Artificial blood vessel: the Holy Grail of peripheral vascular surgery." J Vasc Surg **41**(2): 349-54.

Kannan, R. Y., et al. (2005). "Current status of prosthetic bypass grafts: a review." J Biomed Mater Res B Appl Biomater **74**(1): 570-81.

Kao, W. J., et al. (1995). "Role for interleukin-4 in foreign-body giant cell formation on a poly(etherurethane urea) in vivo." J Biomed Mater Res **29**(10): 1267-75.

Katti, K. S. (2004). "Biomaterials in total joint replacement." Colloids Surf B Biointerfaces **39**(3): 133-42.

Kelly-Welch, A. E., et al. (2003). "Interleukin-4 and interleukin-13 signaling connections maps." Science **300**(5625): 1527-8.

Kerr, M. K., et al. (2000). "Analysis of variance for gene expression microarray data." J Comput Biol **7**(6): 819-37.

Kidd, K. R., et al. (2005). "Stimulated Endothelial Cell Adhesion and Angiogenesis with Laminin-5 Modification of Expanded Polytetrafluoroethylene." Tissue Engineering **11**(9/10).

Kidd, K. R., et al. (2002). "Angiogenesis and neovascularization associated with extracellular matrix-modified porous implants." J Biomed Mater Res **59**(2): 366-77.

Kidd, K. R., et al. (2003). "Accelerated endothelialization of interpositional 1-mm vascular grafts." J Surg Res **113**(2): 234-42.

Kidd, K. R. and S. K. Williams (2004). "Laminin-5-enriched extracellular matrix accelerates angiogenesis and neovascularization in association with ePTFE." J Biomed Mater Res **69A**(2): 294-304.

Kirkpatrick, C. J., et al. (2002). "Tissue response and biomaterial integration: the efficacy of in vitro methods." Biomol Eng **19**(2-6): 211-7.

Kleinert, L. B., et al. (1996). "The neointima formed in endothelial cell sodded ePTFE vascular grafts results from both cellular-hyperplasia and extracellular-hypertrophy." Cell Transplant **5**(4): 475-82.

Kodelja, V., et al. (1997). "Differences in angiogenic potential of classically vs alternatively activated macrophages." Immunobiology **197**(5): 478-93.

Kotanides, H. and N. C. Reich (1996). "Interleukin-4-induced STAT6 recognizes and activates a target site in the promoter of the interleukin-4 receptor gene." J Biol Chem **271**(41): 25555-61.

Kyriakides, T. R. and P. Bornstein (2003). "Matricellular proteins as modulators of wound healing and the foreign body response." Thromb Haemost **90**(6): 986-92.

Kyriakides, T. R., et al. (1999). "Mice that lack the angiogenesis inhibitor, thrombospondin 2, mount an altered foreign body reaction characterized by increased vascularity." Proc Natl Acad Sci U S A **96**(8): 4449-54.

Langlais, F. (1985). "[New biomaterials in orthopedics]." Presse Med **14**(26): 1424-8.

Lehman, W., et al. (2000). "Tropomyosin and actin isoforms modulate the localization of tropomyosin strands on actin filaments." J Mol Biol **302**(3): 593-606.

Lemons, J. and J. Natiella (1986). "Biomaterials, biocompatibility, and peri-implant considerations." Dent Clin North Am **30**(1): 3-23.

Li, J., et al. (2003). "Angiogenesis in wound repair: Angiogenic growth factors and the extracellular matrix." Microsc Res Tech **60**(1): 107-14.

Lloyd, A. W., et al. (1999). "The development of in vitro biocompatibility tests for the evaluation of intraocular biomaterials." J Mater Sci Mater Med **10**(10/11): 621-7.

Long, M. and H. J. Rack (1998). "Titanium alloys in total joint replacement--a materials science perspective." Biomaterials **19**(18): 1621-39.

Longin, A., et al. (1993). "Comparison of anti-fading agents used in fluorescence microscopy: image analysis and laser confocal microscopy study." J Histochem Cytochem **41**(12): 1833-40.

Lu, H. K., et al. (2004). "Comparison of Th1/Th2 cytokine profiles of initial wound healing of rats induced by PDCM and e-PTFE." J Biomed Mater Res B Appl Biomater **68**(1): 75-80.

Lysaght, M. J. and J. A. O'Loughlin (2000). "Demographic scope and economic magnitude of contemporary organ replacement therapies." Asaio J **46**(5): 515-21.

Ma, J., et al. (2003). "Regulation of macrophage activation." Cell Mol Life Sci **60**(11): 2334-46.

Marcotte, E. M., et al. (1999). "A combined algorithm for genome-wide prediction of protein function." Nature **402**(6757): 83-6.

Martin, P. (1997). "Wound healing--aiming for perfect skin regeneration." Science **276**(5309): 75-81.

McNally, A. K. and J. M. Anderson (1995). "Interleukin-4 induces foreign body giant cells from human monocytes/macrophages. Differential lymphokine regulation of macrophage fusion leads to morphological variants of multinucleated giant cells." Am J Pathol **147**(5): 1487-99.

McNally, A. K. and J. M. Anderson (2003). "Foreign body-type multinucleated giant cell formation is potently induced by alpha-tocopherol and prevented by the diacylglycerol kinase inhibitor R59022." Am J Pathol **163**(3): 1147-56.

McNally, A. K., et al. (1996). "Interleukin-4-induced macrophage fusion is prevented by inhibitors of mannose receptor activity." Am J Pathol **149**(3): 975-85.

Merzkirch, C., et al. (2001). "Engineering of vascular ingrowth matrices: are protein domains an alternative to peptides?" Anat Rec **263**(4): 379-87.

Mikos, A. G., et al. (1998). "Host response to tissue engineered devices." Adv Drug Deliv Rev **33**(1-2): 111-139.

Mosser, D. M. (2003). "The many faces of macrophage activation." J Leukoc Biol **73**(2): 209-12.

Naldini, A. and F. Carraro (1999). "Hypoxia modulates cyclin and cytokine expression and inhibits peripheral mononuclear cell proliferation." J Cell Physiol **181**(3): 448-54.

Ono, M., et al. (2001). "Quantitative comparison of anti-fading mounting media for confocal laser scanning microscopy." J Histochem Cytochem **49**(3): 305-12.

Porcheray, F., et al. (2005). "Macrophage activation switching: an asset for the resolution of inflammation." Clin Exp Immunol **142**(3): 481-9.

Ragno, S., et al. (2001). "Changes in gene expression in macrophages infected with Mycobacterium tuberculosis: a combined transcriptomic and proteomic approach." Immunology **104**(1): 99-108.

Rah, D. K. (2000). "Art of replacing craniofacial bone defects." Yonsei Med J **41**(6): 756-65.

Ratcliffe, A. (2000). "Tissue engineering of vascular grafts." Matrix Biol **19**(4): 353-7.

Ratner, B. D. (2001). "Replacing and renewing: synthetic materials, biomimetics, and tissue engineering in implant dentistry." J Dent Educ **65**(12): 1340-7.

Ratner, B. D. (2002). "Reducing capsular thickness and enhancing angiogenesis around implant drug release systems." J Control Release **78**(1-3): 211-8.

Ratner, B. D. and S. J. Bryant (2004). "Biomaterials: where we have been and where we are going." Annu Rev Biomed Eng **6**: 41-75.

Rosengren, A. and L. M. Bjursten (2003). "Pore size in implanted polypropylene filters is critical for tissue organization." J Biomed Mater Res **67A**(3): 918-26.

Rothenberg, M. and S. Hogan (2006). "The Eosinophil." Annu Rev Immunol **24**(5): 1-28.

Saito, N., et al. (2005). "Synthetic biodegradable polymers as drug delivery systems for bone morphogenetic proteins." Adv Drug Deliv Rev **57**(7): 1037-48.

Salzmann, D. L., et al. (1997). "The effects of porosity on endothelialization of ePTFE implanted in subcutaneous and adipose tissue." J Biomed Mater Res **34**(4): 463-76.

Salzmann, D. L., et al. (1999). "Inflammation and neovascularization associated with clinically used vascular prosthetic materials." Cardiovasc Pathol **8**(2): 63-71.

Saulot, V., et al. (2002). "Presence of autoantibodies to the glycolytic enzyme alpha-enolase in sera from patients with early rheumatoid arthritis." Arthritis Rheum **46**(5): 1196-201.

Schachtrupp, A., et al. (2003). "Individual inflammatory response of human blood monocytes to mesh biomaterials." Br J Surg **90**(1): 114-20.

Schena, M., et al. (1998). "Microarrays: biotechnology's discovery platform for functional genomics." Trends Biotechnol **16**(7): 301-6.

Schwartz, M. A., et al. (2005). "Gene expression in tissue associated with extracellular matrix modified ePTFE." J Biomed Mater Res A **73A**(1): 30-8.

Sharkawy, A. A., et al. (1997). "Engineering the tissue which encapsulates subcutaneous implants. I. Diffusion properties." J Biomed Mater Res **37**(3): 401-12.

Sharkawy, A. A., et al. (1998). "Engineering the tissue which encapsulates subcutaneous implants. II. Plasma-tissue exchange properties." J Biomed Mater Res **40**(4): 586-97.

Shen, M., et al. (2004). "Effects of adsorbed proteins and surface chemistry on foreign body giant cell formation, tumor necrosis factor alpha release and procoagulant activity of monocytes." J Biomed Mater Res A **70**(4): 533-41.

Sherwood, L. (1997). Human physiology : from cells to systems. Belmont, CA, Wadsworth Pub. Co.

Singh, R. J., et al. (1992). "Photobleaching of merocyanine 540: involvement of singlet molecular oxygen." Photochem Photobiol **55**(4): 483-9.

Stein, M., et al. (1992). "Interleukin 4 potently enhances murine macrophage mannose receptor activity: a marker of alternative immunologic macrophage activation." J Exp Med **176**(1): 287-92.

Subramanian, A. and D. M. Miller (2000). "Structural analysis of alpha-enolase. Mapping the functional domains involved in down-regulation of the c-myc protooncogene." J Biol Chem **275**(8): 5958-65.

Tang, L. and J. W. Eaton (1995). "Inflammatory responses to biomaterials." Am J Clin Pathol **103**(4): 466-71.

Tassiopoulos, A. K. and H. P. Greisler (2000). "Angiogenic mechanisms of endothelialization of cardiovascular implants: a review of recent investigative strategies." J Biomater Sci Polym Ed **11**(11): 1275-84.

te Velde, A. A., et al. (1988). "Modulation of phenotypic and functional properties of human peripheral blood monocytes by IL-4." J Immunol **140**(5): 1548-54.

Trivedi, N., et al. (2000). "Improved vascularization of planar membrane diffusion devices following continuous infusion of vascular endothelial growth factor." Cell Transplant **9**(1): 115-24.

Updike, S. J., et al. (2000). "A subcutaneous glucose sensor with improved longevity, dynamic range, and stability of calibration." Diabetes Care **23**(2): 208-14.

van Bilsen, P. H., et al. (2004). "Ongoing foreign body reaction to subcutaneous implanted (heparin) modified Dacron in rats." J Biomed Mater Res **68A**(3): 423-7.

Van Gelder, R. N., et al. (1990). "Amplified RNA synthesized from limited quantities of heterogeneous cDNA." Proc Natl Acad Sci U S A **87**(5): 1663-7.

van Luyn, M. J., et al. (1998). "Modulation of the tissue reaction to biomaterials. II. The function of T cells in the inflammatory reaction to crosslinked collagen implanted in T-cell-deficient rats." J Biomed Mater Res **39**(3): 398-406.

Vandgama, V. (2003). "Implant Reconstruction History." September 28, 2005, from http://www.dentalinsurance.co.uk/implants/implant_history.htm.

Venter, J. C., et al. (2001). "The sequence of the human genome." Science **291**(5507): 1304-51.

Vignery, A., et al. (1989). "Polarized distribution of Na+,K+-ATPase in giant cells elicited in vivo and in vitro." J Histochem Cytochem **37**(8): 1265-71.

Vroman, L., et al. (1980). "Interaction of high molecular weight kininogen, factor XII, and fibrinogen in plasma at interfaces." Blood **55**(1): 156-9.

Ward, W. K., et al. (2003). "Vascularizing the tissue surrounding a model biosensor: how localized is the effect of a subcutaneous infusion of vascular endothelial growth factor (VEGF)?" Biosens Bioelectron **19**(3): 155-63.

Ward, W. K., et al. (2002). "The effect of microgeometry, implant thickness and polyurethane chemistry on the foreign body response to subcutaneous implants." Biomaterials **23**(21): 4185-92.

Warner, G. C., et al. (2004). "Molecular classification of oral cancer by cDNA microarrays identifies overexpressed genes correlated with nodal metastasis." Int J Cancer **110**(6): 857-68.

Wataha, J. C. (2001). "Principles of biocompatibility for dental practitioners." J Prosthet Dent **86**(2): 203-9.

Wendelboe, A. M., et al. (2003). "Relationships between body mass indices and surgical replacements of knee and hip joints." Am J Prev Med **25**(4): 290-5.

Werner, S. and R. Grose (2003). "Regulation of wound healing by growth factors and cytokines." Physiol Rev **83**(3): 835-70.

Wiggins, M. J., et al. (2001). "Biodegradation of polyether polyurethane inner insulation in bipolar pacemaker leads." J Biomed Mater Res **58**(3): 302-7.

Williams, D. F. (1987). Definitions in Biomaterials. Progress in Biomedical Engineering. Amsterdam, Elsevier. **4**.

Wisniewski, N., et al. (2001). "Decreased analyte transport through implanted membranes: differentiation of biofouling from tissue effects." J Biomed Mater Res **57**(4): 513-21.

Wisniewski, N., et al. (2000). "Characterization of implantable biosensor membrane biofouling." Fresenius J Anal Chem **366**(6-7): 611-21.

Zdrahala, R. J. (1996). "Small caliber vascular grafts. Part I: state of the art." J Biomater Appl **10**(4): 309-29.

Zhao, Q., et al. (1991). "Foreign-body giant cells and polyurethane biostability: in vivo correlation of cell adhesion and surface cracking." J Biomed Mater Res **25**(2): 177-83.